Dynamics and Stability of Pinned-Clamped Coaxial Cylindrical Shells Conveying Viscous Flow

by

Bin Tian

This thesis was submitted to the Faculty of Graduate Studies and Research in partial fulfillment of the requirements for the Master of Engineering degree.

Department of Mechanical Engineering
McGill University
Montréal, Québec, Canada

The shortened version of the thesis title:

Stability of Pinned-Clamped Coaxial
Shells Conveying Viscous Flow

Abstract

This thesis presents a theoretical study of the stability of *pinned-clamped* and *clamped-pinned* coaxial cylindrical shells conveying internal and/or annular incompressible viscous fluid flow.

In the present analytical model, fluid viscous effects are taken into consideration. Generally, the viscous nature of the fluid results in both *steady* and *unsteady* viscosity-related loads being exerted on the shells, the latter of which are approximated by their *inviscid* counterpart in this thesis. Upstream pressurization of the flow (to overcome frictional pressure drop) and skin friction on the shell surfaces are taken into account, generating time-averaged normal and tangential loads on the shells. In this model, the shell motions are described by Flügge's shell equations, suitably modified to incorporate the time-averaged stress resultants arising from viscous effects. The *unsteady* fluid-dynamic forces in these equations are formulated from potential flow theory: the perturbation pressures on the shells are determined from the perturbation velocity potentials via the unsteady Bernoulli equation; those velocity potentials are governed by the Laplace equation, which is solved by the Fourier transform technique.

For the *clamped-pinned* system, since the downstream end of the shell is simply supported, a so-called out-flow model is utilized in modelling the decay of flow perturbations beyond the pinned end.

Comparison is made with the existing results for clamped-clamped and clamped-free cases.

Finally, future work is suggested with regard to setting up a new analytical model with the *unsteady* viscous effects taken into account.

Résumé

Cette thèse présente une étude théorique sur la stabilité de coques cylindriques coaxialles *épinglées-encastrées* et *encastrées-épinglées*, dont la coque interne et/ou l'espace annulaire sont soumis à un écoulement de fluide visqueux et incompressible.

Dans le modèle présent analytique, les effets fluides visqeux sont partiellement pris en considération. Généralement, le nature visqueuse du fluide aboutit à de forces visqueuses *stationnaires* et *instationnaires* agissant sur la coque, la dernière desquelles est négligée dans cette thèse. La pressurisation en amont dans l'écoulement (pour surmonter la chute de pression frictionelle) et la friction agissant sur la surface de la coque sont tenues en compte, générant les forces normales et tangentieles temps permanentes agissant sur la coque. Dans ce modèle, les déplacements des coques sont décrits par les équations de Flügge, modifiées convenablement afin d'incorporer les forces permanentes provenant des effets visqueux. Les forces fluides dynamiques *instationaires* dans ces équations sont formulées par la théorie des écoulements potentiels: les perturbations de pression sur la coque sont déterminées via l'équation instationnaire de Bernoulli après que l'équation de Laplace est solutionnée en utilisant la technique de la transformée de Fourier.

Pour le systéme *encastré-épinglé*, puisque le bout de la coque en aval est supporté simplement, un modèle dit *out-flow model* est utilisé pour modéliser l'amortissement des perturbations de l'écoulement audelà du bout épinglé.

Une comparaison est faite avec les résultats existants pour les cas encastré-encastré et encastré-libre.

Finalement, des travaux connexes futurs sont suggérés dans le but d'établir un nouveau modèle analytique avec tenant compte des effets visqueux *instationnaires*.

Acknowledgements

I wish to express my sincere gratitude to my thesis supervisors, Prof. M.P. Païdoussis and Prof. A.K. Misra, for their guidance, encouragement and assistance during the course of the inverstigation.

The financial support provided by my supervisors through NSERC and FCAR is gratefully acknowledged.

Finally, I wish to thank my wife, Xiaofeng Li, for her love, support and encouragement.

Contents

List of Figures

List of Tables

Nomenclature

Symbol	Description
a	inner-shell radius
$A_m, \ldots, F_m$	constants [see equations (2.29) and (2.30)]
b	outer-shell radius
d_i	$2a$, mean diameter of the inner shell
d_h	$2(b-a)$, hydraulic diameter
E_i, E_o	Young's moduli of the inner-shell and outer-shell materials
f_i, f_o	friction factors of the inner and outer flows [see equation (2.80)]
h_i, h_o	wall-thicknesses of the inner and outer shell
I_n, K_n	modified Bessel functions of order n
k	axial wave-number [see equation (2.104)]
k_i	$h_i^2/12a^2$
k_o	$h_o^2/12b^2$
ℓ	L'/L
L	length of the flexible portion of the shell
L'	total length in which flow perturbations are non-zero
m	axial wave-number
M	number of comparison functions taken [see equation (2.113)]
M_x	bending moment
$M_{x\theta}$	twisting moment

n	circumferential wave-number
N_x	axial (normal) force per unit length
$N_{x\theta}$	shearing force per unit length
$N_{xI}, N_{\theta I}, N_{x\theta I}$	axial, hoop, and shear stress resultants [see equations (2.95) and (2.96)]
p_e	perturbation pressure surrounding the outer shell
p_i, p_o	perturbation pressures in the inner and annular flow [see equation (2.28)]
P	instantaneous pressure in the perturbed flow field [see equation (2.25)]
$P_i(x,r)$	time-averaged pressure of the inner fluid [see equation (2.75)]
$P_o(x,r)$	time-averaged pressure of the annular fluid [see equation (2.77)]
P_s	stagnation pressure [see equation (2.25)]
$\bar{P}$	mean, undisturbed pressure in the flow [see equation (2.27)]
$\bar{P}_{rIi}$	steady radial differential pressure on the inner shell [see equation (2.83)]
$\bar{P}_{rIo}$	steady radial differential pressure on the outer shell [see equation (2.87)]
$\bar{P}_{xIi}$	traction load on the inner shell [see equation (2.85)]
$\bar{P}_{xIo}$	traction load on the outer shell [see equation (2.90)]
q_{1i}, q_{2i}, q_{3i}	steady viscous forces acting on the inner shell [see equation (2.98)]

q_{1o}, q_{2o}, q_{3o}	steady viscous forces acting on the outer shell [see equation (2.98)]
q_i, q_o	unsteady inviscid forces acting on the inner and outer shells [see equation (2.58)]
Q_x	,ransverse shearing force per unit length
r	radial coordinate
r_m	radius at which the mean velocity is maximum in the turbulent flow [see equation (2.79)]
$\mathrm{Re}_i, \mathrm{Re}_o$	Reynolds numbers of the inner and annular flows
$R_m(x)$	functional form of an out-flow model
t	physical time
u_i, v_i, w_i	axial, circumferential, and radial displacements of the inner shell
u_o, v_o, w_o	axial, circumferential, and radial displacements of the outer shell
U_i, U_o	mean, undisturbed velocities of the inner and annular flows
$U_{\tau i}$	stress velocity on the interior surface of the inner shell [see equation (2.76)]
$U_{\tau oi}$	stress velocity on the exterior surface of the inner shell [see equation (2.86)]
$U_{\tau oo}$	stress velocity on the interior surface of the outer shell [see equation (2.78)]
$\mathcal{U}_i, \mathcal{U}_o$	reference flow velocities [see equation (2.52)]
V_x, V_θ, V_r	components of the mean-flow velocity vector $\mathbf{V}$
V'_x, V'_θ, V'_r	fluctuation velocity components of the turbulent flow
x	axial coordinate
y	coordinate measured from the wall

α	Fourier-transform variable (Chapter 2)
γ_i	$\rho_{si}a^2(1-\nu_i^2)/E_i$
γ_o	$\rho_{so}b^2(1-\nu_o^2)/E_o$
ε	r/L
ε_i	a/L
ε_o	b/L
θ	polar coordinate
μ_i, μ_o	structural damping factors of the inner-shell and outer-shell materials
ν_i, ν_o	(i) Poisson's ratios of the inner-shell and outer-shell materials (ii) kinematic viscosities of the inner and annular fluids
ξ	x/L
ρ_i, ρ_o	densities of the fluids inside the inner shell and in the annulus
ρ_{si}, ρ_{so}	densities of the inner-shell and outer shell materials
τ_{wi}	fluid frictional force per unit area on the interior surface of the inner shell [see equation (2.76)]
τ_{woi}	fluid frictional force per unit area on the exterior surface of the inner shell [see equation (2.86)]
τ_{woo}	fluid frictional force per unit area on the interior surface of the outer shell [see equation (2.78)]
ϕ_i, ϕ_o	velocity potential perturbations of the inner and annular flows
χ_i, χ_o	viscous damping coefficients of the inner-shell and outer-shell materials
Ψ	velocity potential
Ω	angular frequency of oscillation

Chapter 1

Introduction

The dynamics and stability of cylindrical structures containing, or immersed in, flowing fluid have been investigated quite intensively over the past thirty years or so. Although the research in this field is fundamental, applications are found in many engineering constructions, such as in the power-generating, chemical, and petrochemical industries; e.g., in the form of piping of all kinds, marine risers, and chimneys; fuel pins, monitoring, and control rods in nuclear reactors; heat exchanger tube arrays and bundles of electrical conductors in transmission lines; and thin-walled shrouds and flow-containment shells in nuclear reactors, aircraft engines, jet pumps; etc..

Generally, cylindrical structures may be excited by either *axial* flow or *cross* flow, the former of which could be divided into three classes, according to the disposition of the flow vis-à-vis the cylindrical structures: (a) axial flow within tubular structures; (b) axial flow outside the cylindrical structures, i.e., along the long axes of the cylinders; (c) annular flow in systems of coaxial cylinders.

Here, only key references will be cited to show historical stages of research development on *axial flow*—the type of flow to be considered in this thesis. This Introduction follows closely the review by Païdoussis (1987).

1.1 Internal Flow in Tubular Structures

This is the oldest and most fundamental problem. A series of experiments by Aitken (1876), on travelling chains and elastic cords, illustrating the balance between motion-induced tensile and centrifugal forces, is perhaps among the earliest work related to the study of dynamics of flexible pipes conveying fluid. Feodos'ev (1951), Housner (1952) and Niordson (1953) were among the first to study the stability of a straight pipe with pinned-pinned ends conveying fluid. With different means of analysis, they obtained the same basic equation of motion and reached the same conclusion that, at sufficiently high velocities, pinned-pinned pipes may buckle like columns subjected to compressive axial loading. This phenomenon is commonly referred to as divergence, which is another term for buckling instability.

Divergence is the expected form of instability for pipes conveying fluid with both ends supported, since the system is conservative. However, it is of the gyroscopic conservative variety, by virtue of the presence of the Coriolis terms; hence, although the system should lose stability by divergence, in principle it could also be subjected to coupled-mode flutter—by coalescence of two modes in the complex-frequency plane. Païdoussis and Issid (1974) determined that, according to linear theory, coupled-mode flutter should occur at approximately twice the critical flow velocity for divergence. The theoretical predictions for divergence of pipes with ends supported have been well confirmed by series of experiments conducted by Naguleswaran and Williams (1968), Liu and Mote (1974), and more recently Jendrzejczyk and Chen (1985). However, by nonlinear analysis, Holmes (1978) and Ch'ng (1978) found that coupled-mode flutter cannot occur, which is also supported by experimental evidence, since post-divergence oscillatory instability has never been observed.

Benjamin (1961a,b) examined the dynamics of a cantilevered system of articulated

pipes containing flowing fluid; this system is non-conservative. It is found that it loses stability by flutter (single degree-of-freedom flutter, otherwise known as a Hopf bifurcation) and possibly by divergence if gravity is operative and if the fluid is sufficiently heavy. The flutter motion of continuously flexible, rather than articulated cantilevered pipes was later verified by Gregory and Païdoussis (1966a,b) theoretically and experimentally. Païdoussis (1970) subsequently found that vertical, continuous flexible pipes are never subject to divergence.

Thin-walled pipes (or cylindrical shells) conveying incompressible fluid flow are subject to both shell- and beam-mode instabilities at sufficiently high flow velocities, as found by Païdoussis and Denise (1970, 1971, 1972) both theoretically and experimentally: shells with both ends clamped lose stability by divergence, while cantilevered ones do so by flutter. In those studies, the motions of the pipe were described by Flügge's thin-shell equations and the fluid forces were obtained by potential flow theory; reasonably good agreement was obtained between analytical results and experiments. Similar predictions were also reported for the case of pinned-pinned shells by Weaver and Unny (1973). The problem was later re-examined by Shayo and Ellen (1974), who derived asymptotic expressions for the generalized pressures, thus avoiding considerable numerical computation required in previous methods of solution, and showed the relationship between travelling wave and standing wave instabilities for shells of large length-to-radius ratio. The problem was further studied by Pham and Misra (1981) with special attention given to the effect of a superimposed linearly varying or constant axial loading on the shell.

It should be specially mentioned that Shayo and Ellen (1978) studied the importance of the behaviour of the fluid beyond the free end of the shell on the dynamics of cantilevered shells conveying fluid, an aspect not considered in earlier analyses because

of the utilization of different methods of solution (e.g., Païdoussis and Denise 1972), by introducing the so-called *downstream flow models* to describe fluid behaviour in that region, in conjunction with the Fourier-transform technique.

Horáček and Zolotarev (1984) investigated the effects of different symmetric and nonsymmetric boundary conditions upon thin-walled pipes conveying inviscid fluid flow. They suggested that, for a *clamped-pinned* system, if the fluid in the shell flows from the clamped to the pinned end or, for a *free-clamped* system, from the free to the clamped end, the system loses stability for any arbitrarily small internal flow velocity (in the absence of any structural damping). They pointed out that this phenomenon does not correspond sufficiently to physical reality.

1.2 External Axial Flow around Cylindrical Structures

The dynamics and stability of cylinders in external axial flow are closely similar to those of a pipe conveying fluid.

The first theoretical study on unconfined axial flow by Païdoussis (1966a) showed that cylinders with ends supported lose stability by divergence and at higher flow velocities by coupled-mode flutter; similarly, cantilevered cylinders first lose stability by divergence, but then at higher flow velocities by *single*-mode flutter. It is of particular interest that in this case the post-divergence behaviour, whether it is coupled-mode flutter for cylinders supported at both ends or single-mode flutter for cantilevered ones, actually *does* materialize in the experiments (Païdoussis 1966b).

If the flow about the cylinder is confined, by a conduit or by adjacent structures, then the virtual mass of the fluid becomes larger and the instabilities occur at

lower flow velocities (Païdoussis 1973), but the fundamental nature of the stability behaviour is not altered. A more sophisticated analysis of the problem was conducted by Païdoussis and Ostoja-Starzewski (1981), on the effect of slenderness of the cylinder and compressibility of the fluid, but once again the fundamentals of the stability behaviour are the same. Interestingly, compressibility was found to have only a minor effect on the stability of the system—at least, for the range of system parameters investigated.

Chen (1975) was the first to examine the dynamics of arrays of parallel cylinders in dense fluid, bringing to light the important fluid-dynamic coupling in their motions, especially when the cylinders are closely spaced relatively to one another. Because of this coupling, and because the diagonal terms in the virtual mass matrix are much larger than for a solitary cylinder, the instabilities occur at much lower flow velocities than for either a solitary flexible cylinder or a flexible cylinder surrounded by rigid ones. This was studied further, and more completely, in the case of cylinder clusters within a flow-containing pipe (confined flow) by Païdoussis and Suss (1977). Both invisid and viscous hydrodynamic coupling in motions of the cylinders was treated; in addition, the confinement of the fluid, due to the small spacing among cylinders as well as between the channel wall and the adjacent cylinders, was taken into account completely. It was found that the theoretical model and experiment agree qualitatively in most essential features of the dynamical behaviour of the system, and quantitative agreement for the critical flow velocities was found to be remarkably good (Païdoussis 1979; Païdoussis, Curling and Gagnon 1982).

The stability of tubular cylindrical and conical beams simultaneously subjected to both internal and external axial flow was examined theoretically and experimentally by Hannoyer and Païdoussis (1978, 1979a,b).

All of the foregoing refer to flow-induced instabilities of cylindrical bodies of sufficient wall-thickness, if hollow at all, that they may be treated as beams.

1.3 Annular Flow in Coaxial Cylindrical Structures

It should be mentioned that annular-flow-induced instabilities are sometimes referred to as leakage-flow-induced oscillations, or instabilities, which reflects the fact that in most cases of practical concern, the annular flow passage is quite narrow. Some of the practical situations where annular-flow-induced instabilities have occurred are: control rods in guide tubes, fuel strings in coolant channels, and feedwater spargers, in various types of nuclear reactors; and certain types of jet pumps, pistons, and valves.

Some work on the stability of flexible cylinders in axisymmetrically confined flow was undertaken by Païdoussis and Pettigrew (1979), and Païdoussis and Ostoja-Starzewski (1981). The mathematical models developed therein are in principle applicable to any degree of confinement; however, the viscous effects in very narrow passages cannot reliably be adapted from those formulated for less confined flows, casting some doubt on the validity of that aspect of the model.

Hobson (1982) considered a rigid cylindrical body, hinged at one point and coaxially positioned in a flow-carrying duct, generally of nonuniform cross-sectional area; he showed that, at sufficiently high flow velocities of the annular fluid, oscillatory instability ensued, via a negative-damping mechanism. Moreover, the model was capable of dealing, in an approximate manner and some degree of empiricism, with situations of sudden constriction or enlargement in the flow passage.

A more rigorous, purely analytical model was formulated by Mateescu and Païdoussis (1985), once again for a rigid body (the *center-body*) hinged at one point and coaxially positioned in a flow-carrying conduit. It was found that there is a critical location of the hinge: if the hinge is situated downstream of that location, then the system may lose stability at sufficiently high flow velocity; the necessary flow velocity becoming progressively smaller as the hinge is moved farther downstream. The fluid-dynamic forces become larger as the annular passage becomes narrower, destabilizing the system. The rigid body model was extended to take into account, in an approximate manner, viscous effects (Mateescu and Païdoussis 1988). One of the principal findings of this work is that viscous effects stabilize the system, becoming more important as the annulus becomes narrower, which is reasonable on physical grounds. Recently, the theory has been further extended to deal with turbulent annular flow (Mateescu, Païdoussis and Bélanger 1991b).

The first studies on stability of coaxial shells with annular flow were independently conducted by Weppelink (1979) and Païdoussis, Chan and Misra (1984). The latter study considered shells conveying incompressible or compressible inviscid fluid in the annulus and in the inner shell. For the clamped-clamped system considered, it was found that stability was lost, at sufficient high flow, by divergence, followed by either divergence in another mode or by coupled-mode flutter. It was also found that, for annular flow, the critical flow velocity is lowered as the annulus is made narrower. If both shells are flexible, the instability threshold is lower than if the outer shell is rigid, the system losing stability first in the antisymmetric modes. The effect of compressibility on the dynamics of the system is rather small. The analytical model was subsequently extended to take into account the steady viscous effects due to surface traction and pressurization (to overcome frictional pressure drop) by

Païdoussis, Misra and Chan (1985). It was found that pressurization in the flow within the inner shell tends to stabilize the system, as is physically reasonable. In contrast, pressurization in the annular flow is destabilizing, if the outer shell is rigid. On the other hand, pressurization in the annular flow when both shells are flexible could either stabilize or destabilize the system, depending on the system parameters; this becomes clear when it is realized that in this case the effect on the inner shell is destabilizing, whereas it is stabilizing on the outer shell, and that motions of the two are coupled.

El Chebair, Misra and Païdoussis (1990) attempted to account for the unsteady, time-dependent viscous forces in an approximate way by adapting the work originally developed for quiescent fluids by Yeh and Chen (1977) to flowing fluids. This attempt was only partially successful, having run into difficulties when the no-slip boundary condition was rigorously applied at the shell surface in the method of solution. Although the Navier-Stokes equations were used for the calculation of the unsteady viscous forces exerted on the shells, they were in fact never solved. In any event, for shells with both ends supported, unsteady viscous forces were found to have only a slight influence on the dynamics of the system. At the same time, the first experimental study of annular-flow-induced instabilities of clamped-clamped coaxial shells was undertaken (El Chebair, Païdoussis and Misra 1989), which verified the dynamical behaviour of the system, qualitatively very well indeed, but quantitatively only within the usual margin of uncertainty associated with the effect of shell imperfections.

Recently, two new analytical models for study of the stability of clamped-free coaxial cylindrical shells subjected to internal and annular incompressible viscous flow were presented by Païdoussis, Nguyen and Misra (1991), and Nguyen (1992). In the first model, Flügge's shell equations were used to describe the shell motions; in

solving the governing equations of motion, the complexity of the free-end boundary conditions of the shells was dealt with by the *extended* form of the Galerkin method. It was found that, for internal flow, with the system parameters taken for the analysis, loss of stability is not always by flutter; for some large circumferential wave numbers, divergence occurs first, followed by single- or coupled-mode flutter. In the case of annular flow, the system may lose stability either by flutter directly, or by divergence, followed by flutter at a higher flow. In the second model, much attention was given to the unsteady viscous effects of the *annular flow* on the stability of the system with narrow annular gaps. Such effects, which had been neglected in previous studies, were evaluated in a formal manner for the first time. It was found that, for sufficiently small widths of the annular gap, the unsteady viscous effects of the annular flow destabilize the system, and they become diminished as the gap is reduced. Both new theories agreed quite well with the experimental results.

1.4 Objectives and Thesis Organization

The primary objective of this thesis is to develop an analytical model for predicting instabilities of pinned-clamped and clamped-pinned coaxial cylindrical shells subjected to flowing incompressible viscous fluid in the annular region between the two shells and/or within the inner shell, and to compare the results with those obtained for clamped-clamped and cantilevered systems. Another objective is to verify the conclusion by Horáček and Zolotarev (1984) who suggested that clamped-pinned and free-clamped systems lose stability for any arbitrarily small flow velocity.

The analytical model takes into consideration the main effects of fluid viscosity, namely, the steady (time-independent) viscous loads on the shells. The unsteady fluid

forces are calculated approximately by neglecting unsteady viscous effects and using potential flow theory, the solution of which is then obtained by means of the Fourier transform technique.

This thesis consists of five chapters. Chapter 1 has given a brief review of previous studies closely related to the research work of the thesis. It has also stated the objectives undertaken by the thesis, and now presents the outline of the thesis.

In Chapter 2, the development of the analytical model for predicting instabilities of pinned-clamped and/or clamped-pinned coaxial cylindrical shells conveying internal and/or annular flows is given in detail. Presented are (a) the formulation of the problem with Flügge's modified shell equations and potential flow theory, (b) the solution of the fluid-dynamic forces acting on the shells by means of the Fourier-transform generalized-force approach, (c) the solution of the governing equations of motion with the Galerkin method.

Chapter 3 has presented the results of calculations conducted to verify some important aspects of the present theory. Thus, (a) the natural frequencies of a cylindrical shell *in vacuo* were calculated to assess how well the Galerkin solution works; (b) to check the computer program under the condition of the fluid being conveyed is inviscid, comparison was made between the results of the present theory and those of beam theory.

Chapter 4 is focused on calculations and analytical results. Both systems of pinned-clamped and clamped-pinned shells are considered. Calculations are conducted for (a) internal flow only, (b) annular flow only, and for the effects on stability of (c) gap width, (d) shell length, (e) shell-wall thickness.

Finally, Chapter 5 wraps up the thesis with a summary of the important findings of the thesis, conclusions regarding the contributions of the thesis, and recommendations

for future work.

Chapter 2

An Analytical Model

2.1 Introduction

The main purpose of this chapter is to develop an analytical model to investigate the dynamics and stability of either pinned-clamped or clamped-pinned coaxial cylindrical shells conveying internal and/or annular incompressible flowing fluid. In this study, the physical system is replaced by a pre-stressed flexible shell subjected to inviscid flow. The key assumption here is that the forces pre-stressing the shells are the same as those resulting from flow pressurization and traction effects on the shells surfaces in the original system. The unsteady fluid forces will be formulated with potential-flow theory. Thus, although steady viscous effects are taken into account, unsteady viscous effects are not.

The following theory is presented for the general system in which both shells are flexible. Certain important aspects of the theory will be verified by solving a set of problems that have been studied before and comparing the results with the existing ones. For practical reasons, the theory will then be used to study a simple case with the outer shell replaced by a rigid cylindrical tube whereas the inner one remains

flexible. This simplified system, nevertheless, still retains most of the important dynamical characteristics of the general one.

2.2 Formulation of the Analytical Model

2.2.1 System Definitions and Assumptions

The system under consideration is shown in Figure 2.1. It consists of two coaxial cylindrical shells of length L. In the case of the pinned-clamped system, the shells are assumed to be pinned at the upstream end ($x = 0$) and clamped at the downstream end ($x = L$) onto semi-infinite rigid cylinders of same radii and wall thicknesses as the two shells; in the clamped-pinned case the situation is reversed. The inner and outer shells have mean radii a and b, and wall thicknesses h_i and h_o, respectively, such that h_i/a, $h_o/b \ll 1$. The shells are assumed to be elastic and isotropic with Young's moduli E_i and E_o, densities ρ_{si} and ρ_{so} and Poisson's ratios ν_i and ν_o; in all cases subscripts i and o being associated with the inner and outer shell, respectively. Incompressible fluid is generally flowing both inside the inner shell and in the annulus, with densities ρ_i and ρ_o , and flow velocities U_i and U_o, respectively.

Shell motions are assumed to be sufficiently small, so that linear shell theory may be employed. As already mentioned, these perturbations will be formulated using potential-flow theory. Nevertheless, the flows are considered to be viscous, in the steady sense, and hence pressurization, necessary to overcome pressure drop, and traction effects on shells are indeed taken into consideration. Finally, in the case of the pinned-clamped system, the perturbations are assumed to vanish immediately upstream and downstream of the flexible shells, whilst in the clamped-pinned case the perturbations are assumed to vanish upstream and far downstream of the flexible

shell.

2.2.2 Governing Equations of Motion

In its most general form, in the present theory both cylinders are considered to be flexible thin shells. Shell motions are described by Flügge's (1960) shell equations, as modified by Païdoussis, Misra and Chan (1985) to take into account the stress resultants due to steady viscous effects.

With inner-shell and outer-shell quantities characterized by subscripts i and o, respectively, the equations of motion for the two shells are given by

$$L_{1i}(u_i,v_i,w_i) = u_i'' + \frac{1}{2}(1-\nu_i)u_i^{\bullet\bullet} + \frac{1}{2}(1+\nu_i)v_i'^{\bullet} + \nu_i w_i' + k_i\{\frac{1}{2}(1-\nu_i)u_i^{\bullet\bullet} - w_i''' + \frac{1}{2}(1-\nu_i)w_i'^{\bullet\bullet}\} + [q_{1i}u_i'' + q_{2i}(v_i^{\bullet} + w_i) + q_{3i}(u_i^{\bullet\bullet} - w_i')] - \gamma_i\{\frac{\partial^2 u_i}{\partial t^2}\} = 0, \quad (2.1)$$

$$L_{2i}(u_i,v_i,w_i) = \frac{1}{2}(1+\nu_i)u_i'^{\bullet} + v_i^{\bullet\bullet} + \frac{1}{2}(1-\nu_i)v_i'' + w_i^{\bullet} + k_i\{\frac{3}{2}(1-\nu_i)v_i'' - \frac{1}{2}(3-\nu_i)w_i'^{\bullet\bullet}\} + [q_{1i}v_i'' + q_{3i}(v_i^{\bullet\bullet} + w_i^{\bullet})] - \gamma_i\{\frac{\partial^2 v_i}{\partial t^2}\} = 0, \quad (2.2)$$

$$L_{3i}(u_i,v_i,w_i) = \nu_i u_i' + v_i^{\bullet} + w_i + k_i\{\frac{1}{2}(1-\nu_i)u_i'^{\bullet\bullet} - u_i''' - \frac{1}{2}(3-\nu_i)v_i'^{\bullet\bullet} + \nabla_i^4 w_i + 2w_i^{\bullet\bullet} + w_i\} - [q_{1i}w_i'' + q_{3i}(u_i' - v_i^{\bullet} + w_i^{\bullet\bullet})] + \gamma_i\{\frac{\partial^2 w_i}{\partial t^2} - \frac{q_i}{\rho_{si}h_i}\} = 0, \quad (2.3)$$

$$L_{1o}(u_o,v_o,w_o) = u_o'' + \frac{1}{2}(1-\nu_o)u_i^{\bullet\bullet} + \frac{1}{2}(1+\nu_o)v_o'^{\bullet} + \nu_o w_o' + k_o\{\frac{1}{2}(1-\nu_o)u_o^{\bullet\bullet} - w_o''' + \frac{1}{2}(1-\nu_o)w_o'^{\bullet\bullet}\} + [q_{1o}u_o'' + q_{2o}(v_o^{\bullet} + w_o) + q_{3o}(u_o^{\bullet\bullet} - w_o')] - \gamma_o\{\frac{\partial^2 u_o}{\partial t^2}\} = 0, \quad (2.4)$$

$$L_{2o}(u_o,v_o,w_o) = \frac{1}{2}(1+\nu_o)u_o'^{\bullet} + v_o^{\bullet\bullet} + \frac{1}{2}(1-\nu_o)v_o'' + w_o^{\bullet} + k_o\{\frac{3}{2}(1-\nu_o)v_o'' - \frac{1}{2}(3-\nu_o)w_o'^{\bullet\bullet}\} + [q_{1o}v_o'' + q_{3o}(v_o^{\bullet\bullet} + w_o^{\bullet})] - \gamma_o\{\frac{\partial^2 v_o}{\partial t^2}\} = 0, \quad (2.5)$$

$$L_{3o}(u_o,v_o,w_o) = \nu_o u_o' + v_o^{\bullet} + w_o + k_o\{\frac{1}{2}(1-\nu_o)u_o'^{\bullet\bullet} - u_o''' - \frac{1}{2}(3-\nu_o)v_o'^{\bullet\bullet} + \nabla_o^4 w_o + 2w_o^{\bullet\bullet} + w_o\} - [q_{1o}w_o'' + q_{3o}(u_o' - v_o^{\bullet} + w_o^{\bullet\bullet})] + \gamma_o\{\frac{\partial^2 w_o}{\partial t^2} - \frac{q_o}{\rho_{so}h_o}\} = 0, \quad (2.6)$$

where

$$(\,)^{\bullet} = \frac{\partial(\,)}{\partial\theta},\ (\,)' = a\frac{\partial(\,)}{\partial x},\ (\,)'' = b\frac{\partial(\,)}{\partial x},\ k_i = \frac{1}{12}(\frac{h_i}{a})^2,\ k_o = \frac{1}{12}(\frac{h_o}{b})^2,$$

$$\gamma_i = \frac{\rho_{si} a^2 (1-\nu_i^2)}{E_i},\ \gamma_o = \frac{\rho_{so} b^2 (1-\nu_o^2)}{E_o},\ \nabla_i^2 = a^2 \frac{\partial^2}{\partial x^2} + \frac{\partial^2}{\partial \theta^2},\ \nabla_o^2 = b^2 \frac{\partial^2}{\partial x^2} + \frac{\partial^2}{\partial \theta^2};$$

$u(x,\theta,t), v(x,\theta,t)$ and $w(x,\theta,t)$ are the axial, circumferential and radial displacements of the middle surface of the undeformed shell; q_1, q_2 and q_3 denote the nondimensional forces associated with steady viscous effects (Section 2.3.3); $q_i = (p_i - p_o)|_{r=a}$ and $q_o = (p_o - p_e)|_{r=b}$, with p_i, p_o and p_e being the perturbation pressures in the inner fluid, the annular fluid and the fluid surrounding the outer shell, respectively. Thus, q_i and q_o represent the unsteady radial forces acting on the shells per unit area (Section 2.3.2.3).

Shell motions must satisfy the following boundary conditions:(i) at the clamped end, u, v, w and $\partial w/\partial x$ are all equal to zero; (ii) at the pinned end, $v = w = 0$ and since the flexible shell can slide along the rigid cylinder, the normal force N_x and the bending moment M_x must vanish. Thus , in terms of shell displacements, these boundary conditions are equivalent to

(i) at a clamped end,

$$u_i = v_i = w_i = 0, \qquad \frac{\partial w_i}{\partial x} = 0; \tag{2.7}$$

$$u_o = v_o = w_o = 0, \qquad \frac{\partial w_o}{\partial x} = 0; \tag{2.8}$$

(ii) at a pinned end,

$$v_i = w_i = 0, \tag{2.9}$$

$$u_i' + \nu_i \dot{v}_i + \nu_i w_i - k_i w_i'' = 0, \tag{2.10}$$

$$w_i'' + \nu_i \ddot{w}_i - \nu_i \dot{v}_i - u_i' = 0, \tag{2.11}$$

$$v_o = w_o = 0, \tag{2.12}$$

$$u_o' + \nu_o \dot{v}_o + \nu_o w_o - k_o w_o''' = 0, \tag{2.13}$$

$$w_o''' + \nu_o \ddot{w}_o - \nu_o \dot{v}_o - u_o' = 0. \tag{2.14}$$

2.2.3 Perturbation Pressures

As mentioned in the last section, the unsteady fluid forces (q_i and q_o) in the governing equations of motion are simply the differences between the perturbation pressures on the two sides of the shell. Thus, the determination of these forces reduces to that of the perturbation pressures. Since the analysis here applies equally to internal and annular flows, the subscripts i and o will be suppressed, until required for clarity.

The perturbation pressures will be formulated by means of potential flow theory[1]. Thus, for this purpose, the flow is considered to be inviscid and irrotational and also isentropic. Hence, the velocity $\mathbf{V}$ may be expressed in terms of a velocity potential $\Psi(x,\theta,r,t)$, such that

$$\mathbf{V} = \nabla\Psi. \tag{2.15}$$

Moreover, Ψ is considered to consist of a steady component due to the mean, undisturbed flow velocity U in the x-direction and an unsteady component ϕ associated with perturbations due to shell motions; in other words,

$$\Psi = Ux + \phi. \tag{2.16}$$

Hence, from equation (2.15), the velocity components of the perturbed flow field may be expressed as

$$V_x = U + \frac{\partial\phi}{\partial x}, \quad V_\theta = \frac{1}{r}\frac{\partial\phi}{\partial\theta}, \quad V_r = \frac{\partial\phi}{\partial r}. \tag{2.17}$$

With the substitution of equation (2.16) into (2.15) and then into the continuity equation for an incompressible flow, $\nabla\cdot\mathbf{V} = 0$, ϕ is found to be governed by the Laplace equation,

$$\frac{\partial^2\phi}{\partial r^2} + \frac{1}{r}\frac{\partial\phi}{\partial r} + \frac{1}{r^2}\frac{\partial^2\phi}{\partial\theta^2} + \frac{\partial^2\phi}{\partial x^2} = 0, \tag{2.18}$$

[1]This is clearly an approximation. Nevertheless, as mentioned in the foregoing, certain aspects of the viscous nature of the fluid flow *are* taken into account (Section 2.3.3)

which is subject to the impermeability boundary conditions on the shell surface(s), requiring that

$$V_r = \left.\frac{\partial \phi}{\partial r}\right|_{ss} = \frac{\partial w}{\partial t} + U\frac{\partial w}{\partial x}. \tag{2.19}$$

Thus, for the annular flow, equations (2.18) and (2.19) take the form

$$\frac{\partial^2 \phi_o}{\partial r^2} + \frac{1}{r}\frac{\partial \phi_o}{\partial r} + \frac{1}{r^2}\frac{\partial^2 \phi_o}{\partial \theta^2} + \frac{\partial^2 \phi_o}{\partial x^2} = 0; \tag{2.20}$$

$$\left.\frac{\partial \phi_o}{\partial r}\right|_{r=a} = \begin{cases} \dfrac{\partial w_i}{\partial t} + U_o\dfrac{\partial w_i}{\partial x} & \text{for } 0 \le x \le L, \\ 0 & \text{for } x < 0 \text{ and } x \gg L; \end{cases} \tag{2.21}$$

$$\left.\frac{\partial \phi_o}{\partial r}\right|_{r=b} = \begin{cases} \dfrac{\partial w_o}{\partial t} + U_o\dfrac{\partial w_o}{\partial x} & \text{for } 0 \le x \le L, \\ 0 & \text{for } x < 0 \text{ and } x \gg L. \end{cases} \tag{2.22}$$

A similar set of equations also applies to the internal flow,

$$\frac{\partial^2 \phi_i}{\partial r^2} + \frac{1}{r}\frac{\partial \phi_i}{\partial r} + \frac{1}{r^2}\frac{\partial^2 \phi_i}{\partial \theta^2} + \frac{\partial^2 \phi_i}{\partial x^2} = 0; \tag{2.23}$$

$$\left.\frac{\partial \phi_i}{\partial r}\right|_{r=a} = \begin{cases} \dfrac{\partial w_i}{\partial t} + U_i\dfrac{\partial w_i}{\partial x} & \text{for } 0 \le x \le L, \\ 0 & \text{for } x < 0 \text{ and } x \gg L. \end{cases} \tag{2.24}$$

Here, a note should be given, concerning the boundary conditions (2.21), (2.22) and (2.24). Since ϕ_i and ϕ_o are both shell-motion-induced, it is reasonable to assume that $\phi_i = \phi_o = 0$ for $x < 0$; i.e., flows entering the system are undisturbed. On the other hand, for the pinned-clamped system it can be assumed that $\phi_i = \phi_o = 0$ for $x > L$. But for the clamped-pinned system, since the downstream end of the shell has a varying slope, it is *unrealistic* to assume that $\phi_i = \phi_o = 0$ for $x = L + \Delta L$, where $\Delta L \to 0$. However, ϕ_i and ϕ_o should vanish when ΔL is sufficiently large; this matter is discussed in detail in Appendix C.

Once ϕ has been determined, the perturbed pressure may be evaluated from Bernoulli's equation for unsteady flow,

$$\frac{\partial \Psi}{\partial t} + \frac{1}{2}V^2 + \frac{P}{\rho} = \frac{P_s}{\rho}, \tag{2.25}$$

where $V^2 = V_x^2 + V_\theta^2 + V_r^2$, P_s is the stagnation pressure, and P is the pressure in the perturbed flow field. Expressing the pressure in terms of its mean, undisturbed value $\bar{P}$ and its perturbation counterpart p, such that $P = \bar{P} + p$, and substituting (2.16) and (2.17) into equation (2.25) gives

$$\left\{\frac{1}{2}U^2 + \frac{\bar{P}}{\rho} - \frac{P_s}{\rho}\right\} + \left\{\frac{\partial\phi}{\partial t} + U\frac{\partial\phi}{\partial x} + \frac{p}{\rho}\right\} + \frac{1}{2}\left\{(\frac{\partial\phi}{\partial r})^2 + (\frac{1}{r}\frac{\partial\phi}{\partial\theta})^2 + (\frac{\partial\phi}{\partial x})^2\right\} = 0 \quad (2.26)$$

In this equation, the first term is time-independent, while the second and third ones are time-dependent. Equation (2.26) therefore implies that its first two terms must individually vanish, giving

$$\bar{P} = P_s - \frac{1}{2}\rho U^2, \quad (2.27)$$

$$p = -\rho\left\{\frac{\partial\phi}{\partial t} + U\frac{\partial\phi}{\partial x}\right\}, \quad (2.28)$$

for which it has been assumed that all second-order perturbations, grouped in the third term of equation (2.26), are negligibly small—by considering motions of the shell to be small. It is seen that p is readily given by (2.28) once ϕ has been determined from equations (2.20)-(2.22) for the annular flow, or from equations (2.23) and (2.24) for the internal flow.

2.3 Method of Solution

2.3.1 Introduction

In Section 2.2 two different sets of equations were presented, which are integral parts of the theory and must be solved sequentially.

The first set of equations, known as the Laplace equations, needs to be solved in order to determine the unsteady fluid-dynamic forces exerted on the shells. The method

to be used for the solution for these equations is the Fourier-Transform Generalized-Force technique (Section 2.3.2), also employed by Païdoussis *et al.* (1984, 1985). Such forces, once calculated, are substituted into Flügge's modified shell equations, which are then solved with Galerkin's method (Section 2.3.4). With regard to the second set of equations, all steady viscosity-related forces on the shells have been evaluated and given by Païdoussis, Misra and Chan (1985); since the same procedure will be followed here, only the final results will be presented without details of the derivation (Section 2.3.3).

For the purpose of satisfying equations (2.1)-(2.6), the solution for the shell displacements is expressed in the following functional forms:

$$\left\{ \begin{array}{c} u_i \\ v_i \\ w_i \end{array} \right\} = \sum_{n=1}^{\infty} \sum_{m=1}^{\infty} \left\{ \begin{array}{c} A_m \cos n\theta (a\partial/\partial x) \\ B_m \sin n\theta \\ C_m \cos n\theta \end{array} \right\} \Phi_m(x) e^{i\Omega t}, \tag{2.29}$$

$$\left\{ \begin{array}{c} u_o \\ v_o \\ w_o \end{array} \right\} = \sum_{n=1}^{\infty} \sum_{m=1}^{\infty} \left\{ \begin{array}{c} D_m \cos n\theta (b\partial/\partial x) \\ E_m \sin n\theta \\ F_m \cos n\theta \end{array} \right\} \Phi_m(x) e^{i\Omega t}, \tag{2.30}$$

where m and n are the axial and circumferential wave number, respectively; A_m, ..., F_m are constants to be determined; $\Phi_m(x)$ are appropriate eigenfunctions for the x-variations of shell displacements, here taken to be the eigenfunctions of a clamped-pinned or a pinned-clamped beam, and Ω is the angular frequency of oscillation.

The solutions to the perturbation velocity potentials and pressures are taken to be of the form

$$\left\{ \begin{array}{c} \phi_i \\ p_i \end{array} \right\} = \sum_{n=1}^{\infty} \left\{ \begin{array}{c} \bar{\phi}_i(x,r) \\ \bar{p}_i(x,r) \end{array} \right\} \cos n\theta \, e^{i\Omega t}, \left\{ \begin{array}{c} \phi_o \\ p_o \end{array} \right\} = \sum_{n=1}^{\infty} \left\{ \begin{array}{c} \bar{\phi}_o(x,r) \\ \bar{p}_o(x,r) \end{array} \right\} \cos n\theta \, e^{i\Omega t}. \tag{2.31}$$

The determination of $\bar{\phi}_i$, $\bar{\phi}_o$, $\bar{p}_i$ and $\bar{p}_o$ is the subject of the analysis of the next

section.

2.3.2 Solution for the Perturbation Pressures

2.3.2.1 Annular Flow

Substituting ϕ_o from equation (2.31) into (2.20) and taking the Fourier transform of the resulting equation gives

$$\sum_{n=1}^{\infty}\left\{\frac{\partial^2\bar{\phi}_o^*}{\partial r^2}+\frac{1}{r}\frac{\partial\bar{\phi}_o^*}{\partial r}-\left(\alpha^2+\frac{n^2}{r^2}\right)\bar{\phi}_o^*\right\}\cos n\theta=0, \tag{2.32}$$

where $\bar{\phi}_o^*$ denotes the Fourier transform of $\bar{\phi}_o$, defined by

$$\bar{\phi}_o^*(\alpha,r)=\int_{-\infty}^{\infty}\bar{\phi}_o(x,r)e^{i\alpha x}dx, \tag{2.33}$$

and $e^{i\Omega t}\neq 0$ (in fact,$|e^{i\Omega t}|=1$) has been taken into consideration.

It is noted that the right-hand side of equation (2.32) is zero whereas the left-hand side is an infinite series of $\cos n\theta$. Since $\cos n\theta$, $n=1,2,\ldots,\infty$ form an orthonormal set, the coefficient of $\cos n\theta$ for any given n must equal zero, or

$$\frac{\partial^2\bar{\phi}_o^*}{\partial r^2}+\frac{1}{r}\frac{\partial\bar{\phi}_o^*}{\partial r}-\left(\alpha^2+\frac{n^2}{r^2}\right)\bar{\phi}_o^*=0. \tag{2.34}$$

Equation (2.34) is known as Bessel's modified equation, admitting solutions of the general form

$$\bar{\phi}_o^*(\alpha,r)=C_{1o}I_n(\alpha r)+C_{2o}K_n(\alpha r), \tag{2.35}$$

where $I_n(\alpha r)$ and $K_n(\alpha r)$ are the nth-order modified Bessel functions of the first and second kinds, respectively, and C_{1o} and C_{2o} are constants of integration to be determined from the boundary conditions at the shell surfaces, namely equations (2.21) and (2.22).

The procedure to evaluate C_{1o} and C_{2o} is as follows. Equations (2.29)-(2.31) are appropriately substituted into equations (2.21) and (2.22), then the Fourier transforms of the resultant equations are taken, and finally $\bar{\phi}_o^*$ is replaced by its functional form in (2.35). Thus, boundary conditions (2.21) and (2.22) are effectively equivalent to

$$\sum_{n=1}^{\infty} \{[\alpha I_n'(\alpha a)]\, C_{1o} + [\alpha K_n'(\alpha a)]\, C_{2o}\} \cos n\theta =$$

$$\sum_{n=1}^{\infty} \left\{ i(\Omega - U_o\alpha) \sum_{m=1}^{\infty} C_m [\Phi_m^*(\alpha) + R_m^*(\alpha)] \right\} \cos n\theta, \tag{2.36}$$

$$\sum_{n=1}^{\infty} \{[\alpha I_n'(\alpha b)]\, C_{1o} + [\alpha K_n'(\alpha b)]\, C_{2o}\} \cos n\theta =$$

$$\sum_{n=1}^{\infty} \left\{ i(\Omega - U_o\alpha) \sum_{m=1}^{\infty} F_m [\Phi_m^*(\alpha) + R_m^*(\alpha)] \right\} \cos n\theta. \tag{2.37}$$

Before C_{1o} and C_{2o} are obtained from equation (2.36) and (2.37), it is important to discuss the reasons for introducing into these equations the new function $R_m^*(\alpha)$, which is the Fourier transform of $R_m(x)$ (refer to Appendix C).

As previously touched upon, the method of solution being employed is the Fourier transform method (see, for example, Bracewell 1974), implicit in which is the specification of $\bar{\phi}(x,r)$, $\partial\bar{\phi}/\partial x$, and $\bar{p}(x,r)$ at $\pm\infty$, whereas the variations of these quantities are dependent on x through the beam-eigenfunction expansions, which are specified only within the interval $[0, L]$. Furthermore, on physical grounds, although it may reasonably be argued that perturbations in flow and pressure are nearly zero for $x < 0$ (and hence at $x = -\infty$), the same would be quite unreasonable if applied for $x > L$ in the case of the clamped-pinned system; perturbations should die out in a finite length beyond the pinned end of shells and do so as smoothly as in reality. Hence, the need

arises, both mathematically and physically, of specifying how $\bar{\phi}$ and $\bar{p}$ decay beyond $x = L$—since decay they must, on physical grounds, by dissipation and diffusion. The functional form of the decay of perturbations is given by $R_m(x)$, which may be visualized as an *extension* of the beam eigenfunctions $\Phi_m(x)$, $0 \leq x \leq L$. For the pinned-clamped system, however, it is just assumed that $R_m(x) \equiv 0$.

The functional form of $R_m(x)$ constitutes what has been termed an *out-flow* model; such models were first proposed by Shayo and Ellen (1978) and later elaborated further by Païdoussis, Luu and Laithier (1986). Since such models cause some difficulties because of numerical non-convergence, a more proper model was suggested by Païdoussis, Nguyen and Misra (1991). The detailed description of such a model and its corresponding functional form of $R_m(x)$ may be found in Appendix C.

Equating the coefficients of $\cos n\theta$ on the two sides of (2.36) and of (2.37) leads to

$$[\alpha I_n'(\alpha a)]\, C_{1o} + [\alpha K_n'(\alpha a)]\, C_{2o} = i(\Omega - U_o\alpha) \sum_{m=1}^{\infty} C_m[\Phi_m^*(\alpha) + R_m^*(\alpha)], \qquad (2.38)$$

$$[\alpha I_n'(\alpha b)]\, C_{1o} + [\alpha K_n'(\alpha b)]\, C_{2o} = i(\Omega - U_o\alpha) \sum_{m=1}^{\infty} F_m[\Phi_m^*(\alpha) + R_m^*(\alpha)], \qquad (2.39)$$

from which C_{1o} and C_{2o} are found to be

$$C_{1o} = \frac{i(\Omega - U_o\alpha)}{\alpha} \sum_{m=1}^{\infty} \left\{ \frac{-K_n'(\alpha b)C_m + K_n'(\alpha a)F_m}{I_n'(\alpha b)K_n'(\alpha a) - I_n'(\alpha a)K_n'(\alpha b)} \right\} [\Phi_m^*(\alpha) + R_m^*(\alpha)], \qquad (2.40)$$

$$C_{2o} = \frac{i(\Omega - U_o\alpha)}{\alpha} \sum_{m=1}^{\infty} \left\{ \frac{I_n'(\alpha b)C_m - I_n'(\alpha a)F_m}{I_n'(\alpha b)K_n'(\alpha a) - I_n'(\alpha a)K_n'(\alpha b)} \right\} [\Phi_m^*(\alpha) + R_m^*(\alpha)]. \qquad (2.41)$$

As a result of (2.40) and (2.41), equation (2.35) may be rewritten as

$$\bar{\phi}_o^*(\alpha, r) = \frac{i(\Omega - U_o\alpha)}{\alpha} \sum_{m=1}^{\infty} \{[W_{1n}(\alpha, r)C_m + W_{2n}(\alpha, r)F_m][\Phi_m^*(\alpha) + R_m^*(\alpha)]\}, \qquad (2.42)$$

where

$$W_{1n}(\alpha, r) = \frac{I_n'(\alpha b)K_n(\alpha r) - I_n(\alpha r)K_n'(\alpha b)}{I_n'(\alpha b)K_n'(\alpha a) - I_n'(\alpha a)K_n'(\alpha b)}, \qquad (2.43)$$

$$W_{2n}(\alpha, r) = \frac{I_n(\alpha r)K_n'(\alpha a) - I_n'(\alpha a)K_n(\alpha r)}{I_n'(\alpha b)K_n'(\alpha a) - I_n'(\alpha a)K_n'(\alpha b)}; \qquad (2.44)$$

in these expressions C_m and F_m have been defined in equations (2.29) and (2.30), respectively; prime denotes differentiation with respect to the argument of Bessel's modified functions. To obtain $\bar{p}_o^*$, equations (2.31) are substituted into (2.28), and then the Fourier transform of the resultant equation is taken with $\phi_o^*(\alpha, r)$ replaced by its value in (2.42) and, finally, the coefficients of $\cos n\theta$ on the two sides of the equation are equated, giving

$$\bar{p}_o^*(\alpha, r) = \frac{\rho_o(\Omega - U_o\alpha)^2}{\alpha} \sum_{m=1}^{\infty} \{[W_{1n}(\alpha, r)C_m + W_{2n}(\alpha, r)F_m][\Phi_m^*(\alpha) + R_m^*(\alpha)]\}. \quad (2.45)$$

2.3.2.2 Internal Flow

With the same procedure as was carried out for the annular flow, $\bar{\phi}_i^*(\alpha, r)$ for the internal flow is also found to be governed by a modified Bessel equation, similar to equation (2.34),

$$\frac{\partial^2 \bar{\phi}_i^*}{\partial r^2} + \frac{1}{r}\frac{\partial \bar{\phi}_i^*}{\partial r} - \left(\alpha^2 + \frac{n^2}{r^2}\right)\bar{\phi}_i^* = 0, \quad (2.46)$$

which admits solutions of the form

$$\bar{\phi}_i^*(\alpha, r) = C_{1i} I_n(\alpha r) + C_{2i} K_n(\alpha r). \quad (2.47)$$

Here, it should be recalled that $\lim_{r\to 0} K_n(\alpha r) = \infty$. Hence, for $\bar{\phi}_i^*$ to be finite as r approaches 0, C_{2i} must be set to zero ($C_{2i} = 0$). Meanwhile, C_{1i} is determined from boundary condition (2.24). Substituting (2.29) and (2.31) into (2.24), taking the Fourier transform of the resulting equation and making use of (2.47), and finally equating the coefficients of $\cos n\theta$ on the two sides of the equation yields

$$[\alpha I_n'(\alpha a)]C_{1i} = i(\Omega - U_i\alpha) \sum_{m=1}^{\infty} C_m[\Phi_m^*(\alpha) + R_m^*(\alpha)], \quad (2.48)$$

or equivalently,

$$C_{1i} = \frac{i(\Omega - U_i\alpha)}{\alpha} \sum_{m=1}^{\infty} \frac{C_m}{I_n'(\alpha a)}[\Phi_m^*(\alpha) + R_m^*(\alpha)]. \quad (2.49)$$

With C_{1i} given by (2.49) and $C_{2i} = 0$, equation (2.47) becomes

$$\bar{\phi}_i^*(\alpha, r) = \frac{i(\Omega - U_i\alpha)}{\alpha} \sum_{m=1}^{\infty} \frac{I_n(\alpha r)}{I_n'(\alpha a)} C_m[\Phi_m^*(\alpha) + R_m^*(\alpha)]; \tag{2.50}$$

thus, $\bar{p}_i^*(\alpha, r)$ can now be obtained from (2.28). Proceeding in the same manner as was done for $\bar{p}_o^*(\alpha, r)$ results in

$$\bar{p}_i^*(\alpha, r) = \frac{\rho_i(\Omega - U_i\alpha)^2}{\alpha} \sum_{m=1}^{\infty} \frac{I_n(\alpha r)}{I_n'(\alpha a)} C_m[\Phi_m^*(\alpha) + R_m^*(\alpha)]. \tag{2.51}$$

2.3.2.3 Nondimensionalization and Generalized Forces

As it is more convenient to deal with dimensionless quantities, equations (2.1)-(2.6) will be nondimensionalized prior to being solved. For this purpose, the following reference velocities and forces per unit area are defined:

$$\begin{gathered} \mathcal{U}_i = \left[\frac{E_i}{\rho_{si}(1-\nu_i^2)}\right]^{1/2}, \quad \mathcal{U}_o = \left[\frac{E_o}{\rho_{so}(1-\nu_o^2)}\right]^{1/2}, \\ \bar{q}_i = \frac{\rho_{si} h_i L}{\gamma_i} = \frac{E_i h_i L}{a^2(1-\nu_i^2)}, \quad \bar{q}_o = \frac{\rho_{so} h_o L}{\gamma_o} = \frac{E_o h_o L}{b^2(1-\nu_o^2)}, \end{gathered} \tag{2.52}$$

from which the following dimensionless parameters are introduced:

$$\begin{gathered} \bar{U}_i = \frac{U_i}{\mathcal{U}_i}, \ \bar{U}_o = \frac{U_o}{\mathcal{U}_o}, \ \bar{\Omega}_i = \frac{\Omega a}{\mathcal{U}_i}, \ \bar{\Omega}_o = \frac{\Omega b}{\mathcal{U}_o}, \ \Omega_r = \frac{\bar{\Omega}_i}{\bar{\Omega}_o} = \frac{a\mathcal{U}_o}{b\mathcal{U}_i}, \\ \varepsilon = \frac{r}{L}, \ \varepsilon_i = \frac{a}{L}, \ \varepsilon_o = \frac{b}{L}, \ \bar{\alpha} = \alpha L, \ \xi = \frac{x}{L}, \ \ell = \frac{L'}{L}, \\ \bar{A}_m = \frac{A_m}{L}, \ \bar{B}_m = \frac{B_m}{L}, \ \bar{C}_m = \frac{C_m}{L}, \ \bar{D}_m = \frac{D_m}{L}, \ \bar{E}_m = \frac{E_m}{L}, \ \bar{F}_m = \frac{F_m}{L}. \end{gathered} \tag{2.53}$$

Thus, in terms of (2.52) and (2.53), the perturbation pressures evaluated in (2.45) and (2.51) may be written as

$$\bar{p}_i^*(\bar{\alpha}, \varepsilon) = \frac{\rho_i \mathcal{U}_i^2}{\bar{\alpha}} \left\{\frac{\bar{\Omega}_i}{\varepsilon_i} - \bar{U}_i\bar{\alpha}\right\}^2 \sum_{m=1}^{\infty} \frac{I_n(\bar{\alpha}\varepsilon)}{I_n'(\bar{\alpha}\varepsilon_i)} \bar{C}_m[\Phi_m^*(\bar{\alpha}) + R_m^*(\bar{\alpha})], \tag{2.54}$$

$$\begin{aligned} \bar{p}_o^*(\bar{\alpha}, \varepsilon) = \frac{\rho_o \mathcal{U}_o^2}{\bar{\alpha}} \left\{\frac{\bar{\Omega}_i}{\varepsilon_o \Omega_r} - \bar{U}_o\bar{\alpha}\right\}^2 \sum_{m=1}^{\infty} \left\{W_{1n}(\bar{\alpha}, \varepsilon)\bar{C}_m + W_{2n}(\bar{\alpha}, \varepsilon)\bar{F}_m\right\} \\ \times \{\Phi_m^*(\bar{\alpha}) + R_m^*(\bar{\alpha})\}, \end{aligned} \tag{2.55}$$

where

$$W_{1n}(\bar{\alpha},\varepsilon) = \frac{I_n'(\bar{\alpha}\varepsilon_o)K_n(\bar{\alpha}\varepsilon) - I_n(\bar{\alpha}\varepsilon)K_n'(\bar{\alpha}\varepsilon_o)}{I_n'(\bar{\alpha}\varepsilon_o)K_n'(\bar{\alpha}\varepsilon_i) - I_n'(\bar{\alpha}\varepsilon_i)K_n'(\bar{\alpha}\varepsilon_o)}, \tag{2.56}$$

$$W_{2n}(\bar{\alpha},\varepsilon) = \frac{I_n(\bar{\alpha}\varepsilon)K_n'(\bar{\alpha}\varepsilon_i) - I_n'(\bar{\alpha}\varepsilon_i)K_n(\bar{\alpha}\varepsilon)}{I_n'(\bar{\alpha}\varepsilon_o)K_n'(\bar{\alpha}\varepsilon_i) - I_n'(\bar{\alpha}\varepsilon_i)K_n'(\bar{\alpha}\varepsilon_o)}. \tag{2.57}$$

Finally, the terms q_i and q_o in equations (2.3) and (2.6), respectively, are given by

$$q_i = (p_i - p_o)|_{r=a}\,, \quad q_o = (p_o - p_e)|_{r=b} = p_o|_{r=b}\,, \tag{2.58}$$

where the quiescent fluid surrounding the outer shell has been assumed to have a negligibly small inertial effect on the dynamics of the system (e.g., if the fluid is air), or $p_e = 0$; p_i and p_o are obtainable from (2.54) and (2.55), respectively, after inverse Fourier transformation and utlization of (2.31). The following analysis will be devoted to the evaluation of the generalized forces associated with perturbation pressures in the flows.

For the inner shell, if q_i is taken to have the form

$$q_i(\xi,\theta,t) = \sum_{n=1}^{\infty}\sum_{m=1}^{\infty} Q_{mn}(\xi)\cos n\theta e^{i\Omega t}, \tag{2.59}$$

then substituting (2.31) and (2.59) into the first of (2.58), taking its Fourier transform and utilizing (2.54) and (2.55), then taking inverse transform and equating the coefficients of $\cos n\theta$ on the two sides of the resulting equation will give

$$\begin{aligned} Q_{mn}(\xi) = {} & \frac{\rho_i \mathcal{U}_i^2 \bar{C}_m}{2\pi}\int_{-\infty}^{\infty}\frac{1}{\bar{\alpha}}\left\{\frac{\bar{\Omega}_i}{\varepsilon_i} - \bar{U}_i\bar{\alpha}\right\}^2\left\{\frac{I_n(\bar{\alpha}\varepsilon)}{I_n'(\bar{\alpha}\varepsilon_i)}\right\}[\Phi_m^*(\bar{\alpha}) + R_m^*(\bar{\alpha})]e^{-i\bar{\alpha}\xi}d\bar{\alpha} \\ & -\frac{\rho_o \mathcal{U}_o^2}{2\pi}\int_{-\infty}^{\infty}\frac{1}{\bar{\alpha}}\left\{\frac{\bar{\Omega}_i}{\varepsilon_o\Omega_r} - \bar{U}_o\bar{\alpha}\right\}^2\left\{W_{1n}(\bar{\alpha},\varepsilon)\bar{C}_m + W_{2n}(\bar{\alpha},\varepsilon)\bar{F}_m\right\} \\ & \times\{\Phi_m^*(\bar{\alpha}) + R_m^*(\bar{\alpha})\}e^{-i\bar{\alpha}\xi}d\bar{\alpha}. \end{aligned} \tag{2.60}$$

In the process of solving the equations of motion by the Galerkin method (Section 2.3.4), all the terms are made to have the same common factor L. It is noted that the

resulting term $\gamma_i q_i/(\rho_{s_i} h_i L)$ from equation (2.3) is simply $q_i/\bar{q}_i$, with $\bar{q}_i$ having been defined in (2.52). Thus, for later convenience, $Q_{mn}(\xi)$ needs to be nondimensionalized with respect to $\bar{q}_i$. In the present method of solution, $Q_{mn}(\xi)$ is eventually multiplied by $\Phi_k(\xi)$ and integrated over the domain [0,1] of ξ. Hence, the dimensionless generalized force may be written as

$$\bar{Q}_{kmn} = \frac{1}{\bar{q}_i}\int_0^1 \Phi_k(\xi) Q_{mn}(\xi) d\xi. \tag{2.61}$$

Substitution of (2.60) into (2.61) gives

$$\begin{aligned}\bar{Q}_{kmn} = {} & \frac{\rho_i \mathcal{U}_i^2 \bar{C}_m}{2\pi \bar{q}_i}\int_{-\infty}^{\infty}\frac{1}{\bar{\alpha}}\left\{\frac{\bar{\Omega}_i}{\varepsilon_i} - \bar{U}_i\bar{\alpha}\right\}^2\left\{\frac{I_n(\bar{\alpha}\varepsilon)}{I_n'(\bar{\alpha}\varepsilon_i)}\right\}\{H_{km}(\bar{\alpha}) + N_{km}(\bar{\alpha})\}d\bar{\alpha} \\ & - \frac{\rho_o \mathcal{U}_o^2}{2\pi \bar{q}_i}\int_{-\infty}^{\infty}\frac{1}{\bar{\alpha}}\left\{\frac{\bar{\Omega}_i}{\varepsilon_o\Omega_r} - \bar{U}_o\bar{\alpha}\right\}^2\left\{W_{1n}(\bar{\alpha},\varepsilon)\bar{C}_m + W_{2n}(\bar{\alpha},\varepsilon)\bar{F}_m\right\} \\ & \times \{H_{km}(\bar{\alpha}) + N_{km}(\bar{\alpha})\}d\bar{\alpha},\end{aligned} \tag{2.62}$$

where $H_{km}(\bar{\alpha})$ and $N_{km}(\bar{\alpha})$are defined as

$$H_{km}(\bar{\alpha}) = \left\{\int_0^1 \Phi_k(\xi)e^{-i\bar{\alpha}\xi}d\xi\right\}\left\{\int_0^1 \Phi_m(\xi)e^{i\bar{\alpha}\xi}d\xi\right\}, \tag{2.63}$$

$$N_{km}(\bar{\alpha}) = \left\{\int_0^1 \Phi_k(\xi)e^{-i\bar{\alpha}\xi}d\xi\right\}\left\{\int_1^\ell R_m(\xi)e^{i\bar{\alpha}\xi}d\xi\right\}, \tag{2.64}$$

both of which can be determined analytically. The evaluation of $H_{km}(\bar{\alpha})$ and $N_{km}(\bar{\alpha})$ is presented in Appendices B and C, respectively. $\bar{Q}_{kmn}$ may also be expressed explicitly as a quadratic function of $\bar{\Omega}_i$,

$$\bar{Q}_{kmn} = \left\{q^{(1)}_{kmn}\bar{C}_m + r^{(1)}_{kmn}\bar{F}_m\right\}\bar{\Omega}_i^2 + 2\left\{q^{(2)}_{kmn}\bar{C}_m + r^{(2)}_{kmn}\bar{F}_m\right\}\bar{\Omega}_i + \left\{q^{(3)}_{kmn}\bar{C}_m + r^{(3)}_{kmn}\bar{F}_m\right\}, \tag{2.65}$$

where

$$\begin{aligned}q^{(j)}_{kmn} = {} & (-1)^{j+1}\frac{\rho_i \mathcal{U}_i^2}{2\pi\bar{q}_i}\left\{\frac{\bar{U}_i^{j-1}}{\varepsilon_i^{3-j}}\right\}\int_{-\infty}^{\infty}\bar{\alpha}^{j-2}\left\{\frac{I_n(\bar{\alpha}\varepsilon_i)}{I_n(\bar{\alpha}\varepsilon_i)}\right\}\{H_{km}(\bar{\alpha}) + N_{km}(\bar{\alpha})\}d\bar{\alpha} \\ & + (-1)^j\frac{\rho_o \mathcal{U}_o^2}{2\pi\bar{q}_i}\left\{\frac{\bar{U}_o^{j-1}}{(\varepsilon_o\Omega_r)^{3-j}}\right\}\int_{-\infty}^{\infty}\bar{\alpha}^{j-2}W_{1n}(\bar{\alpha}\varepsilon_i)\{H_{km}(\bar{\alpha}) + N_{km}(\bar{\alpha})\}d\bar{\alpha}, \\ r^{(j)}_{kmn} = {} & (-1)^j\frac{\rho_o \mathcal{U}_o^2}{2\pi\bar{q}_i}\left\{\frac{\bar{U}_o^{j-1}}{(\varepsilon_o\Omega_r)^{3-j}}\right\}\int_{-\infty}^{\infty}\bar{\alpha}^{j-2}W_{2n}(\bar{\alpha}\varepsilon_i)\{H_{km}(\bar{\alpha}) + N_{km}(\bar{\alpha})\}d\bar{\alpha},\end{aligned}$$

with the value of j being 1, 2 or 3.

Similarly, for the outer shell, q_o may be written as

$$q_o(\xi,\theta,t)=\sum_{n=1}^{\infty}\sum_{m=1}^{\infty}S_{mn}(\xi)\cos n\theta e^{i\Omega t}; \tag{2.66}$$

using the same procedure as was carried out for the generalized force on the inner shell results in

$$\bar{S}_{kmn}=\left\{s^{(1)}_{kmn}\bar{C}_m+t^{(1)}_{kmn}\bar{F}_m\right\}\bar{\Omega}_i^2+2\left\{s^{(2)}_{kmn}\bar{C}_m+t^{(2)}_{kmn}\bar{F}_m\right\}\bar{\Omega}_i+\left\{s^{(3)}_{kmn}\bar{C}_m+t^{(3)}_{kmn}\bar{F}_m\right\}, \tag{2.67}$$

where

$$s^{(j)}_{kmn}=(-1)^{j+1}\frac{\rho_o\mathcal{U}_o^2}{2\pi\bar{q}_o}\left\{\frac{\bar{U}_o^{j-1}}{(\varepsilon_o\Omega_r)^{3-j}}\right\}\int_{-\infty}^{\infty}\bar{\alpha}^{j-2}W_{1n}(\bar{\alpha}\varepsilon_o)\{H_{km}(\bar{\alpha})+N_{km}(\bar{\alpha})\}d\bar{\alpha},$$

$$t^{(j)}_{kmn}=(-1)^{j+1}\frac{\rho_o\mathcal{U}_o^2}{2\pi\bar{q}_o}\left\{\frac{\bar{U}_o^{j-1}}{(\varepsilon_o\Omega_r)^{3-j}}\right\}\int_{-\infty}^{\infty}\bar{\alpha}^{j-2}W_{2n}(\bar{\alpha}\varepsilon_o)\{H_{km}(\bar{\alpha})+N_{km}(\bar{\alpha})\}d\bar{\alpha}.$$

To recap, what has been done in the foregoing analysis is the derivation of the unsteady fluid-dynamic forces exerted on two coaxial cylindrical flexible shells due to the internal and annular flows. For the system with a flexible shell concentrically inside a rigid cylinder, the force on the outer cylinder [equation (2.67)] is of no practical interest, while the one on the inner shell, equation (2.65), reduces to

$$\bar{Q}_{kmn}=\left\{q^{(1)}_{kmn}\bar{C}_m\right\}\bar{\Omega}_i^2+\left\{2q^{(2)}_{kmn}\bar{C}_m\right\}\bar{\Omega}_i+\left\{q^{(3)}_{kmn}\bar{C}_m\right\}, \tag{2.68}$$

where the $q^{(j)}_{kmn}$ are the same as those defined for equation (2.65). Note that, in this case, since $\mathcal{U}_o=\infty$, the following term in equation (2.65) should be redefined as:

$$(-1)^j\frac{\rho_o\mathcal{U}_o^2}{2\pi\bar{q}_i}\left\{\frac{\bar{U}_o^{j-1}}{(\varepsilon_o\Omega_r)^{3-j}}\right\}=(-1)^j\frac{\rho_o\mathcal{U}_i^2}{2\pi\bar{q}_i}\left\{\frac{\hat{U}_o^{j-1}}{\varepsilon_i^{3-j}}\right\},\quad \hat{U}_o=\frac{U_o}{\mathcal{U}_i}.$$

For the reason to be discussed next, attention is now focused on $W_{1n}(\bar{\alpha},\varepsilon_i)$, which appeared in the second integrand of $q^{(j)}_{kmn}$ and can be obtained directly from (2.56),

$$W_{1n}(\bar{\alpha},\varepsilon_i)=\frac{I_n'(\bar{\alpha}\varepsilon_o)K_n(\bar{\alpha}\varepsilon_i)-I_n(\bar{\alpha}\varepsilon_i)K_n'(\bar{\alpha}\varepsilon_o)}{I_n'(\bar{\alpha}\varepsilon_o)K_n'(\bar{\alpha}\varepsilon_i)-I_n'(\bar{\alpha}\varepsilon_i)K_n'(\bar{\alpha}\varepsilon_o)}. \tag{2.69}$$

It is seen that, as the radius of the outer cylinder becomes very large, $\epsilon_o \to \infty$, i.e. when the inner shell becomes simultaneously subjected to internal and *unconfined external* axial flows, this becomes a configuration similar to that analyzed by Hannoyer and Païdoussis (1978) with beam theory. The present theory is sufficiently general to handle such a problem; all that needs to be done here is to evaluate $\lim_{\epsilon_o \to \infty} W_{1n}(\bar{\alpha}, \epsilon_i)$, because $W_{1n}(\bar{\alpha}, \epsilon_i)$, given by (2.69), has the form ∞/∞ as ϵ_o approaches ∞. From the limiting values of the modified Bessel functions,

$$\lim_{x \to \infty} I_n(x) = \infty, \quad \lim_{x \to \infty} K_n(x) = 0,$$

and from their recurrence relationships,

$$I_n'(x) = \frac{n}{x} I_n(x) + I_{n+1}(x),$$
$$K_n'(x) = \frac{n}{x} K_n(x) - K_{n+1}(x),$$

it may be seen that

$$\lim_{x \to \infty} I_n'(x) = \infty, \quad \lim_{x \to \infty} K_n'(x) = 0. \tag{2.70}$$

As a result of (2.70), the limiting value of (2.69) is found to be

$$\lim_{\epsilon_o \to \infty} W_{1n}(\bar{\alpha}, \epsilon_i) = \lim_{\epsilon_o \to \infty} \frac{I_n'(\bar{\alpha}\epsilon_o) K_n(\bar{\alpha}\epsilon_i)}{I_n'(\bar{\alpha}\epsilon_o) K_n'(\bar{\alpha}\epsilon_i)} = \frac{K_n(\bar{\alpha}\epsilon_i)}{K_n'(\bar{\alpha}\epsilon_i)}. \tag{2.71}$$

2.3.3 Steady Viscous Effects

As explained earlier, the viscous nature of the fluid results in both steady and unsteady viscosity-related loads being exerted on the shells, the latter of which are not considered in this thesis but will be the subject of future investigation. The steady loads have already been derived by Païdoussis, Misra and Chan (1985) from the time-averaged Navier-Stokes equations for the case of clamped-clamped shells. The same

procedure will be followed here to calculate such loads acting on the clamped-pinned and pinned-clamped shells. Since details of the derivation have been given (Païdoussis *et al.* 1985), they will not be repeated here; however, the final results with all the assumptions involved will be presented.

The steady loads are evaluated under the assumption of a fully-developed turbulent, incompressible flow. The fluid pressure and the surface frictional force inside a circular cylinder and in the annulus between two coaxial cylinders are derived by further assuming that the cylinders are rigid.

Figure 2.1 is referred to once more in this section. The flow velocity components in the cylindrical coordinates x, θ and r are $V_x + V_x'$, V_θ' and V_r', respectively; V_x is the mean velocity in the axial direction while V_x', V_θ' and V_r' are the fluctuating velocity components of the turbulent flow (here, $V_\theta = V_r = 0$). For a flow velocity V_x and static pressure P, the time-averaged Navier-Stokes equations may be written as (Laufer 1953):

$$\frac{1}{\rho}\frac{\partial P}{\partial x} = -\frac{1}{r}\frac{d}{dr}\left\{r\overline{V_x'V_r'}\right\} + \frac{\nu}{r}\frac{d}{dr}\left\{r\frac{dV_x}{dr}\right\}, \tag{2.72}$$

$$\frac{1}{\rho}\frac{\partial P}{\partial r} = -\frac{1}{r}\frac{d}{dr}\left\{r\overline{(V_r')^2}\right\} + \frac{\overline{(V_\theta')^2}}{r}, \tag{2.73}$$

$$0 = \frac{d}{dr}\left\{\overline{V_r'V_\theta'}\right\} + 2\frac{\overline{V_r'V_\theta'}}{r}, \tag{2.74}$$

where $\overline{(\ )}$ denotes the time mean of ( ); ρ and ν are the density and the kinematic viscosity of the fluid, respectively. These equations apply to both internal and annular flows.

After lengthy mathematical manipulations, the solutions of the above equations for the internal and annular fluid regions are obtained. The results of interest are given below.

- For the internal flow,

$$P_i(x,r) = -2\left(\frac{\rho_i}{a}\right)U_{\tau i}^2 x - \rho_i\overline{(V_{ri}')^2} + \rho_i\int_a^r \frac{\overline{(V_{\theta i}')^2} - \overline{(V_{ri}')^2}}{r}dr + P_i(0,a), \quad (2.75)$$

with $U_{\tau i}$, the so-called stress velocity, being given by

$$U_{\tau i} = \left\{-\nu_i\frac{dV_{xi}}{dr}\bigg|_{r=a}\right\}^{1/2} = \left\{\frac{\tau_{wi}}{\rho_i}\right\}^{1/2} = \left\{\frac{1}{8}f_i U_i^2\right\}^{1/2}, \quad (2.76)$$

where U_i is the mean axial velocity of the internal fluid, τ_{wi} is the fluid frictional force per unit area on the interior surface of the inner shell, $P_i(x,r)$ is the time-averaged pressure of the internal fluid, and $P_i(0,a)$ is the internal-fluid pressure at the position $x = 0$, $r = a$.

- For the annular flow,

$$P_o(x,r) = -\left\{\frac{2b}{b^2 - r_m^2}\right\}\rho_o U_{\tau oo}^2 x - \rho_o\overline{(V_{ro}')^2} + \rho_o\int_a^r \frac{\overline{(V_{\theta o}')^2} - \overline{(V_{ro}')^2}}{r}dr + P_o(0,a), \quad (2.77)$$

with $U_{\tau oo}$ being the stress velocity on the inner surface of the outer shell,

$$U_{\tau oo} = \left\{-\nu_o\frac{dV_{xo}}{dr}\bigg|_{r=b}\right\}^{1/2} = \left\{\frac{\tau_{woo}}{\rho_o}\right\}^{1/2} = \left\{\frac{1}{8}\frac{b^2 - r_m^2}{b(b-a)}f_{oo}U_o^2\right\}^{1/2}; \quad (2.78)$$

here U_o is the mean axial velocity of the annular fluid, τ_{woo} is the fluid frictional force per unit area on the interior surface of the outer shell, $P_o(x,r)$ is the annular time-averaged pressure, $P_o(0,a)$ is the annular-fluid pressure at $x = 0$ and $r = a$, and r_m is the radius at which the mean velocity V_{xo} is maximum.

In equations (2.77) and (2.78), r_m cannot be evaluated analytically; it is therefore determined from a multi-linear representation of Brighton and Jones' (1964) experimental measurements. Nevertheless, these measurements showed that if $a/b \geq 0.8$ then r_m can be approximated by its counterpart in the case of laminar flow; in other words,

$$r_m = \left\{\frac{b^2 - a^2}{2\ln(b/a)}\right\}^{1/2}. \quad (2.79)$$

The friction factor f, appearing in equations (2.76) and (2.78), is a function of the Reynolds number, Re, and of the relative roughness of the cylinder, k/d, where k is the average height of surface protrusions and d is the diameter of the cylinder. The friction factor may be found graphically from a Moody diagram, which is a plot of f versus Re for different values of k/d. Alternatively, it may be determined from a number of empirical formulas. A common practice is to use the Colebrook equation (Murdock 1976),

$$\frac{1}{\sqrt{f}} = -2\log_{10}\left\{\frac{k/d}{3.7} + \frac{2.51}{\mathrm{Re}\sqrt{f}}\right\}. \tag{2.80}$$

To avoid solving the above implicit equation, Moody himself derived the following approximation, which matches equation (2.80) to within $\pm 5\%$ for $k/d \leq 0.015$ and $\mathrm{Re} \leq 10^7$:

$$f_a = 0.0055\left\{1 + \left[20000\left(\frac{k}{d}\right) + \frac{10^6}{\mathrm{Re}}\right]^{1/3}\right\}. \tag{2.81}$$

The accuracy of f_a can be significantly improved if f_a is substituted back into equation (2.80), namely

$$\frac{1}{\sqrt{f}} = -2\log_{10}\left\{\frac{k/d}{3.7} + \frac{2.51}{\mathrm{Re}\sqrt{f_a}}\right\}; \tag{2.82}$$

the value of f so obtained is then within $\pm 0.7\%$ that of equation(2.80) for $k/d \leq 0.05$ and $\mathrm{Re} \leq 10^8$.

Equations (2.81) and (2.82) are valid for both internal and annular flows. For internal flow, d_i is the diameter of the inner cylinder, $2a$, and $\mathrm{Re}_i = U_i d_i/\nu_i = 2aU_i/\nu_i$. For annular flow, d_o is equal to the equivalent hydraulic diameter $d_h = 2(b-a)$, and $\mathrm{Re}_o = U_o d_o/\nu_o = 2(b-a)U_o/\nu_o$.

With the fluid pressures determined, the basic loads on the shells can now be evaluated. The steady radial differential pressure on the inner shell is given by $\bar{P}_{rIi} =$

$P_i(x,a) - P_o(x,a)$ which, in terms of (2.75) and (2.77), may be written as

$$\bar{P}_{rI_i} = \left\{ \frac{2b}{b^2 - r_m^2} \rho_o U_{\tau oo}^2 - \frac{2\rho_i}{a} U_{\tau i}^2 \right\} x + P_i(0,a) - P_o(0,a), \tag{2.83}$$

where subscript I stands for *initial* or steady-state, and use has been made of the condition that at the surfaces of the inner shell,

$$\overline{(V_{\tau i}')^2}\Big|_{r=a} = \overline{(V_{\tau o}')^2}\Big|_{r=a} = 0.$$

$P_i(0,a)$ and $P_o(0,a)$ may be determined from equations (2.75) and (2.77), respectively, if the static pressures of the two flows at either end of the shell are known. Here, the inner and annular static pressure are set equal at $x = L$, i.e.,

$$\Delta P_i = P_i(0,a) - P_o(0,a) = \frac{2\rho_i}{a} U_{\tau i}^2 L - \frac{2b}{b^2 - r_m^2} \rho_o U_{\tau oo}^2 L. \tag{2.84}$$

The corresponding surface traction in the axial direction on the inner shell is $\bar{P}_{xI_i} = \tau_{wi} + \tau_{woi}$, or,

$$\bar{P}_{xI_i} = \rho_i U_{\tau i}^2 + \rho_o U_{\tau oi}^2, \tag{2.85}$$

with τ_{woi} being the fluid frictional force per unit area on the exterior surface of the inner shell, $U_{\tau i}$ being the stress velocity defined in equation (2.76), and $U_{\tau oi}$ being the stress velocity on the outer surface of the inner shell,

$$U_{\tau oi} = \left\{ -\nu_o \frac{dV_{xo}}{dr}\bigg|_{r=a} \right\}^{1/2} = \left\{ \frac{\tau_{woi}}{\rho_o} \right\}^{1/2} = \left\{ \frac{1}{8} \frac{r_m^2 - a^2}{a(b-a)} f_{oi} U_o^2 \right\}^{1/2}. \tag{2.86}$$

Similarly, with the presumption that the outer shell is surrounded by quiescent fluid at pressure P_e, the steady radial differential pressure on the outer shell is found from $\bar{P}_{rI_o} = P_o(x,b) - P_e$, or

$$\bar{P}_{rI_o} = -\left\{ \frac{2b}{b^2 - r_m^2} \rho_o U_{\tau oo}^2 \right\} x + \rho_o \int_a^b \frac{\overline{(V_{\theta o}')^2} - \overline{(V_{ro}')^2}}{r} dr + P_o(0,a) - P_e, \tag{2.87}$$

where the fact that $\overline{(V'_{ro})^2}\big|_{r=b} = 0$ has been utilized. Also the annular and the outer static pressures are assumed equal at $x = L$,

$$\Delta P_o = P_o(0,a) - P_e = \frac{2b}{b^2 - r_m^2}\rho_o U_{roo}^2 L. \tag{2.88}$$

The quantities in the integral in equation (2.87) correspond to the mean-squared tangential and radial flow velocities in the annular flow; the value of this integral is quoted from Païdoussis *et al.* (1985),

$$I = \int_a^b \frac{\overline{(V'_{\theta o})^2} - \overline{(V'_{ro})^2}}{r} dr = \left\{0.7864 - \frac{0.56 r_m}{b - r_m} + \left[\frac{0.56 r_m^2}{(b-r_m)^2} - \frac{0.5064 r_m}{b - r_m}\right] \ln\left(\frac{b}{r_m}\right)\right\} U_{roo}^2$$

$$- \left\{0.7864 - \frac{0.56 r_m}{r_m - a} + \left[\frac{0.56 r_m^2}{(r_m-a)^2} - \frac{0.5064 r_m}{r_m - a}\right] \ln\left(\frac{r_m}{a}\right)\right\} U_{roi}^2, \tag{2.89}$$

and has been found to be numerically rather insignificant, as compared to the other terms on the right-hand side of equation (2.87). Finally, the corresponding traction load on the outer shell is given by

$$\bar{P}_{xIo} = \tau_{woo} = \rho_o U_{roo}^2. \tag{2.90}$$

It is noted that, for both internal and annular flows, equations (2.85) and (2.90), as well as (2.83) and (2.87), may be expressed in the functional forms

$$\bar{P}_{xI} = B, \quad \bar{P}_{rI} = -(Cx + D), \tag{2.91}$$

where

$$\begin{aligned}
B_i &= \rho_i U_{ri}^2 + \rho_o U_{roi}^2, & B_o &= \rho_o U_{roo}^2, \\
C_i &= \frac{2\rho_i}{a} U_{ri}^2 - \frac{2b}{b^2 - r_m^2}\rho_o U_{roo}^2, & C_o &= \frac{2b}{b^2 - r_m^2}\rho_o U_{roo}^2, \\
D_i &= -\Delta P_i, & D_o &= -(\rho_o I + \Delta P_o),
\end{aligned} \tag{2.92}$$

with ΔP_i, ΔP_o and I being defined in (2.84), (2.88) and (2.89), respectively.

Now that the pressures and stresses acting on the shells have been fully determined, they will be transformed into the terms q_{1i} to q_{3i} in equations (2.1)-(2.3) and q_{1o} to q_{3o} in equations (2.4)-(2.6). By balancing forces on an infinitesimal shell element in the $x-$, $\theta-$ and $r-$direction, the stress resultants may be determined and are found to be

$$N_{\theta I} = \bar{P}_{rI}\bar{r}, \quad \frac{\partial N_{x\theta I}}{\partial x} = -\frac{1}{\bar{r}}\frac{\partial N_{\theta I}}{\partial \theta}, \quad \frac{\partial N_{xI}}{\partial x} = -\bar{P}_{xI} - \frac{1}{\bar{r}}\frac{\partial N_{x\theta I}}{\partial \theta}, \tag{2.93}$$

where $N_{\theta I}$ and N_{xI} are the hoop and axial stress resultants, respectively, while $N_{x\theta I}$ is the shear stress resultant; $\bar{r}$ is equal to a for the inner shell and b for the outer one. In (2.93), the first equation shows that $N_{\theta I}$ is independent of θ, or $\partial N_{\theta I}/\partial\theta = 0$; hence the second equation becomes $N_{x\theta I} = f_1(\theta)$, and the third simplifies to $\partial N_{xI}/\partial x = -\bar{P}_{xI} - \frac{1}{\bar{r}}f_1'(\theta)$ or $N_{xI} = -Bx + f_2(\theta)$. However, since the shells are axisymmetric, $N_{x\theta I}$ and N_{xI} must be functionally independent of θ; in other words,

$$N_{x\theta I} = C_1, \quad N_{xI} = -Bx + C_2, \tag{2.94}$$

where C_1 and C_2 may be determined from the boundary conditions, as follows:

(i) for the pinned-clamped system, at $x = 0, N_{x\theta I} = 0$ or $C_1 = 0$, and $N_{xI} = 0$ (the pinned end of the flexible shell can slide along the rigid cylinder, for the reasons explained in Section 2.3.4), or $C_2 = 0$. Thus, with the substitution of these values into (2.94) and $\bar{P}_{rI}$ from (2.91) into(2.93), the following relationships are obtained:

$$N_{xI} = -Bx, \quad N_{\theta I} = -\bar{r}(Cx + D), \quad N_{x\theta I} = 0; \tag{2.95}$$

(ii) for the clamped-pinned system, at $x = 0, N_{x\theta I} = 0$ or $C_1 = 0$; at $x = L, N_{xI} = 0$ (the pinned end of the flexible shell can slide along the rigid cylinder), or $C_2 = BL$. With a similar procedure, it is easy to get,

$$N_{xI} = -B(x - L), \quad N_{\theta I} = -\bar{r}(Cx + D), \quad N_{x\theta I} = 0. \tag{2.96}$$

Finally, the terms q_1 to q_3 may be calculated from the following relationships (Païdoussis, Misra and Chan 1985):

$$q_1 = \left\{\frac{1-\nu^2}{Eh}\right\} N_{xI}, \quad q_2 = \left\{\frac{\bar{r}(1-\nu^2)}{Eh}\right\} \bar{P}_{xI}, \quad q_3 = \left\{\frac{1-\nu^2}{Eh}\right\} N_{\theta I}, \tag{2.97}$$

where subscripts i or o may be added as necessary, with $\bar{r} = a$ or b, respectively. It is noted that q_1, q_2 and q_3 as given by (2.98) are dimensionless and may be expressed in the following functional terms:

$$q_1 = \hat{A}_1\xi + \hat{B}_1, \quad q_2 = \hat{B}_2, \quad q_3 = \hat{A}_3\xi + \hat{B}_3, \tag{2.98}$$

where ξ is a nondimensionalized length variable defined in (2.53), and

$$\hat{A}_1 = -\left\{\frac{1-\nu^2}{Eh}\right\} BL, \quad \hat{A}_3 = -\left\{\frac{1-\nu^2}{Eh}\right\} CL\bar{r},$$

$$\hat{B}_1 = \begin{cases} 0, & \text{pinned-clamped} \\ \left\{\frac{1-\nu^2}{Eh}\right\} BL, & \text{clamped-pinned} \end{cases} \tag{2.99}$$

$$\hat{B}_2 = \left\{\frac{1-\nu^2}{Eh}\right\} B\bar{r}, \quad \hat{B}_3 = -\left\{\frac{1-\nu^2}{Eh}\right\} D\bar{r},$$

are all dimensionless constants, resulting from the substitution of (2.91), (2.95) and(2.96) into (2.98).

Thus, equations (2.98), together with (2.84), (2.88), (2.89) and (2.92), fully specify these dimensionless steady viscous forces acting on the shells.

2.3.4 Solution to the Governing Equations of Motion

With the unsteady generalized fluid forces and steady viscous friction acting on the shells completely determined, the solution for the governing equations of motion (2.1)-(2.6) subject to the pinned-clamped and clamped-pinned boundary conditions can

now be carried out using Galerkin's method, of which the variational statement can be written as

$$\delta E = \delta E_i + \delta E_o = 0, \tag{2.100}$$

with

$$\delta E_i = \int_0^{2\pi} \left\{ \frac{\mathcal{D}_i}{\varepsilon_i} \int_0^1 [L_{1i}\delta u_i + L_{2i}\delta v_i - L_{3i}\delta w_i] d\xi \right\} d\theta, \tag{2.101}$$

$$\delta E_o = \int_0^{2\pi} \left\{ \frac{\mathcal{D}_o}{\varepsilon_o} \int_0^1 [L_{1o}\delta u_o + L_{2o}\delta v_o - L_{3o}\delta w_o] d\xi \right\} d\theta, \tag{2.102}$$

where $\mathcal{D}_i = E_i h_i/(1-\nu_i^2)$ and $\mathcal{D}_o = E_o h_o/(1-\nu_o^2)$; and subscripts i and o are associated with the inner and outer shells, respectively. The minus signs associated with the terms $L_{3i}\delta w_i$ in (2.101) and $L_{3o}\delta w_o$ in (2.102) are necessary, as L_{3i} and L_{3o} represent the negative of the load per unit surface (unit length and unit radian).

Since δE_i and δE_o are generally independent, the implication of equation (2.100) is that both δE_i and δE_o must individually vanish, or

$$\delta E_i = 0, \quad \delta E_o = 0, \tag{2.103}$$

and hence these two equations must be solved simultaneously. Each of the variational statements (2.103) may be derived from an extended form of the principle of virtual work (Altman and De Oliveira 1988) or from Hamilton's principle. It should be mentioned here that all the boundary conditions (2.7)-(2.14) are automatically satisfied by the comparison functions chosen for u, v and w [equations (2.29) and (2.30)].

As the procedure to solve the first equation of (2.103) is *exactly* identical to that of the second one, only the former will be presented in full herein, whereas the final results from the second equation will be given in Appendix D.

The variations in u_i, v_i and w_i are simply derived from (2.29). Expressed in terms of dimensionless parameters as were defined in (2.53), these variations may be written

as follows:

$$\left\{\begin{array}{c}\delta u_i\\ \delta v_i\\ \delta w_i\end{array}\right\} = L\sum_{l=1}^{\infty}\sum_{k=1}^{\infty}\left\{\begin{array}{c}\delta\bar{A}_k\cos l\theta(\varepsilon_i\partial/\partial\xi)\\ \delta\bar{B}_k\sin l\theta\\ \delta\bar{C}_k\cos l\theta\end{array}\right\}\Phi_k(\xi)e^{i\Omega t}. \tag{2.104}$$

In the above expressions, for the purpose of evaluating (2.101), different indices have been used for the two summations--k and l denote the axial and circumferential wave numbers, respectively.

Substituting (2.29) and (2.59) into equations (2.1)-(2.3) and multiplying the resulting L's by the appropriate variations in (2.104) yields the following products

$$L_{1i}\delta u_i = \sum_{l=1}^{\infty}\sum_{n=1}^{\infty}\cos l\theta\cos n\theta f_{1L}(n), \tag{2.105}$$

$$L_{2i}\delta v_i = \sum_{l=1}^{\infty}\sum_{n=1}^{\infty}\sin l\theta\sin n\theta f_{2L}(n), \tag{2.106}$$

$$L_{3i}\delta w_i = \sum_{l=1}^{\infty}\sum_{n=1}^{\infty}\cos l\theta\cos n\theta f_{3L}(n), \tag{2.107}$$

where

$$\begin{aligned} f_{1L}(n) = {} & L^2e^{2i\Omega t}\sum_{k=1}^{\infty}\sum_{m=1}^{\infty}\delta\bar{A}_k\Big\{\Big[\Big(\bar{\Omega}_i^2-\frac{n^2}{2}(1+k_i)(1-\nu_i)-q_{3i}n^2\Big)\varepsilon_i^2\Phi_k'(\xi)\Phi_m'(\xi)\\ & +(1+q_{1i})\varepsilon_i^4\Phi_k'''(\xi)\Phi_m'(\xi)\Big]\bar{A}_m+\Big[\frac{n}{2}(1+\nu_i)\varepsilon_i^2\Phi_k'(\xi)\Phi_m'(\xi)\\ & +q_{2i}n\varepsilon_i\Phi_k'(\xi)\Phi_m(\xi)\Big]\bar{B}_m+\Big[\Big(\nu_i-\frac{n^2k_i}{2}(1-\nu_i)-q_{3i}\Big)\varepsilon_i^2\Phi_k'(\xi)\Phi_m'(\xi)\\ & -k_i\varepsilon_i^4\Phi_k'(\xi)\Phi_m'''(\xi)+q_{2i}\varepsilon_i\Phi_k'(\xi)\Phi_m(\xi)\Big]\bar{C}_m\Big\}, \end{aligned} \tag{2.108}$$

$$\begin{aligned} f_{2L}(n) = {} & L^2e^{2i\Omega t}\sum_{k=1}^{\infty}\sum_{m=1}^{\infty}\delta\bar{B}_k\Big\{-\Big[\frac{n}{2}(1+\nu_i)\varepsilon_i^2\Phi_k(\xi)\Phi_m''(\xi)\Big]\bar{A}_m\\ & +\Big[\Big(\bar{\Omega}_i^2-n^2(1+q_{3i})\Big)\Phi_k(\xi)\Phi_m(\xi)\\ & +\Big(\frac{1}{2}(1+3k_i)(1-\nu_i)+q_{1i}\Big)\varepsilon_i^2\Phi_k(\xi)\Phi_m''(\xi)\Big]\bar{B}_m\\ & +\Big[\frac{nk_i}{2}(3-\nu_i)\varepsilon_i^2\Phi_k(\xi)\Phi_m''(\xi)-n(1+q_{3i})\Phi_k(\xi)\Phi_m(\xi)\Big]\bar{C}_m\Big\}, \end{aligned} \tag{2.109}$$

$$f_{3L}(n) = L^2e^{2i\Omega t}\sum_{k=1}^{\infty}\sum_{m=1}^{\infty}\delta\bar{C}_k\Big\{\Big[\Big(\nu_i-\frac{n^2k_i}{2}(1-\nu_i)-q_{3i}\Big)\varepsilon_i^2\Phi_k(\xi)\Phi_m''(\xi)$$

$$
\begin{aligned}
&- k_i\varepsilon_i^4\lambda_m^4\,\Phi_k(\xi)\Phi_m(\xi)\Big]\,\bar{A}_m + \Big[n(1+q_{3i})\Phi_k(\xi)\Phi_m(\xi)\\
&-\frac{nk_i}{2}(3-\nu_i)\varepsilon_i^2\Phi_k(\xi)\Phi_m''(\xi)\Big]\,\bar{B}_m\\
&+\Big[\Big(1+k_i\varepsilon_i^4\lambda_m^4+k_i(n^2-1)^2+n^2q_{3i}-\bar{\Omega}_i^2\Big)\,\Phi_k(\xi)\Phi_m(\xi)\\
&-(2k_in^2+q_{1i})\varepsilon_i^2\Phi_k(\xi)\Phi_m''(\xi)\Big]\,\bar{C}_m-\frac{1}{\bar{q}_i}\Phi_k(\xi)Q_{mn}(\xi)\Big\}, \qquad (2.110)
\end{aligned}
$$

where the eigenvalues for a pinned-clamped beam, λ_m, are the roots of the transcendental equation $\tanh\lambda_m = \tan\lambda_m$; more information on λ_m may be found in Appendix A.

Before further analysis is made, it is useful to recall the orthogonality property of the sine and cosine functions: for any two integers l and n,

$$
\int_0^{2\pi}\cos l\theta\cos n\theta\,d\theta=\int_0^{2\pi}\sin l\theta\sin n\theta\,d\theta=\begin{cases}0 & \text{if } l\neq n,\\ \pi & \text{if } l=n;\end{cases}
$$

this leads to

$$
\begin{aligned}
\int_0^{2\pi}\Big\{\sum_{l=1}^{\infty}\sum_{n=1}^{\infty}\cos l\theta\cos n\theta\,f_c(n)\Big\}\,d\theta &= \sum_{l=1}^{\infty}\sum_{n=1}^{\infty}\Big\{\int_0^{2\pi}\cos l\theta\cos n\theta\Big\}\,f_c(n)\,d\theta\\
&= \sum_{n=1}^{\infty}\pi f_c(n), \qquad (2.111)\\
\int_0^{2\pi}\Big\{\sum_{l=1}^{\infty}\sum_{n=1}^{\infty}\sin l\theta\sin n\theta\,f_s(n)\Big\}\,d\theta &= \sum_{l=1}^{\infty}\sum_{n=1}^{\infty}\Big\{\int_0^{2\pi}\sin l\theta\sin n\theta\Big\}\,f_s(n)\,d\theta\\
&= \sum_{n=1}^{\infty}\pi f_s(n), \qquad (2.112)
\end{aligned}
$$

where $f_c(n)$ and $f_s(n)$ are some particular functions of n. In effect, equations (2.111) and (2.112) show how the terms $\cos l\theta\cos n\theta$ and $\sin l\theta\sin n\theta$ in equations (2.105)-(2.107) are *decoupled* once the Galerkin method is applied via equation (2.100).

Now, if all the terms q_{1i}, q_{2i} and q_{3i} in equations (2.108)-(2.110) are replaced by their functional forms in (2.98), then substituting (2.105)-(2.107) into (2.101) and performing (i) the integration over the domain $[0,2\pi]$ of θ with (2.111) and (2.112)

taken into account and (ii) the integration over the domain $[0,1]$ of ξ will lead to

$$\pi L^2 e^{2i\Omega t}\left(\frac{\mathcal{D}_i}{\varepsilon_i}\right)\sum_{n=1}^{\infty}\sum_{k=1}^{M}\{W_{1kn}\delta\bar{A}_k + W_{2kn}\delta\bar{B}_k + W_{3kn}\delta\bar{C}_k\} = 0,$$

and because $\pi L^2 e^{2i\Omega t}(\mathcal{D}_i/\varepsilon_i) \neq 0$ for all t,

$$\sum_{n=1}^{\infty}\sum_{k=1}^{M}\{W_{1kn}\delta\bar{A}_k + W_{2kn}\delta\bar{B}_k + W_{3kn}\delta\bar{C}_k\} = 0. \tag{2.113}$$

In equation (2.113), M is the number of admissible functions taken for the analysis, thus replacing the upper limits of the summations of the axial wave numbers in (2.29) and (2.104), i.e. $1 \leq k \leq M$ and $1 \leq m \leq M$. The coefficients $W_{1kn}, W_{2kn}, W_{3kn}$ are functions of $\bar{A}_m$, $\bar{B}_m$, $\bar{C}_m$ associated with the inner shell,

$$\begin{aligned}
W_{1kn} = \sum_{m=1}^{M}\Bigg\{\Bigg[\Bigg(\bar{\Omega}_i^2 - \frac{n^2}{2}\left[(1+k_i)(1-\nu_i) + 2\hat{B}_{3i}\right]\Bigg)\varepsilon_i^2\int_0^1 \Phi_k'(\xi)\Phi_m'(\xi)d\xi \\
- n^2\varepsilon_i^2\hat{A}_{3i}\int_0^1 \xi\Phi_k'(\xi)\Phi_m(\xi)d\xi + (1+\hat{B}_{1i})\varepsilon_i^4\int_0^1 \Phi_k'(\xi)\Phi_m'''(\xi)d\xi \\
+\varepsilon_i^4\hat{A}_{1i}\int_0^1 \xi\Phi_k'(\xi)\Phi_m'''(\xi)d\xi\Bigg]\bar{A}_m + \Bigg[\frac{n}{2}(1+\nu_i)\varepsilon_i^2\int_0^1 \Phi_k'(\xi)\Phi_m'(\xi)d\xi \\
+n\varepsilon_i\hat{B}_{2i}\int_0^1 \Phi_k'(\xi)\Phi_m(\xi)d\xi\Bigg]\bar{B}_m \\
+\Bigg[\Bigg(\nu_i - \frac{n^2k_i}{2}(1-\nu_i) - \hat{B}_{3i}\Bigg)\varepsilon_i^2\int_0^1 \Phi_k'(\xi)\Phi_m'(\xi)d\xi \\
-\varepsilon_i^2\hat{A}_{3i}\int_0^1 \xi\Phi_k'(\xi)\Phi_m'(\xi)d\xi \\
-k_i\varepsilon_i^4\int_0^1 \Phi_k'(\xi)\Phi_m'''(\xi)d\xi + \varepsilon_i\hat{B}_{2i}\int_0^1 \Phi_k'(\xi)\Phi_m(\xi)d\xi\Bigg]\bar{C}_m\Bigg\},
\end{aligned} \tag{2.114}$$

$$\begin{aligned}
W_{2kn} = \sum_{m=1}^{M}\Bigg\{\Bigg[-\frac{n}{2}(1+\nu_i)\varepsilon_i^2\int_0^1 \Phi_k(\xi)\Phi_m''(\xi)d\xi\Bigg]\bar{A}_m \\
+\Bigg[[\bar{\Omega}_i^2 - n^2(1+\hat{B}_{3i})]\int_0^1 \Phi_k(\xi)\Phi_m(\xi)d\xi - n^2\hat{A}_{3i}\int_0^1 \xi\Phi_k(\xi)\Phi_m(\xi)d\xi \\
+\Bigg(\frac{1}{2}(1+3k_i)(1-\nu_i) + \hat{B}_{1i}\Bigg)\varepsilon_i^2\int_0^1 \Phi_k(\xi)\Phi_m''(\xi)d\xi \\
+\varepsilon^2\hat{A}_{1i}\int_0^1 \xi\Phi_k(\xi)\Phi_m''(\xi)d\xi\Bigg]\bar{B}_m + \Bigg[\frac{nk_i}{2}(3-\nu_i\varepsilon_i^2\int_0^1 \Phi_k(\xi)\Phi_m''(\xi)d\xi \\
-n(1+\hat{B}_{3i}\int_0^1 \Phi_k(\xi)\Phi_m(\xi)d\xi - n\hat{A}_{3i}\int_0^1 \xi\Phi_k(\xi)\Phi_m(\xi)d\xi\Bigg]\bar{C}_m\Bigg\},
\end{aligned} \tag{2.115}$$

$$\begin{aligned}
W_{3kn} = \sum_{m=1}^{M}\Bigg\{\Bigg[\Bigg(-\frac{n^2k_i}{2}(1-\nu_i) - \nu_i + \hat{B}_{3i}\Bigg)\varepsilon_i^2\int_0^1 \Phi_k(\xi)\Phi_m''(\xi)d\xi
\end{aligned}$$

$$
\begin{aligned}
&+\varepsilon_i^2 \hat{A}_{3i} \int_0^1 \xi \Phi_k(\xi) \Phi_m''(\xi) d\xi + k_i \varepsilon_i^4 \lambda_m^4 \int_0^1 \Phi_k(\xi) \Phi_m(\xi) d\xi \Big] \bar{A}_m \\
&+ \Big[\frac{nk_i}{2}(3-\nu_i)\varepsilon_i^2 \int_0^1 \Phi_k(\xi) \Phi_m''(\xi) d\xi - n(1+\hat{B}_{3i}) \int_0^1 \Phi_k(\xi) \Phi_m(\xi) d\xi \\
&- n \hat{A}_{3i} \int_0^1 \xi \Phi_k(\xi) \Phi_m(\xi) d\xi \Big] \bar{B}_m \\
&+ \Big[\Big(\bar{\Omega}_i^2 - [1 + k_i \varepsilon_i^4 \lambda_m^4 + k_i (n^2-1)^2 + n^2 \hat{B}_{3i}] \Big) \int_0^1 \Phi_k(\xi) \Phi_m(\xi) d\xi \\
&- n^2 \hat{A}_{3i} \int_0^1 \xi \Phi_k(\xi) \Phi_m(\xi) d\xi + (2k_i n^2 + \hat{B}_{1i}) \int_0^1 \Phi_k(\xi) \Phi_m''(\xi) d\xi \\
&+ \varepsilon_i^2 \hat{A}_{1i} \int_0^1 \xi \Phi_k(\xi) \Phi_m''(\xi) d\xi \Big] \bar{C}_m + \frac{1}{\bar{q}_i} \int_0^1 \Phi_k(\xi) Q_{mn}(\xi) d\xi \Big\}, \qquad (2.116)
\end{aligned}
$$

where $\hat{A}_{1i}, \ldots, \hat{B}_{3i}$ are as defined in equations (2.99).

Because $\delta \bar{A}_k$, $\delta \bar{B}_k$ and $\delta \bar{C}_k$ are totally arbitrary, equation (2.113) is equivalent to

$$
\sum_{n=1}^{\infty} W_{1kn} = 0, \quad \sum_{n=1}^{\infty} W_{2kn} = 0, \quad \sum_{n=1}^{\infty} W_{3kn} = 0. \qquad (2.117)
$$

As may be seen from equations (2.114)-(2.116), each term of any of the above three series is a function of n and is independent of other terms in the same series. Equations (2.117) thus imply that individual W_{1kn}, W_{2kn} and W_{3kn} must be equal to zero, namely

$$
\begin{aligned}
W_{1kn} &= \sum_{m=1}^{M} \{ J_{kmn}^{1,1} \bar{A}_m + J_{kmn}^{1,2} \bar{B}_m + J_{kmn}^{1,3} \bar{C}_m + J_{kmn}^{1,4} \bar{D}_m + J_{kmn}^{1,5} \bar{E}_m + J_{kmn}^{1,6} \bar{F}_m \} = 0, \\
&\vdots \qquad (2.118) \\
W_{3kn} &= \sum_{m=1}^{M} \{ J_{kmn}^{3,1} \bar{A}_m + J_{kmn}^{3,2} \bar{B}_m + J_{kmn}^{3,3} \bar{C}_m + J_{kmn}^{3,4} \bar{D}_m + J_{kmn}^{3,5} \bar{E}_m + J_{kmn}^{3,6} \bar{F}_m \} = 0.
\end{aligned}
$$

Note that $\bar{D}_m$, $\bar{E}_m$ and $\bar{F}_m$ are arising from the last term in equation (2.116). Similarly, with the foregoing analysis carried out for the second equation of (2.103), the following equations will be obtained

$$
\begin{aligned}
W_{4kn} &= \sum_{m=1}^{M} \{ J_{kmn}^{4,1} \bar{A}_m + J_{kmn}^{4,2} \bar{B}_m + J_{kmn}^{4,3} \bar{C}_m + J_{kmn}^{4,4} \bar{D}_m + J_{kmn}^{4,5} \bar{E}_m + J_{kmn}^{4,6} \bar{F}_m \} = 0, \\
&\vdots \qquad (2.119) \\
W_{6kn} &= \sum_{m=1}^{M} \{ J_{kmn}^{6,1} \bar{A}_m + J_{kmn}^{6,2} \bar{B}_m + J_{kmn}^{6,3} \bar{C}_m + J_{kmn}^{6,4} \bar{D}_m + J_{kmn}^{6,5} \bar{E}_m + J_{kmn}^{6,6} \bar{F}_m \} = 0.
\end{aligned}
$$

Thus, equation (2.100) is in effect equivalent to a set of $6M$ equations, equations (2.118) and (2.119), in which $\bar{A}_m$, $\bar{B}_m$, ..., $\bar{F}_m$ are the unknowns to be solved for.

Equations (2.118) and (2.119) may be grouped together and put in the matrix form

$$\left([M]\bar{\Omega}_i^2 + [C]\bar{\Omega}_i + [K]\right)\{X\} = \{0\}. \tag{2.120}$$

It should be emphasized here that $[M]$, $[C]$ and $[K]$ in equation (2.120) are not the traditional mass, damping and stiffness matrices but are proportional to them. $[M]$, $[C]$ and $[K]$ are the coefficient matrices of $\bar{\Omega}_i^2$, $\bar{\Omega}_i^1$ and $\bar{\Omega}_i^0$, respectively. The elements of $[M]$, $[C]$, $[K]$ and $\{X\}$ are given in Appendix D.

So far, energy dissipated internally in the material of the shells has been neglected. If dissipation is considered to be a hysteretic effect (structural damping), it may be taken into account by replacing Young's modulus E by $E\left(1 + \frac{\mu}{\Omega}\frac{\partial}{\partial t}\right)$ in equations (2.1)-(2.6), where μ is called the structural damping factor. Alternatively, dissipation may be considered to be a viscoelastic effect (viscoelastic damping), in which case E is replaced by $E\left(1 + \chi\frac{\partial}{\partial t}\right)$, where χ is the viscoelastic damping coefficient. In general, E may be replaced by $E\left\{1 + \left(\frac{\mu}{\Omega} + \chi\right)\frac{\partial}{\partial t}\right\}$ with the understanding (purely for convenience) that either μ or χ will be zero for a given system. As a reminder of the notation used in equations (2.1)-(2.6), $E\left\{1 + \left(\frac{\mu}{\Omega} + \chi\right)\frac{\partial}{\partial t}\right\}$ is to be written with the subscript i for equations (2.1)-(2.3), namely $E_i\left\{1 + \left(\frac{\mu_i}{\Omega} + \chi_i\right)\frac{\partial}{\partial t}\right\}$, and with the subscript o for equations (2.4)-(2-6), namely $E_o\left\{1 + \left(\frac{\mu_o}{\Omega} + \chi_o\right)\frac{\partial}{\partial t}\right\}$.

To give a simple illustration of the changes equation (2.120) will be subject to when internal damping is included, it is assumed that both inner and outer shells are made of the same material and hence neither subscript i nor o is required for μ and χ (and other material properties). Equation (2.120) then becomes

$$\left([M]\bar{\Omega}_i^2 + [C]\bar{\Omega}_i + [1 + i(\mu + \chi\Omega)[K]\right)\{X\} = \{0\}. \tag{2.121}$$

Since

$$i\chi\Omega = i\left(\frac{\chi\mathcal{U}_i}{L}\right)\left(\frac{L}{a}\right)\left(\frac{\Omega a}{\mathcal{U}_i}\right) = \left(\frac{i}{\varepsilon_i}\frac{\chi\mathcal{U}_i}{L}\right)\bar{\Omega}_i,$$

equation (2.121) may be rearranged and rewritten as

$$\left([M']\bar{\Omega}_i^2 + [C']\bar{\Omega}_i + [K']\right)\{X\} = \{0\}, \tag{2.122}$$

where

$$[M'] = [M],\ \ [C'] = [C] + \left(\frac{i}{\varepsilon_i}\frac{\chi\mathcal{U}_i}{L}\right)[K],\ \ [K'] = (1+\mu i)[K]. \tag{2.123}$$

If a new vector $\{Y\}$ is introduced and defined as

$$\{Y\} = \left\{\begin{array}{c} \{X\} \\ \bar{\Omega}_i\{X\} \end{array}\right\}, \tag{2.124}$$

equation (2.120) [or equation (2.122) if internal dissipation is to be accounted for] can be transformed into the first-order form

$$\left([P] + \bar{\Omega}_i[Q]\right)\{Y\} = \{0\}, \tag{2.125}$$

where

$$[P] = \left[\begin{array}{cc} [0] & [I] \\ [K] & [C] \end{array}\right],\ \ [Q] = \left[\begin{array}{cc} [-I] & [0] \\ [0] & [M] \end{array}\right],$$

with $[I]$ being the identity matrix of the same order as $[M]$, $[C]$ and $[K]$. Equation (2.125) represents a generalized eigenvalue problem and can readily be solved by any available computer subroutines such as those of IMSL (International Mathematical and Scientific Libraries), giving the eigenfrequencies of the system.

2.3.5 Summary

Section 2.3 has presented in detail (i) the evaluation of the unsteady generalized fluid forces acting on the shells by means of the Fourier transform technique, (ii) all final,

important results for the steady viscous forces appearing in the governing equations of motion, and (iii) the procedure of solving the governing equations of motion using Galerkin's method.

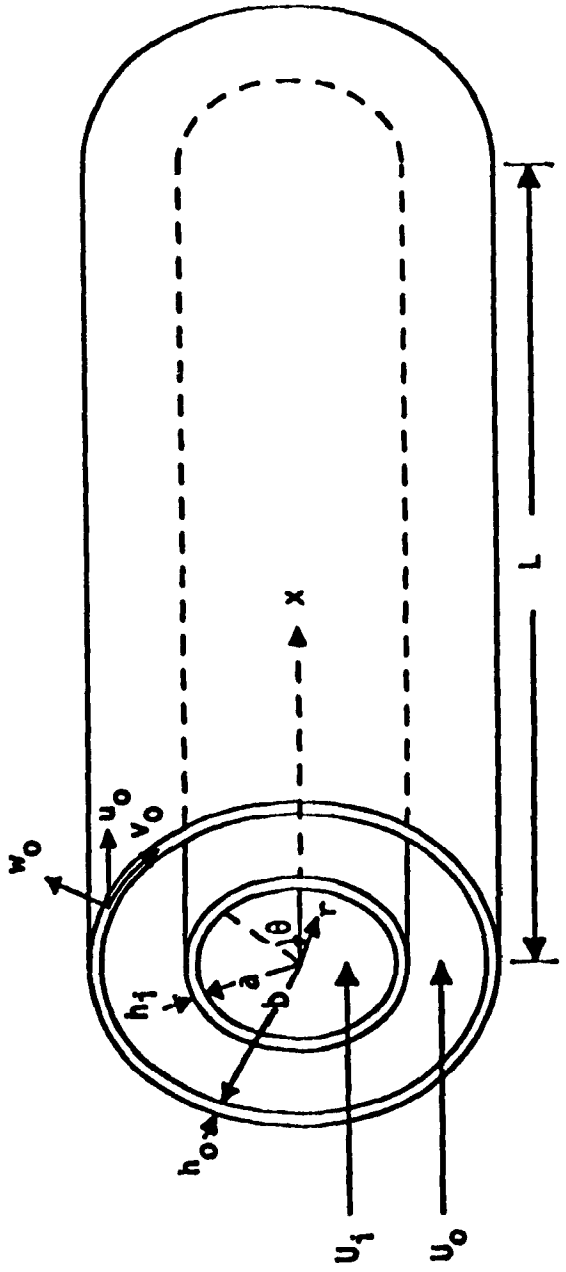

Figure 2.1: Schematic of the system under consideration.

Chapter 3

Verification of the Computer Program

3.1 Introduction

Before the theory presented in the last chapter was actually applied to the system under consideration (Chapter 4), a series of preliminary calculations were conducted to examine different aspects of the theory and to verify the computer program.

Firstly, natural frequencies of a cylindrical shell *in vacuo* were calculated (Section 3.2). The aim of these calculations was to assess how well the Galerkin method works and hence to validate certain segments of the computer program developed for Chapter 4. Thus, equation (2.100) was used to solve the equations of motion [(2.1)-(2.6)] subject to the pinned-clamped and/or clamped-pinned boundary conditions.

Secondly, calculations were conducted for a cylindrical shell conveying inviscid flow (Section 3.3). The purpose of these calculations was to validate the computer program in the case of a shell conveying inviscid flow.

It should be noted that the results to be presented in this chapter were obtained

without steady viscous effects (Section 2.3.3). There were two reasons for doing so: (i) all the above-mentioned aspects are part of the inviscid theory only, and (ii) the present results could be compared with previous theoretical ones which did not involve any viscous effects.

3.2 Natural Frequencies of a Shell in the Absence of Flow

3.2.1 Weingarten's Theory

There already exist many theories to estimate the lowest natural frequencies of cylindrical shells. The one presented here was developed by Weingarten (1964), who neglected the longitudinal and circumferential inertial terms in the Donnell equation. With this simplification, based on the radial character of the motion associated with the lowest natural frequencies, the Donnell equation reduces to:

$$\frac{h_i^2}{12}\nabla^8 w_i + \frac{1-\nu_i^2}{a^2}\frac{\partial^4 w_i}{\partial x^4} + \rho_{si}\frac{1-\nu_i^2}{E_i}\nabla^4\frac{\partial^2 w_i}{\partial t^2} = 0, \tag{3.1}$$

where

$$\nabla^2 = \frac{\partial^2}{\partial x^2} + \frac{1}{a}\frac{\partial^2}{\partial \theta^2},$$

and subscript i stands for the inner shell, corresponding to the present theory.

If it is assumed that

$$w_i = \left(\sum_m C_m e^{i\lambda_{mn}x/L}\right)\cos n\theta \cos \Omega t, \tag{3.2}$$

equation (3.1) becomes

$$\frac{h_i^2}{12}\left(\frac{n}{a}\right)^8\left(1-\frac{\lambda_{mn}^2 a^2}{n^2L^2}\right)^4 + \frac{1-\nu_i^2}{a^2}\left(\frac{\lambda_{mn}}{L}\right)^4 - \left(\frac{\bar{\Omega}_i}{a}\right)^2\left(\frac{n}{a}\right)^4\left(1-\frac{\lambda_{mn}^2 a^2}{n^2L^2}\right)^2 = 0, \tag{3.3}$$

where $\bar{\Omega}_i$ is the dimensionless frequency defined in equation (2.53). This eighth degree equation relating λ_{mn} and $\bar{\Omega}_i$ is reduced to a fourth degree equation by using Yu's (1955) assumption:

$$\frac{|\lambda_{mn}^2|a^2}{n^2L^2} \ll 1, \tag{3.4}$$

which restricts the solution to *long cylinders and high circumferential wave-numbers.*

With this assumption, equation (3.3) is replaced by

$$(1-\nu_i^2)\left(\frac{\lambda_{mn}a}{L}\right)^4 = \bar{\Omega}_i^2 n^4 - \frac{n^8}{12}\frac{h_i^2}{a^2}. \tag{3.5}$$

The lowest estimated dimensionless natural frequency is found by rearranging equation(3.5), as follows:

$$\bar{\Omega}_i^2 = \left[\frac{n^8}{12}\frac{h_i^2}{a^2} + (1-\nu_i^2)\left(\frac{\lambda_{mn}a}{L}\right)^4\right]\frac{1}{n^4}, \tag{3.6}$$

or, in dimensional terms,

$$\Omega_i = \frac{\mathcal{U}_i}{an^2}\left[\frac{n^8}{12}\left(\frac{h_i}{a}\right)^2 + (1-\nu_i^2)\left(\frac{\lambda_{mn}a}{L}\right)^4\right]^{1/2}, \tag{3.7}$$

where λ_{mn} is the mth eigenvalue (axial mode number m), and $\mathcal{U}_i$ is the reference velocity defined in Section 2.3.2.3.

3.2.2 Comparison of the Two Theories

To satisfy Yu's (1955) assumption (3.4), the ratio L/a should be large. The following system parameters were selected for calculations, and it should be noted that $L/a = 20$:

$$E_i = 2.1 \times 10^{11}\ \text{N/m}^2,\quad \nu_i = 0.28,\quad \rho_{si} = 7.8 \times 10^3\ \text{kg/m}^3,$$

$$h_i = 0.8\ \text{mm},\quad a = 50\ \text{mm},\quad L = 1.0\ \text{m};\quad \mu_i \text{ and } \chi_i \text{ are zero.}$$

In addition to a large L/a, for the same reason of meeting Yu' assumption (3.4),(i) the axial mode number m should be fairly low in order to keep λ_m small, and (ii) large n is required. Hence, calculations were conducted with $m = 1 - 3$ and $n = 1 - 12$. From Yu's assumption (3.4), it can be seen that the left-hand side will give the maximum value ($\bar{\Omega}_i = 0.26$ in the case of a pinned-clamped or clamped-pinned shell) when $m = 3$ and $n = 1$, which leads to the worst results when using equation (3.7) for calculating the natural frequencies. For the purpose of comparison, calculations were conducted using the present theory with same system parameters as mentioned above. Results of both Weingarten's and the present theories are presented in Figure 3.1 and Table 3.1.

In Figure 3.1, the results obtained with three comparison functions ($M = 3$) by using the present theory are compared with those obtained by using the estimated natural frequency formula (3.7), i.e. Weingarten's theory. It is seen that the agreement is quite good, except for $n = 1$ and $n = 2$, for which Yu's assumption (3.4) and Donnell's theory (3.1) used by Weingarten are inaccurate. The results improve further, if only slightly, when the calculations are carried out with a larger M the number of comparison functions used, since the natural frequencies then become smaller. However, because the effect of M on the natural frequencies is not overwhelming, especially for low m (= 1,2), quite a number of the calculations that follow have been conducted with $M = 6$, or even 3, to reduce the computing time required.

In general, the theoretical results are better for higher n, the circumferential wave number, and lower m, and *vice versa*, as expected from Yu's assumption (3.4). It is noted that in Figure 3.1 Weingarten's theory gives much greater values when $n = 1$

than the present theory does; in other words, the present theory is better and more general, because it is not restricted by Yu's assumption.

3.3 Natural Frequencies of a Shell Conveying Inviscid Fluid Flow

3.3.1 Straight Pipes Conveying Steady Inviscid Flow

In order to verify the present computer program when internal inviscid fluid flow is taken into account, comparison should be made between the results obtained with the present theory and by previous theory. The theory of straight, thick-walled pipes with steady flow (i.e. the so-called *beam theory*) has been discussed thoroughly. With the assumption that gravity, internal damping, externally imposed tension, and pressurization effects are either absent or neglected, the equation of motion of beam-like pipes conveying inviscid flow takes the particularly simple form

$$E_i I_i \frac{\partial^4 w_i}{\partial x^4} + M_f U_i^2 \frac{\partial^2 w_i}{\partial x^2} + 2 M_f U_i \frac{\partial^2 w_i}{\partial x \partial t} + (M_f + m_s) \frac{\partial^2 w_i}{\partial t^2} = 0, \qquad (3.8)$$

where $E_i I_i$ is the flexural rigidity of the pipe, M_f is the mass of the fluid per unit length flowing with a steady flow velocity U_i, m_s is the mass of the pipe per unit length, and w_i is the lateral deflection of the pipe; x and t are the axial coordinate and time, respectively.

Here only the first mode of beam functions (for the pinned-clamped or clamped-pinned system) is taken, i.e., the radial displacement takes the following form:

$$w_i = C_1 \Phi_1(\xi) e^{i\Omega_i t}. \qquad (3.9)$$

By using Galerkin's method, we have:

$$\int_0^1 \left[\frac{E_i I_i}{L^4} \Phi_i^{(4)}(\xi) + \frac{M_f U_i^2}{L^2} \Phi_i''(\xi) + \frac{2 M_f U_i}{L} i\Omega_i \Phi_i'(\xi) - (M_f + m_s)\Omega_i^2 \Phi_i(\xi) \right] \Phi_i(\xi) d\xi = 0. \tag{3.10}$$

Finally, the frequency can be expressed as

$$\Omega_i = \left[\frac{E_i I_i \left(\frac{\lambda_1}{L}\right)^4 - \frac{M_f U_i^2}{L^2} b_{11}}{M_f + m_s} \right]^{1/2} \tag{3.11}$$

where

$$m_s = 2\pi \left(a + \frac{h_i}{2}\right) h_i \rho_{si}, \quad M_f = \pi a^2 \rho_i,$$
$$I_i = \pi h_i \left(a + \frac{h_i}{2}\right)^3, \qquad U_i = \mathcal{U}_i \bar{U}_i,$$

and b_{11} is the integral involving the first mode beam eigenfunction defined in Appendix A.

3.3.2 Comparison of Results

The following system parameters were chosen for calculations conducted both by using the present theory and the beam theory (3.11):

$E_i = 2.1 \times 10^{11}$ N/m^2, $\nu_i = 0.28$, $\rho_{si} = 7.8 \times 10^3$ kg/m^3, $\rho_i = 1.0 \times 10^3$ kg/m^3, $h_i = 0.8$ mm, $a = 50$ mm, $L = 1.0$ m; μ_i and χ_i are zero.

It is noted that the ratio L/a is 20, to make the system more beam-like. The variation of frequency Ω_i with dimensionless flow velocity $\bar{U}_i$ is shown in Figure 3.2 and Table 3.2. In Figure 3.2, the results obtained with three comparison functions $M = 3$ and with circumferential wave number $n = 1$ (corresponding to the beam-like motion) by using the present theory are compared with those obtained by using

the beam theory (3.11). It is seen that the agreement between the two theories is reasonably good and, in fact, the present results are better, since the frequencies obtained with the present theory are lower than those obtained with the beam theory. Note that Galerkin's method yields upper bounds. The results of the beam theory could of course be improved by increasing the number of the comparison functions to more than just the first comparison function.

3.4 Summary

In Charpter 3 are presented the results of preliminary calculations conducted to verify some important aspects of the present theory.

- To check Galerkin's method, natural frequencies of a pinned-clamped or clamped-pinned shell in the absence of fluid (*in vacuo*) were calculated and found to be in excellent agreement with the results obtained by Weingarten's theory when the circumferential wave number n is large.

- To check the computer program under the condition that the fluid conveyed is inviscid, comparison was made between the results of the present theory and those of beam theory. The agreement is reasonably good.

Table 3.1: Comparison between natural frequencies of a pinned-clamped shell, as calculated by Weingarten's theory and by the present theory with three comparison functions ($M = 3$) , for different circumferential and axial mode numbers, n and m, respectively.

n	Natural Frequencies (kHz)					
	m = 1		m = 2		m = 3	
	Estimated Value	Present Theory	Estimated Value	Present Theory	Estimated Value	Present Theory
1	4.031	2.671	12.972	7.773	27.050	14.388
2	2.233	1.616	3.806	3.116	7.050	5.783
3	4.515	3.824	4.718	4.064	5.405	4.771
4	7.992	7.282	8.029	7.355	8.165	7.545
5	12.483	11.763	12.492	11.810	12.528	11.906
6	17.974	17.250	17.977	17.291	17.990	17.365
7	24.465	23.737	24.466	23.777	24.471	23.845
8	31.954	31.224	31.955	31.263	31.957	31.330
9	40.442	39.711	40.442	39.750	40.443	39.815
10	49.928	49.196	49.928	49.235	49.929	49.301
11	60.413	59.680	60.414	59.720	60.414	59.785
12	71.897	71.163	71.897	71.203	71.897	71.268

Table 3.2: Comparison between the lowest natural frequencies of a pinned-clamped shell (steel) conveying internal fluid (water) with dimensionless velocity $\bar{U}_i$, as calculated by beam theory with one comparison function ($M = 1$) and by the present theory with three comparison functions ($M = 3$), for circumferential wave number $n = 1$ and axial mode number $m = 1$.

Beam Theory		Present Theory	
$\bar{U}_i x10^2$	Frequency Hz	$\bar{U}_i x10^2$	Frequency Hz
0.000	1,278.2	0.000	1,205.6
1.000	1,267.7	1.000	1,191.7
2.000	1,235.5	2.000	1,149.4
3.000	1,179.9	3.000	1,083.5
4.000	1,097.3	4.000	973.8
5.000	980.9	5.000	833.1
6.000	816.5	6.000	643.6
7.000	563.3	7.000	359.1
7.755	134.1	7.200	271.1
7.760	126.1	7.400	138.2
7.765	117.6	7.450	75.5
7.770	108.3	7.452	71.9
7.775	98.2	7.454	68.1
7.780	87.0	7.456	64.0
7.785	74.0	7.458	59.7
7.790	58.1	7.464	44.3
7.795	35.9	7.468	30.0

Figure 3.1: Comparison between natural frequencies of a pinned-clamped shell, as calculated by Weingarten's theory and by the present theory with three comparison functions ($M = 3$), for different circumferential and axial mode numbers, n and m, respectively.

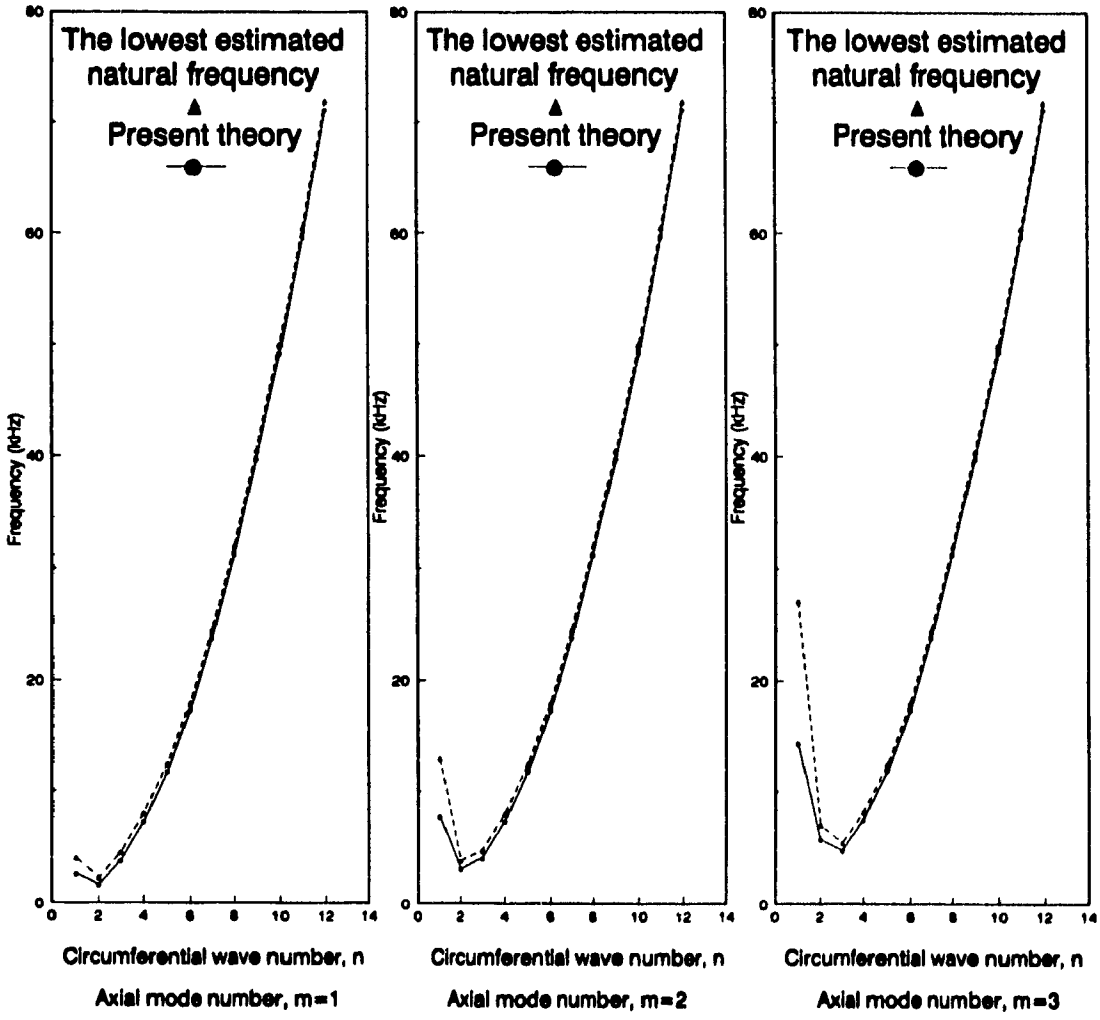

Figure 3.2: Comparison between the lowest natural frequencies of a pinned-clamped shell (steel) conveying internal fluid (water) with dimensionless velocity $\bar{U}_i$, as calculated by beam theory with one comparison function ($M = 1$) and by the present theory with three comparison functions ($M = 3$), for circumferential wave number $n = 1$ and axial mode number $m = 1$.

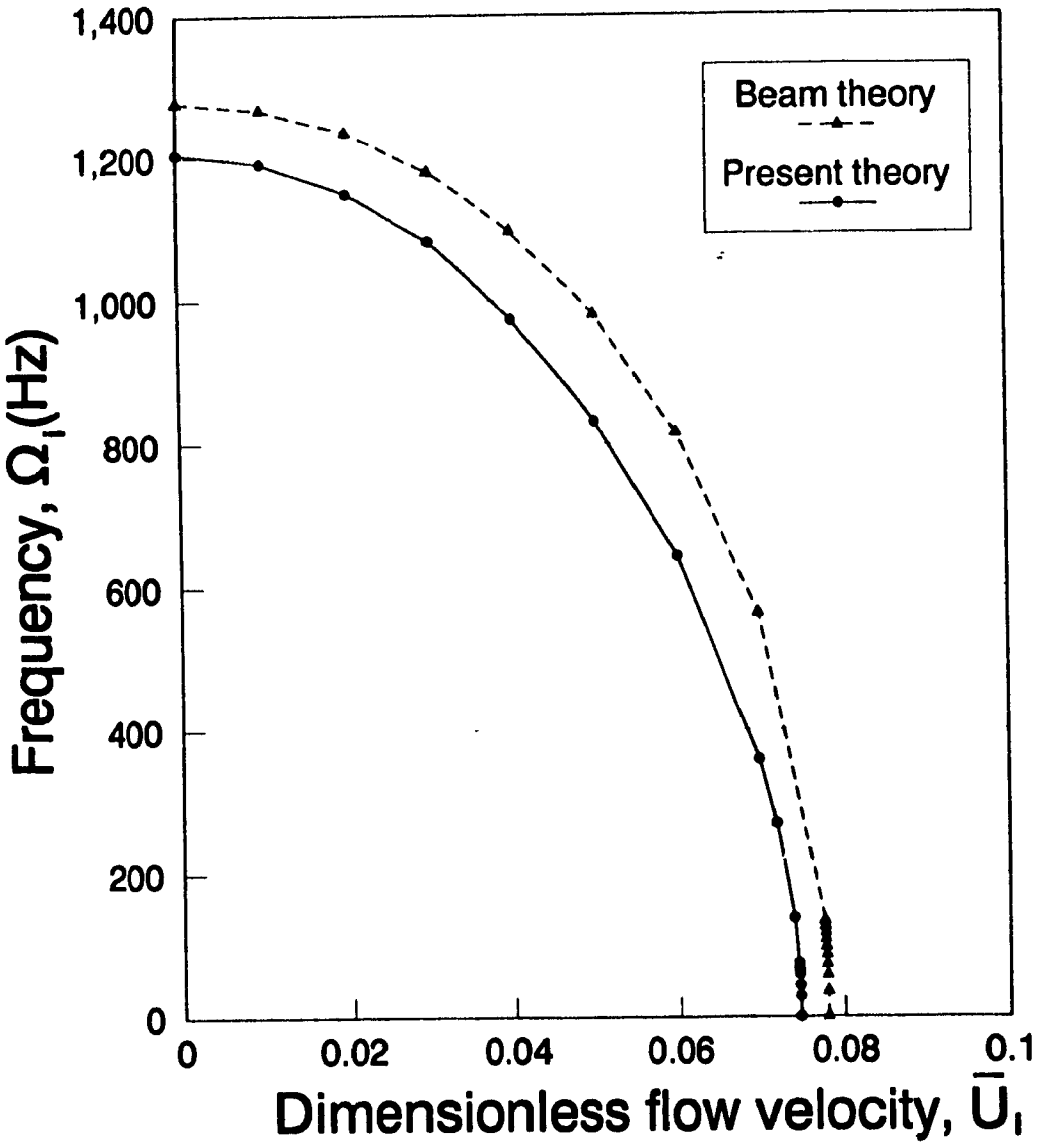

Chapter 4

Theoretical Results

4.1 Introduction

Although the theory given in Sections 2.2 and 2.3 was developed for the general case of two coaxial *flexible* shells, nevertheless for the calculations to be conducted here the outer shell is replaced by a rigid cylinder. This is done partly in order to achieve some computational economy, but also because most physical problems of interest are like that; another reason is that, at least for shells with both ends supported, the dynamical behaviour of such systems is qualitatively the same whether one or both shells are flexible (Païdoussis *et al.* 1984, 1985), the main effect of an outer flexible shell being to diminish the critical flow velocities.

The calculations were conducted for shells with the same geometries and properties as those in earlier studies of clamped-clamped shells (Païdoussis *et al.* 1984, 1985) and of clamped-free shells (Païdoussis *et al.* 1991), namely:

$$E_i = 2.0 \times 10^{11}\,\mathrm{N/m^2},\ \nu_i = 0.3,\ \rho_{si} = 7.8 \times 10^3\,\mathrm{kg/m^3},\ \rho_i = \rho_o = 10^3\,\mathrm{kg/m^3},$$

$b = 100\,\mathrm{mm}$, $a = (10/11)b$ for the so-called 1/10-gap system,

$a = (100/101)b$ for the 1/100-gap system, $L = 1.00\,\mathrm{m}$, $h_i = 0.5\,\mathrm{mm}$;

thus, $\mathcal{U}_i = 5308\,\mathrm{m/s}$ and $\rho_i a/(\rho_{si} h_i) = 23.30.$ (4.1)

It is known (Evensen 1974, Evensen and Olson 1968) that shells are subject to important softening-type nonlinearities. Since the present theory is linear, the results generated are expected to be physically correct only for sufficiently small-amplitude perturbations; thus, the intricate behaviour of the system beyond the first loss of stability as predicted by the present theory may not be reliable. However, the results are still of academic interest and are therefore presented.

Two different cases of flows will be considered and discussed in the following order: (i) internal flow alone, $\bar{U}_o = 0$ (Section 4.3), and (ii) annular flow alone, $\bar{U}_i = 0$ (Section 4.4).

4.2 Some Numerical Considerations

Since the computer program of the present theory was obtained by implementing the computer program written by Nguyen (1992), optimum values of some of the parameters involved in the calculations had been already selected. To save computing time, the same values of these parameters are used in the present calculations:

(i) the integration stepsize (e.g., in the integrals in (2.62)) is $\Delta\bar{\alpha} = 2.0$;

(ii) the domain of integration (for the same numerical integration, approximating $-\infty < z < \infty$) is $(-z, z) = (-200, 200)$;

(iii) the number of comparison functions in the Galerkin expansions is $M = 6$;

(iv) $\ell = 3$, if the out-flow model is taken into account (see Appendix C).

4.3 Internal Flow Alone

4.3.1 General Dynamics of the System

Typical results of the variation of the real and imaginary parts of the dimensionless eigenfrequencies, $\bar{\Omega}_i$, with increasing dimensionless internal flow velocity, $\bar{U}_i$, are shown in Figure 4.1 (for $n = 3$, $m = 1, 2, 3$); the annular fluid is stagnant and its static pressure is equal to that of the internal fluid at $x = L$. These results were obtained with inviscid theory. They are the same whether the system is pinned-clamped or clamped-pinned. Structural damping is ignored in these calculations. The system being conservative, the $\bar{\Omega}_i$ are real, up to the point of loss of stability by divergence at $\bar{U}_i = 2.12 \times 10^{-2}$, which is denoted by A in Figure 4.1. Beyond A, the first ($m = 1$) mode locus bifurcates and the eigenfrequencies become purely imaginary. The behaviour of the second ($m = 2$) mode is different, since its eigenfrequencies never become purely imaginary as those of the first mode do. However, at point B ($\bar{U}_i = 2.73 \times 10^{-2}$), the loci of the first and second modes coalesce and the eigenfrequencies become complex; one of the two has a negative imaginary part, indicating that beyond B the system is subject to coupled-mode flutter.

It is stressed that both results of the pinned-clamped system and of the clamped-pinned (with outflow model) system in the case of inviscid flow are the same, which indicates that the slope effect at the downstream pinned end has little influence upon the stability of the system. This is in contrast to the observation by Horáček and Zolotarev (1984) that a clamped-pinned shell loses stability for any infinitesimally small inviscid flow.

A typical Argand diagram for the pinned-clamped system conveying inner viscous flow is shown in Figure 4.2 (for $n = 3$, $m = 1, 2, 3$). It can be seen that for

the first axial mode ($m = 1$) the system loses stability by divergence at point A ($\bar{U}_i = 3.98 \times 10^{-2}$, which is higher than for inviscid flow), followed by single mode flutter at point B ($\bar{U}_i = 4.17 \times 10^{-2}$), as opposed to coupled-mode flutter for the clamped-clamped system (Païdoussis *et al.* 1985). For the clamped-pinned system, the dynamical behaviour is qualitatively similar to that of the pinned-clamped one.

More extensive results in which n was varied are shown in Table 4.1 for the pinned-clamped system, and in Table 4.2 for the clamped-pinned system. It is seen that all modes are stabilized, by varying degrees, by the inclusion of steady viscous terms. It is also seen that stability according to inviscid theory is lost in the third circumferential mode, $n = 3$, for both the pinned-clamped and clamped-pinned systems. On the other hand, when the steady viscous forces are taken into account, stability is lost in the fifth circumferential mode, $n = 5$, for the pinned-clamped system (Table 4.1), but in the fourth circumferential mode, $n = 4$, for the clamped-pinned system (Table 4.2).

The physical explanation for this stabilizing influence of viscous effects is the same as for clamped-clamped shells (Païdoussis, Misra and Chan 1985): the steady loads due to viscosity induce a tensile hoop stress, and either a tensile axial load in the clamped-pinned system or a compressive axial load in the pinned-clamped system, the former being the dominant factor since the hoop stress is much greater than the axial one. The hoop stress effectively renders the shell stiffer, thus raising the dimensionless critical flow velocity, $\bar{U}_{ic}$. However, this effect is not very pronounced, since for this shell L/a is only 11; calculations for larger L/a will be presented in Section 4.3.3.

A final point of interest in the results of Tables 4.1 and 4.2 is associated with the fact that the dimensionless critical *viscous flow* velocities in the case of the pinned-

clamped system are higher than those in the case of the clamped-pinned system, because the distribution of pre-stress resultants caused by basic loads along the flexible shell is different, which results in the pinned-clamped system being effectively stiffer than the clamped-pinned system in the case of inner viscous flow. This is because the highest levels of hoop pre-stress occur at the upstream end, where the pinned-clamped system is *softest* and hence most susceptible to being stiffened by this pressurization effect (refer to Figure 4.9).

4.3.2 Effect of Annular Gap

The effect of narrowing the annular gap on stability of the system was investigated by means of inviscid theory only. Although the annulus is filled with quiescent fluid, this fluid nevertheless does participate in the dynamics since it adds to the system inertia; examination of the generalized fluid forces [equation (2.62)] on the inner shell shows that setting $\bar{U}_o = 0$ does not totally eliminate the forces associated with the annular fluid. The results for the critical flow velocity, $\bar{U}_{ic}$, corresponding to $n = 1-8$ are shown numerically in Table 4.3 and graphically in Figure 4.3.

It is seen that there is a reduction in $\bar{U}_{ic}$ for $n \geq 3$ as the annular gap size is diminished; a tenfold diminution in the annular gap leads to a 5% reduction in the overall (the lowest) critical velocity $\bar{U}_{ic}$, which corresponds to the $n = 3$ mode. The physical reason for this destabilizing effect of stagnant annular fluid is associated with the correspondingly large increase in virtual, or added, mass. Thus, although the stiffness of the system is not affected by the annular gap size, the increase in added mass may be thought of as an *effective* reduction in stiffness, hence causing a reduction in the *overall* critical flow velocity $\bar{U}_{ic}$, namely $\bar{U}^*_{ic}$. The effect of annular gap on $\bar{U}_{ic}$ for small n ($n = 1, 2$) is negligible, as seen in Figure 4.3.

4.3.3 Effect of Length of the Shell

The results for the overall critical flow velocity $\bar{U}_{ic}^{*}$ and the associated circumferential wave number n are presented in Table 4.4 and Figure 4.4 for different length-to-radius of the shell, L/a; the radius a was fixed at $(10/11) \times 100\,\text{mm}$ as listed in Section 4.1.

According to inviscid-flow theory, $\bar{U}_{ic}^{*}$ is diminished monotonically with increasing L/a. Furthermore, as previously found for the clamped-clamped system (Païdoussis and Denise 1972) and the clamped-free system (Païdoussis *et al.* 1991), the value of n associated with loss of stability becomes smaller as L/a is increased. The situation is slightly more complicated when steady viscous effects are taken into account. As L/a is increased sufficiently, there is a stabilizing effect, with $\bar{U}_{ic}^{*}$ becoming larger ($\bar{U}_{ic}^{*} = 0.0365$ for $L/a = 15$, and even 0.0443 for $L/a = 25$); the physical reason for this phenomenon is that the stabilizing effect of the steady viscous forces of the internal flow, which increases with L/a due to higher pressurization effects, overcomes the destabilizing effect of increased L/a due to the inviscid forces. Here, it should be recalled that the dimensionless $\bar{U}_{ic}$ does not involve length; thus, variations of $\bar{U}_{ic}^{*}$ with L/a correspond to similar variations of the critical *dimensional* flow velocities, U_{ic}^{*}.

Perhaps, the most important point that emerges from Table 4.4 is that the relative difference in $\bar{U}_{ic}^{*}$ between inviscid and viscous versions of the theory increases with L/a: for $L/a = 5$, this difference is 55% (based on the inviscid results) whereas it becomes 175% for $L/a = 25$. It is quite obvious that steady viscous effects are hardly negligible for long shells.

4.4 Annular Flow Alone

4.4.1 General Dynamics of the System

In the present case, the flow is purely annular, while the fluid filling the interior of the inner shell is stagnant. Results were again obtained with both inviscid and viscous versions of the theory, so that steady viscous effects of the annular flow could be assessed.

In the case of inviscid annular flow, typical results of the variation of the real and imaginary parts of the dimensionless eigenfrequencies, $\bar{\Omega}_i$, with increasing dimensionless annular flow velocity, $\bar{U}_o$, are shown in Figure 4.5 (for $n = 3$, $m = 1, 2, 3$); the internal fluid is stagnant and its static pressure is equal to that of the annular fluid at $x = L$, and the system is either pinned-clamped or clamped-pinned. The situation is more complex than that of the inviscid internal flow. The system being conservative, the $\bar{\Omega}_i$ are real, up to the point of loss of stability by divergence, which is denoted by A in Figure 4.5. Beyond A, the first ($m = 1$) mode locus bifurcates and the eigenfrequencies become purely imaginary. Beyond point B, the first mode becomes stable again. The behaviour of the second ($m = 2$) mode is different, since its eigenfrequencies never become purely imaginary as those of the first mode do. However, at point C, the loci of the first and second modes coalesce and the eigenfrequencies become complex; one of these two has a negative imaginary part, indicating that beyond C the system is subject to coupled-mode flutter; beyond point D, the coupled-mode flutter vanishes and the second ($m = 2$) mode becomes stable again, but the first mode loses stability by divergence (although which locus belongs to which mode is really arbitrary after C). Similarly to the behaviour of the second mode, the real parts of the eigenfrequencies of the third ($m = 3$) mode never go to

zero. From Figure 4.5, it is seen that, at point E, the loci of the second and third modes coalesce and the eigenfrequencies become complex, one of which has a negative imaginary part, indicating that beyond E the system is subject to coupled-mode flutter again.

Similarly to the case of internal flow, it is noted that the results for both the pinned-clamped system and of the clamped-pinned (with outflow model) system in the case of inviscid annular flow are the same, which indicates that the slope effect at the downstream pinned end has little influence upon the stability of the system. This is in contrast to the observation by Horáček and Zolotarev (1984).

A typical Argand diagram for the pinned-clamped system conveying annular *viscous flow* is shown in Figure 4.6 (for $n = 3$, $m = 1, 2$). It can be seen that the system loses stability by divergence in the first axial mode ($m = 1$) at $\bar{U}_0 = 0.267 \times 10^{-2}$, which is denoted by A in Figure 4.6. Beyond A, the first-mode locus bifurcates and the eigenfrequencies become purely imaginary. The behaviour of the second mode is similar. At point C, i.e. when $\bar{U}_i = 1.03 \times 10^{-2}$, the eigenfrequencies of both the first and the second mode become complex; one of the two has a negative imaginary part, indicating that beyond C the system is subjected to coupled-mode flutter, similar to coupled-mode flutter for the clamped-clamped system (Païdoussis *et al.* 1985). It should be noted that this flutter is here initiated with vanishingly small real frequency (point C in the figure). For the clamped-pinned system, the dynamical behaviour is qualitatively similar to that of the pinned-clamped one.

The values of $\bar{U}_{oc}$ for different n are shown in Table 4.5 for the pinned-clamped system and in Table 4.6 for the clamped pinned system. It is observed that, for all n, $\bar{U}_{oc}$ according to the viscous theory is much less than that obtained via inviscid theory in both pinned-clamped and clamped-pinned cases. It is also seen that, for

both the pinned-clamped system (Table 4.5) and the clamped-pinned system (Table 4.6), stability according to the inviscid theory is lost in the third circumferential mode, $n = 3$, but when the steady viscous forces taken into account, stability is lost in the fourth circumferential mode, $n = 4$.

The physical explanation for this destabilizing influence of viscous effects is the same as for clamped-clamped shells (Païdoussis *et al.* 1985): the steady loads due to viscosity induce a compressive hoop stress, and either a tensile axial load in the clamped-pinned system or a compressive axial load in the pinned-clamped system, the hoop stress being the dominant factor since it is two orders of magnitude greater than the axial one. The hoop compressive stress effectively reduces the shell stiffness, thus greatly lowering $\bar{U}_{oc}$.

A final point of interest in the results of Table 4.5 and Table 4.6 is associated with the fact that the dimensionless critical viscous flow velocities in the case of the pinned-clamped system are lower than those in the case of the clamped-pinned system, because the distribution of pre-stress resultants caused by basic loads along the flexible shell is different, which results in the pinned-clamped system being effectively more flexible than the clamped-pinned system in the case of annular viscous flow. This is so, for the same reason that was discussed in the last paragragh of Section 4.3.1 (refer to Figure 4.10).

4.4.2 Effect of Length of the Shell

Shown in Figure 4.7 are the results for $\bar{U}_{oc}^{*}$ as a function of the ratio L/a in a 1/10-gap system [i.e., $(b-a)/a = 1/10$]. It should be reiterated here that $\bar{U}_{oc}^{*}$ denotes the overall (lowest) critical flow velocity, whereas $\bar{U}_{oc}$ refers to the critical flow velocity associated with some particular n. Two variants of the theory have been used to

calculate $\bar{U}_{oc}^{*}$; in the inviscid variant, the fluid is assumed to be purely inviscid, while in the viscous variant, steady viscous effects of the flow are taken into account. The system is pinned-clamped.

The value of $\bar{U}_{oc}^{*}$ predicted by the viscous variant of the theory is of the order of three to five times smaller than that by the inviscid counterpart as L/a is varied from 5 to 25. This destabilizing effect of the steady viscous forces with increasing L/a is not surprising since, the destabilizing effect of the crushing compressive load q_3 appearing in equations (2.1)-(2.3) is in fact proportional to L; thus, these results quantify the influence of L/a on stability. The results here are similar to those obtained by Nguyen (1992) for a clamped-clamped system under the same conditions.

In general, as L/a is increased, $\bar{U}_{oc}^{*}$ decreases, and so does the circumferential mode associated with $\bar{U}_{oc}^{*}$. Consequently, if L is large enough, the shell will eventually lose its stability by divergence in the $n = 1$ (beam) mode. This observation is similar to that made earlier by Païdoussis and Denise (1972) for the system of an unconfined clamped-clamped shell containing internal flow.

4.4.3 Effect of Shell Thickness

The variation of $\bar{U}_{oc}^{*}$ with shell thickness, expressed nondimensionally as h_i/a, is plotted in Figure 4.8, for the pinned-clamped system. Again, the steady viscous forces have a destabilizing effect on the system. As may be seen from the figure, $\bar{U}_{oc}^{*}$ increases with h_i/a, whereas the circumferential mode n associated with $\bar{U}_{oc}^{*}$ decreases. The effect of h_i/a on $\bar{U}_{oc}^{*}$ and n may be understood by considering the strain energies resulting from circumferential bending and stretching of the shell.

For shells with both ends supported, if the strain energies are plotted against the circumferential wave number n, it will be observed that the bending energy $\mathcal{E}_b$

increases with n, while the stretching energy $\mathcal{E}_s$ varies in the reverse manner, resulting in a curve for the total strain energy $\mathcal{E}_t$ (i.e., $\mathcal{E}_t = \mathcal{E}_b + \mathcal{E}_s$) of quasi-parabolic form (Arnold and Warburton 1949). The approximate value of n at which $\mathcal{E}_t$ is minimum may be determined when $\mathcal{E}_b = \mathcal{E}_s$. Considering an element of the shell, so small as to be approximated as a plate of thickness h_i, it has been shown (Timoshenko and Woinowsky-Krieger 1959) that for such a plate $\mathcal{E}_b$ is proportional to h_i^3 while $\mathcal{E}_s$ is proportional to h_i. The *notional* relationships between $\mathcal{E}_b$, $\mathcal{E}_s$ and h_i are thus

$$\mathcal{E}_b = C_b n h_i^3, \qquad \mathcal{E}_s = \frac{C_s}{n} h_i,$$

where C_b and C_s are some proportionality constants. Hence, equating $\mathcal{E}_b = \mathcal{E}_s$ leads to

$$n^2 = \frac{C_s}{C_b h_i^2},$$

which implies that, as far as $(\mathcal{E}_t)_{min}$ is concerned, n decreases with increasing h_i, and

$$(\mathcal{E}_t)_{min} = 2\sqrt{C_b C_s} h_i^2.$$

On the other hand, the energy supplied by the flowing fluid $\mathcal{E}_f$, required to overcome $\mathcal{E}_t$ and hence to collapse the shell, comes from the centrifugal fluid-dynamic force, which is known to be proportional to U^2 according to inviscid theory. Implicitly, $\mathcal{E}_f$ is also proportional to U^2,

$$\mathcal{E}_f = U^2 f(n),$$

where $f(n)$ is some unknown function of the circumferential wave number n. It is obvious that the system loses stability when

$$\mathcal{E}_t - \mathcal{E}_f = \mathcal{E}_t - U^2 f(n) = 0.$$

Since $(\mathcal{E}_t)_{min}$ is proportional to h_i^2 and $f(n)$ is a weak function of n, this implies that $\bar{U}_{oc}^*$ will become higher if there is an increase in $(\mathcal{E}_t)_{min}$ due to increasing h_i.

4.5 Comparison of Results

Dimensionless critical flow velocities (of only the annular or the inner fluid) for inviscid and viscous flow with pinned-clamped and clamped-pinned end conditions are shown in Table 4.9 for a 1/10-gap system. For comparison purposes, the results obtained with clamped-clamped (Païdoussis *et al.* 1985) and clamped-free (Païdoussis *et al.* 1991) end conditions are also presented.

It is recalled that the critical velocities obtained from the inviscid theory for pinned-clamped end conditions are identical to those obtained with clamped-pinned ones, which means that the slope effect at the downstream pinned end has little influence upon the stability of the system. This is in contrast to the findings by Horáček and Zolotarev (1984). It may also be noted that in the case of inviscid flow (either only annular or only internal), the system with either pinned-clamped or clamped-pinned end conditions loses stability by divergence first ($\bar{U}_{oc} = 1.14 \times 10^{-2}$, $\bar{U}_{ic} = 2.12 \times 10^{-2}$), followed by coupled-mode flutter ($\bar{U}_{oc} = 1.54 \times 10^{-2}$, $\bar{U}_{ic} = 2.73 \times 10^{-2}$), behaving like one with clamped-clamped end conditions conveying inviscid flow (Païdoussis *et al.* 1984).

Similarly to the cases considered in the previous studies (Païdoussis *et al.* 1985, 1991), viscous effects destabilize pinned-clamped or clamped-pinned shells for annular flow, but stabilize them for internal flow. In contrast to the case of inviscid flow, the critical viscous flow velocities for the pinned-clamped system are not the same as those for the clamped-pinned system but are lower in the case of annular flow and higher in the case of inner flow, because the distribution of pre-stress resultants caused by the basic loads along the shells (induced by pressurization and surface traction) is different, which results in the pinned-clamped system being effectively more flexible than the clamped-pinned system in the case of annular viscous flow, but stiffer in

the case of internal viscous flow. The reason was discussed in the last paragragh of Section 4.3.1. The interested reader can refer to Figures 4.9 and 4.10 from which it is seen that the highest levels of hoop pre-stress resultant N_θ occur at the upstream and are much greater than axial pre-stress resultant N_x.

From Table 4.9, it is noted that in the case of either inviscid or viscous flow, the critical velocities obtained with clamped-pinned or pinned-clamped end conditions are lower than those with clamped-clamped end conditions and higher than those with clamped-free end conditions, since the clamped-pinned or pinned-clamped system is more flexible than the clamped-clamped system and stiffer than the clamped-free system. This is another verification that the present theory is correct, since it makes sense in physical terms.

4.6 Summary

Chapter 4 has presented in detail the results for the dynamical behaviour of the system of either clamped-pinned or pinned-clamped coaxial, thin cylindrical conduits, with the outer cylinder being rigid while the inner one (the shell) remains flexible. The system was subjected to internal flow or annular flow. Investigated were the effects of varying annular gap, of varying length of the shell, and of steady viscous loads on stability of the system.

In the case of *internal flow*, the clamped-pinned or pinned-clamped system loses stability by divergence first. If the fluid is considered to be inviscid, this is followed by coupled-mode flutter; for viscous flow, this is followed by single-mode flutter. For large n ($n > 2$), reducing the annular gap diminishes the critical flow velocities. It is found that the critical velocities are diminished with increasing L/a for inviscid flow,

but they increase with increasing L/a for viscous flow, as discussed in Section 4.3.3. Viscous effects stabilize the system, and result in the clamped-pinned system being effectively more flexible than the pinned-clamped system.

In the case of *annular flow*, the system loses stability by divergence first, followed by coupled-mode flutter. As L/a is increased, the critical flow velocity decreases, as disscused in Section 4.4.2. It is found that the critical velocity increases with increasing h_i/a. In all cases, viscous effects destabilize the system, and result in the clamped-pinned system being stiffer than the pinned-clamped system.

Finally, comparison between results obtained by the present theory and those obtained earlier with clamped-clamped and clamped-free end conditions were presented.

Table 4.1: The dimensionless inner critical flow velocities, $\bar{U}_{ic}$, with $n = 1 - 8$ for the 1/10-gap system subjected to internal flow according to the inviscid and viscous (i.e., including steady viscous effect) versions of the theory, with the axial mode number m involved in each case. The system is pinned-clamped. The instability type is marked as: D=divergence, S=single-mode flutter, C=coupled-mode flutter.

Pinned-Clamped, Internal Flow Only

n	Critical Flow Velocity, $\bar{U}_{ic}$					
	Inviscid Theory	Type	m	Viscous Theory	Type	m
1	0.0726 0.0998	D C	1 1+2	*	*	*
2	0.0285 0.0452	D C	1 1+2	0.0461 0.0505	D S	1 1
3	0.0212 0.0273	D C	1 1+2	0.0398 0.0417	D S	1 1
4	0.0233 0.0262	D C	1 1+2	0.0365 0.0413	D S	1 1
5	0.0259 0.0272	D C	1 1+2	0.0353 0.0420	D S	1 1
6	0.0307 0.0293	D C	1 1+2	0.0393	D	1
7	0.0317 0.0343	D C	1 1+2	*	*	*
8	0.0388 0.0440	D C	1 1+2	*	*	*

* No calculations were conducted for these circumferential modes.

Table 4.2: The dimensionless inner critical flow velocities, $\bar{U}_{ic}$, with $n = 1 - 8$ for the 1/10-gap system subjected to internal flow according to the inviscid and viscous (i.e., including steady viscous effect) versions of the theory, with the axial mode number m involved in each case. The system is clamped-pinned. The instability type is marked as: D=divergence, S=single-mode flutter, C=coupled-mode flutter.

Clamped-Pinned, Internal Flow Only

n	Critical Flow Velocity, $\bar{U}_{ic}$					
	Inviscid Theory	Type	m	Viscous Theory	Type	m
1	0.0726 0.0998	D C	1 1+2	*	*	*
2	0.0285 0.0452	D C	1 1+2	*	*	*
3	0.0212 0.0273	D C	1 1+2	0.0328 0.0424	D S	1 1
4	0.0233 0.0262	D C	1 1+2	0.0315 0.0385	D S	1 1
5	0.0259 0.0272	D C	1 1+2	0.0319 0.0393	D S	1 1
6	0.0307 0.0293	D C	1 1+2	*	*	*
7	0.0317 0.0343	D C	1 1+2	*	*	*
8	0.0388 0.0440	D C	1 1+2	*	*	*

* No calculations were conducted for these circumferential modes.

Table 4.3: The critical flow velocities, $\bar{U}_{ic}$, associated with $n = 1-8$ for the (1/10)- and (1/100)-gap systems subjected to internal flow according to inviscid theory, with the axial mode number m involved in each case. The system is either pinned-clamped or clamped-pinned. The instability type is marked as: D=divergence, C=coupled-mode flutter; thus, 1D means divergence associated with $m = 1$.

n	Critical Flow Velocity, $\bar{U}_{ic}$			
	1/10-Gap	*m*	1/100-Gap	*m*
1	0.0726	1D	0.0743	1D
2	0.0285	1D	0.0295	1D
3	0.0212	1D	0.0201	1D
4	0.0233	1D	0.0217	1D
5	0.0259	1D	0.0238	1D
6	0.0293	1+2C	0.0261	1D
7	0.0317	1D	0.0283	1D
8	0.0388	1D	0.0331	1D

Table 4.4: The effect of varying the length-to-radius ratio on the overall critical flow velocity, $\bar{U}_{ic}^{*}$, for the 1/10-gap system subjected to internal flow only, according to the inviscid and viscous (i.e., including steady viscous effects) versions of the theory; the circumferential wave number n associated with $\bar{U}_{ic}^{*}$ is shown in each case.

L/a	The Overall Critical Flow Velocity $\bar{U}_{ic}^{*}$				
	Inviscid Flow	n	Viscous Flow	n	Difference in %
5	0.0265	4	0.0411	6	55.1%
10	0.0217	3	0.0353	5	62.7%
15	0.0207	3	0.0365	4	76.3%
20	0.0178	2	0.0393	3	120.8%
25	0.0161	2	0.0443	2	175.2%

Table 4.5: The dimensionless annular critical flow velocities, $\bar{U}_{oc}$, with $n = 2 - 5$ for the 1/10-gap system subjected to annular flow according to the inviscid and viscous (i.e., including steady viscous effect) versions of the theory, showing the axial mode number m involved in each case. The system is pinned-clamped. The instability type is marked as: D=divergence, C=coupled-mode flutter.

Pinned-Clamped, Annular Flow Only

n	Critical Flow Velocity, $\bar{U}_{oc}$					
	Inviscid Theory	Type	m	Viscous Theory	Type	m
2	0.0127 0.0212	D C	1 1+2	0.0067 0.0191	D C	1 1+2
3	0.0114 0.0154	D C	1 1+2	0.00267 0.0103	D C	1 1+2
4	0.0144 0.0216	D C	1 1+2	0.00260 0.0093	D C	1 1+2
5	*	*	*	0.00305	D	1

* No calculation was conducted for this circumferential mode.

Table 4.6: The dimensionless annular critical flow velocities, $\bar{U}_{oc}$, with $n = 2 - 5$ for the 1/10-gap system subjected to annular flow according to the inviscid and viscous (i.e., including steady viscous effect) versions of the theory, showing the axial mode number m involved in each case. The system is clamped-pinned. The instability type is marked as: D=divergence, S=single-mode flutter, C=coupled-mode flutter.

Clamped-Pinned, Annular Flow Only

n	Critical Flow Velocity, $\bar{U}_{oc}$					
	Inviscid Theory	Type	m	Viscous Theory	Type	m
2	0.0127 0.0212	D C	1 1+2	*	*	*
3	0.0114 0.0154	D C	1 1+2	0.00306 0.00910	D C	1 1+2
4	0.0144 0.0216	D C	1 1+2	0.00295 0.00851	D S	1 2
5	*	*	*	0.00329 0.00787	D S	1 3

*No calculations were conducted for these circumferential modes.

Table 4.7: The effect of varying the length-to-radius ratio on the overall critical flow velocity, $\bar{U}_{oc}^{*}$, for the 1/10-gap system subjected to annular flow, according to the inviscid and viscous (i.e., including steady viscous effects) versions of the theory; the circumferential mode number n associated with $\bar{U}_{oc}^{*}$ is shown in each case.

L/a	The Overall Critical Flow Velocity $\bar{U}_{oc}^{*}$			
	Inviscid Flow	n	Viscous Flow	n
5	0.0165	4	0.0059	5
10	0.0117	3	0.0029	4
15	0.0097	2	0.0017	3
20	0.0079	2	0.0013	3
25	0.0071	2	0.0011	2

Table 4.8: The effect of varying the thickness-to-radius ratio on the overall critical flow velocity, $\bar{U}^*_{oc}$, for the 1/10-gap system subjected to annular flow, according to the inviscid and viscous (i.e., including steady viscous effects) versions of the theory; the circumferential mode number n associated with $\bar{U}^*_{oc}$ is shown in each case.

h_i/a $\times 10^3$	The Overall Critical Flow Velocity $\bar{U}_{oc}^* \times 10^2$			
	Inviscid Flow	n	Viscous Flow	n
5	1.05	3	0.25	4
10	1.77	2	0.55	3
15	2.29	2	0.97	3
20	2.81	2	1.49	3
25	3.35	2	1.89	2

Table 4.9: Comparison between critical flow velocities, $\bar{U}_{ic}$ and $\bar{U}_{oc}$, as calculated by the present theory and by Païdoussis *et al.* (1985, 1991) for the 1/10-gap system with a rigid outer cylinder, for the circumferential mode number $n = 3$. The instability type is marked as : D=divergence, C=usual coupled-mode flutter*, SM=same-mode coupled-mode flutter, S=single mode flutter. * (C1+2) means: the first ($m = 1$) and the second ($m = 2$) axial modes are involved.

Critical Flow Velocities, $\bar{U}_{ic}x10^2$ and $\bar{U}_{oc}x10^2$					
System	Flow	Inviscid Theory	Type	Viscous Theory	Type
Pinned-Clamped	Annular Flow Only	1.14 1.54	D1 C1+2	0.267 1.03	D1 C1+2
	Internal Flow Only	2.12 2.73	D1 C1+2	3.98 4.17	D1 SM1
Clamped-Pinned	Annular Flow Only	1.14 1.54	D1 C1+2	0.306 0.910	D1 C1+2
	Internal Flow Only	2.12 2.73	D1 C1+2	3.28 4.24	D1 SM1
Clamped-Free (Paidoussis et al. 1991)	Annular Flow Only	2.46	S3	0.28 1.02	D1 C1+2
	Internal Flow Only	2.77	S3	3.11	S3
Clamped-Clamped (Paidoussis et al. 1985)	Annular Flow Only	1.36 1.85	D1 C1+2	0.36 1.04	D1 C1+2
	Internal Flow Only	2.55 3.14	D1 C1+2	4.14 4.86	D1 C1+2

Figure 4.1: The real and imaginary parts of the dimensionless eigenfrequencies, Ω_i, of the 1/10-gap system (see equation (4.1)) with inviscid internal water flow and a stagnant annular fluid (water), as functions of the dimensionless inner flow velocity, $\bar{U}_i$, when the outer cylinder is rigid and the inner shell (steel) is pinned-clamped or clamped-pinned; for $n = 3$, $m = 1, 2, 3$.

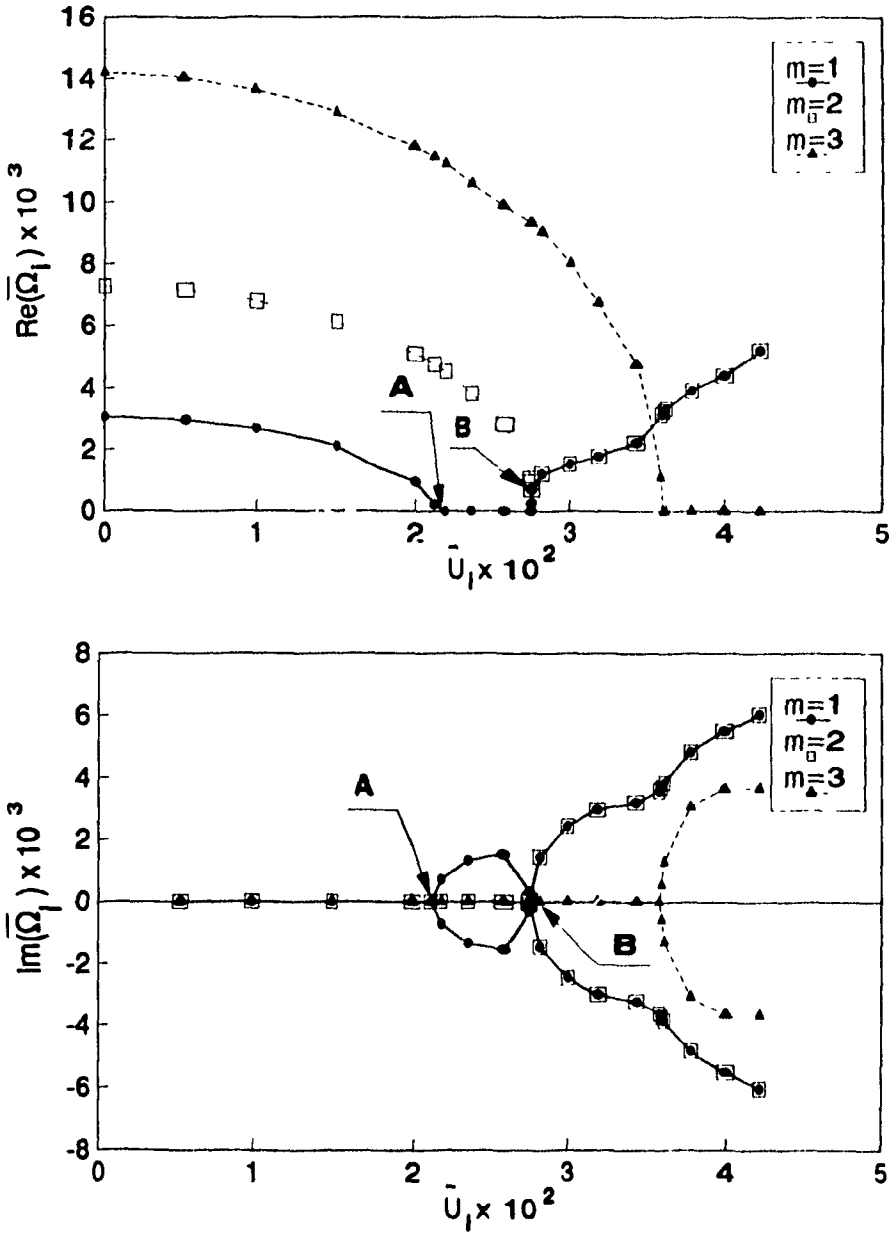

Figure 4.2: The real and imaginary parts of the dimensionless eigenfrequencies, $\bar{\Omega}_i$, of the 1/10-gap system (see equation (4.1)) with viscous internal water flow and a stagnant annular fluid (water), as functions of the dimensionless inner flow velocity, $\bar{U}_i$, when the outer cylinder is rigid and the inner shell (steel) is pinned-clamped; for $n = 3$, $m = 1, 2, 3$.

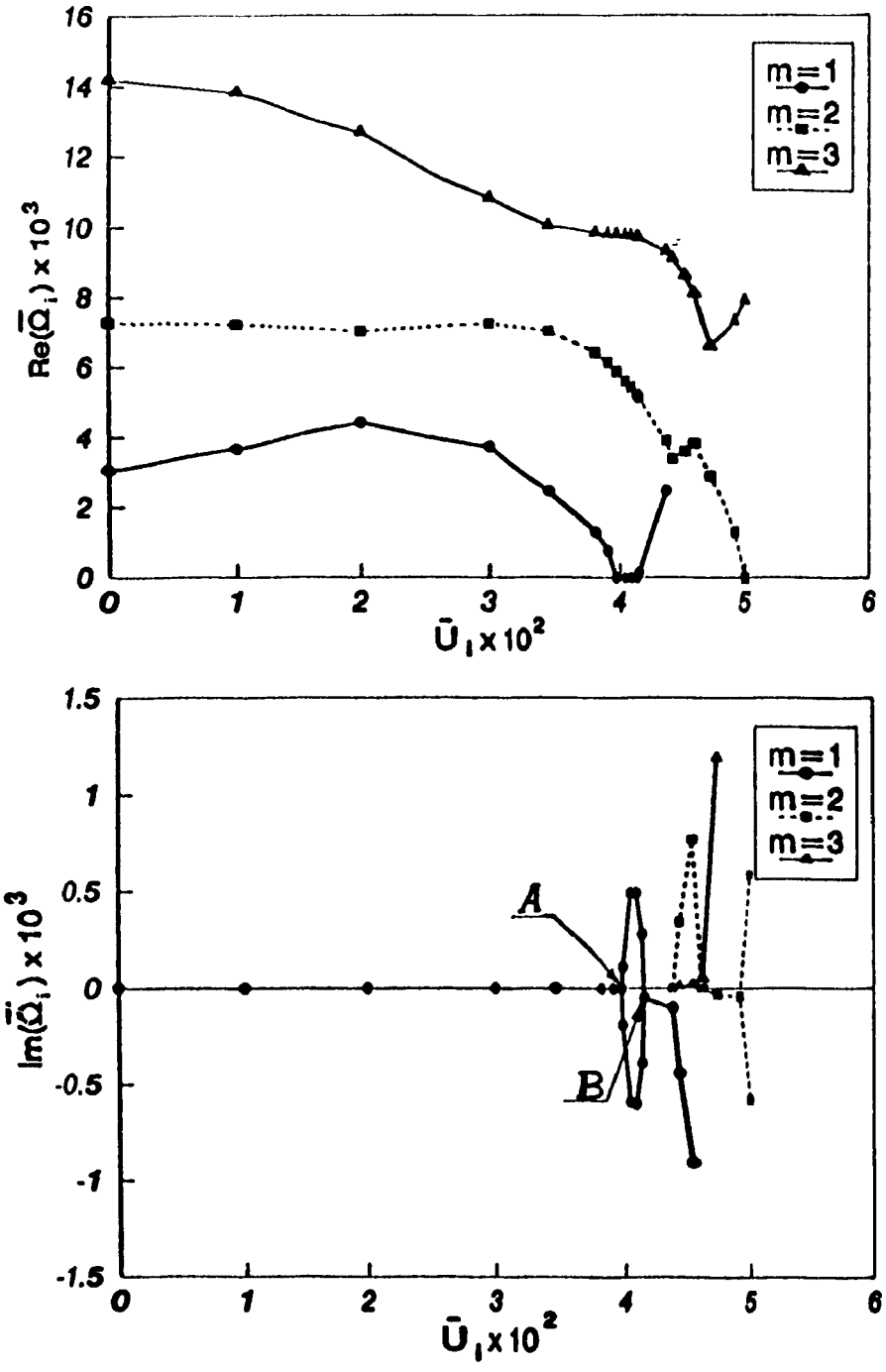

Figure 4.3: The dimensionless critical flow velocity, $\bar{U}_{ic}$, of a pinned-clamped system, surrounded by quiescent annular fluid (water) while conveying internal water flow, as a function of the circumferential wave number n for two different annular gaps. These calculations were done with the inviscid theory.

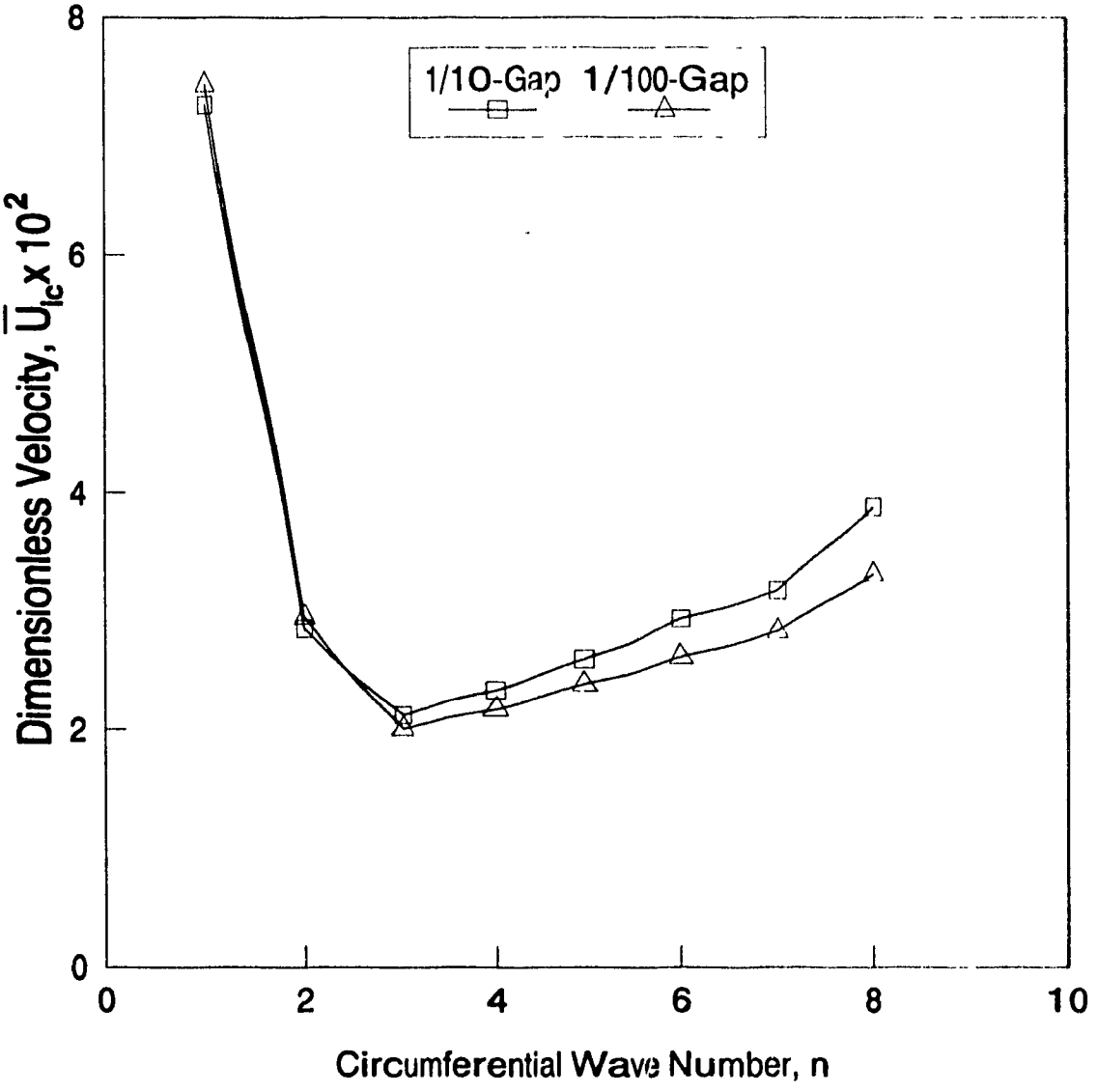

Figure 4.4: The effect of L/c on the overall (lowest) critical dimensionless flow velocity, $\bar{U}_{ic}^{*}$, for the 1/10-gap system conveying internal water flow and quiescent annular fluid (water); the circumferential wave number n associated with the first loss of stability is shown in the figure. The system is pinned-clamped.

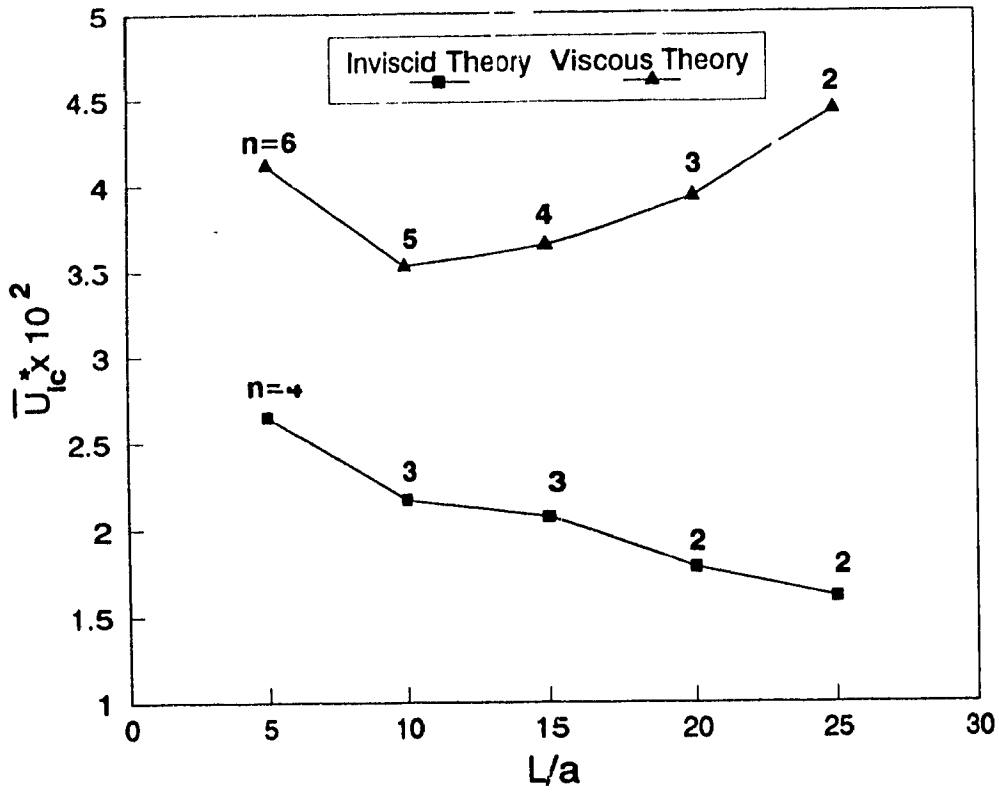

Figure 4.5: The real and imaginary parts of the dimensionless eigenfrequencies, Ω_i, of the 1/10-gap system with inviscid annular water flow and a stagnant internal fluid (water), as functions of the dimensionless annular flow velocity, U_o, when the outer cylinder is rigid and the inner shell is pinned-clamped or clamped-pinned, for $n = 3$, $m = 1,\ 2,\ 3$.

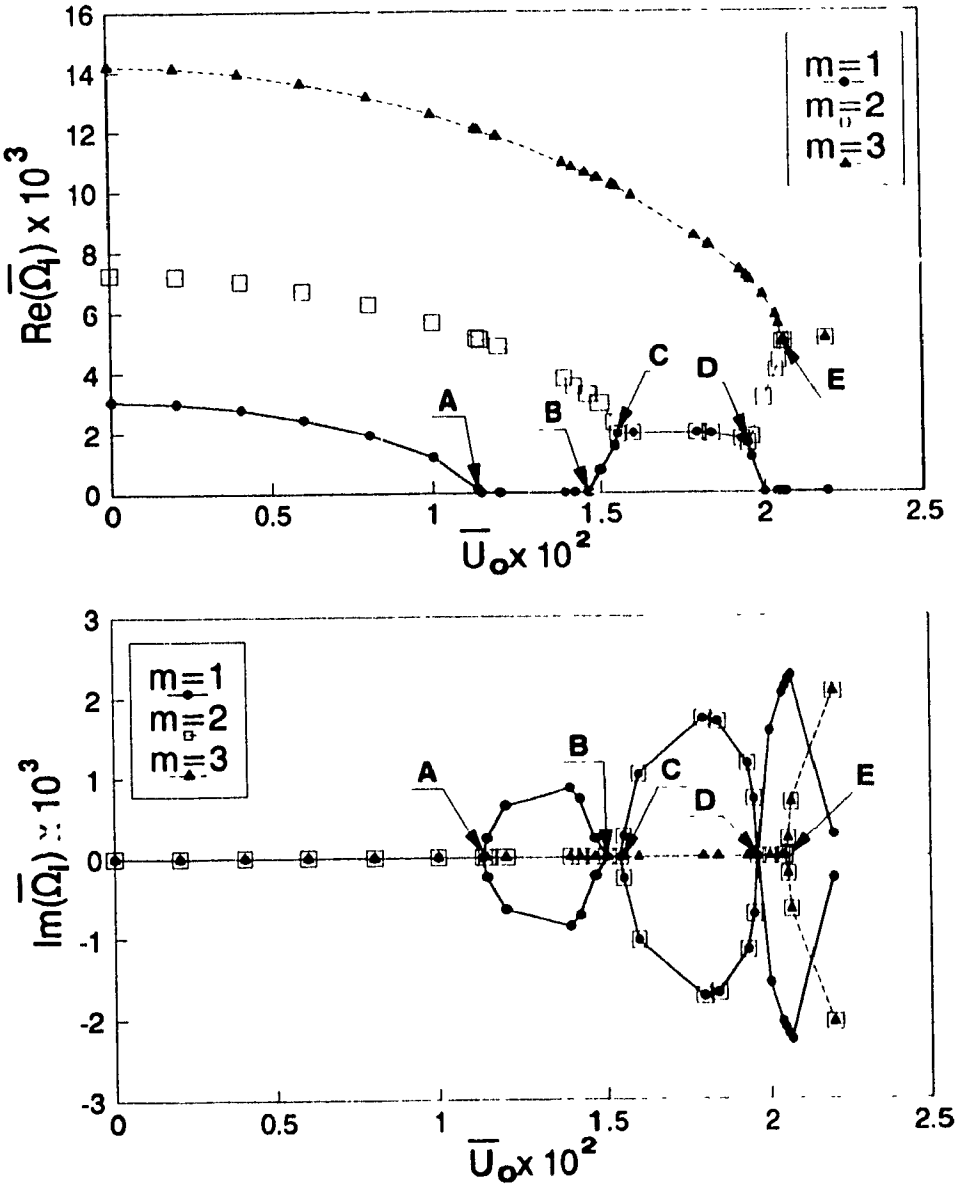

Figure 4.6: Typical Argand diagram involving the real, $\mathrm{Re}(\bar{\Omega}_i)$, and imaginary, $\mathrm{Im}(\bar{\Omega}_i)$, parts of the dimensionless eigenfrequencies of the so-called 1/10-gap system with viscous annular water flow and a stagnant internal fluid (water), as the dimensionless annular flow velocity $\bar{U}_o$ is varied, when the outer cylinder is rigid and the inner shell (steel) is pinned-clamped; for $n = 3$, $m = 1$, 2.

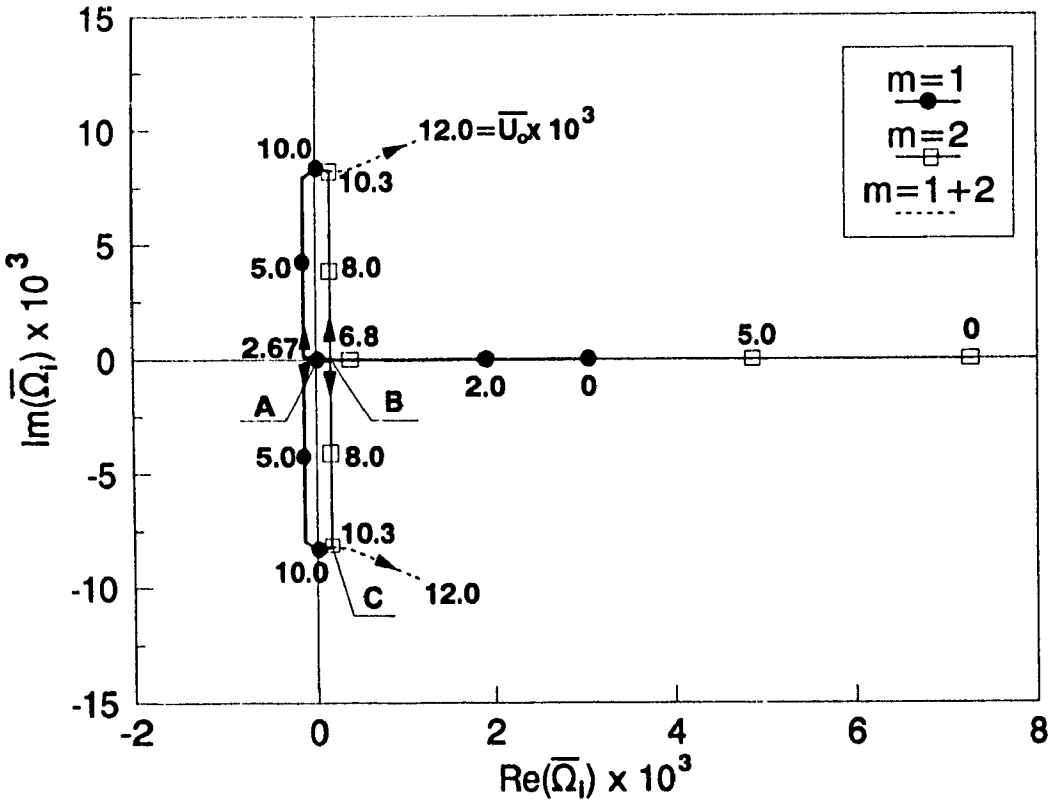

Figure 4.7: The effect of L/a on the overall (lowest) critical dimensionless flow velocity, $\bar{U}^*_{oc}$, for the 1/10-gap system with internal water flow and quiescent annular fluid (water); the circumferential wave number n associated with the first loss of stability is shown in the figure. The system is pinned-clamped.

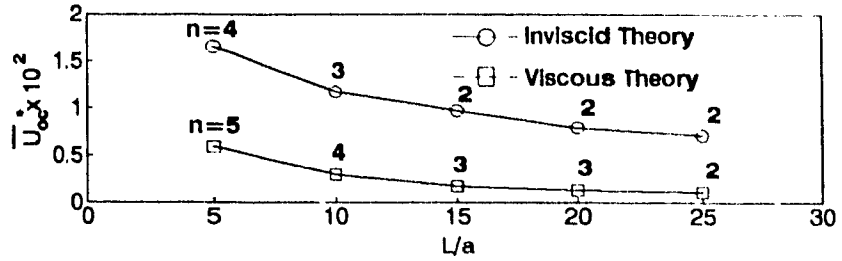

Figure 4.8: The overall critical dimensionless annular flow velocity, $\bar{U}^*_{oc}$, in the 1/10-gap system as a function of the dimensionless wall-thickness of the shell h_1/a, with the circumferential mode, n, associated with the first loss of stability indicated in the figure. The shell (steel) is pinned-clamped and the inner fluid (water) is stagnant.

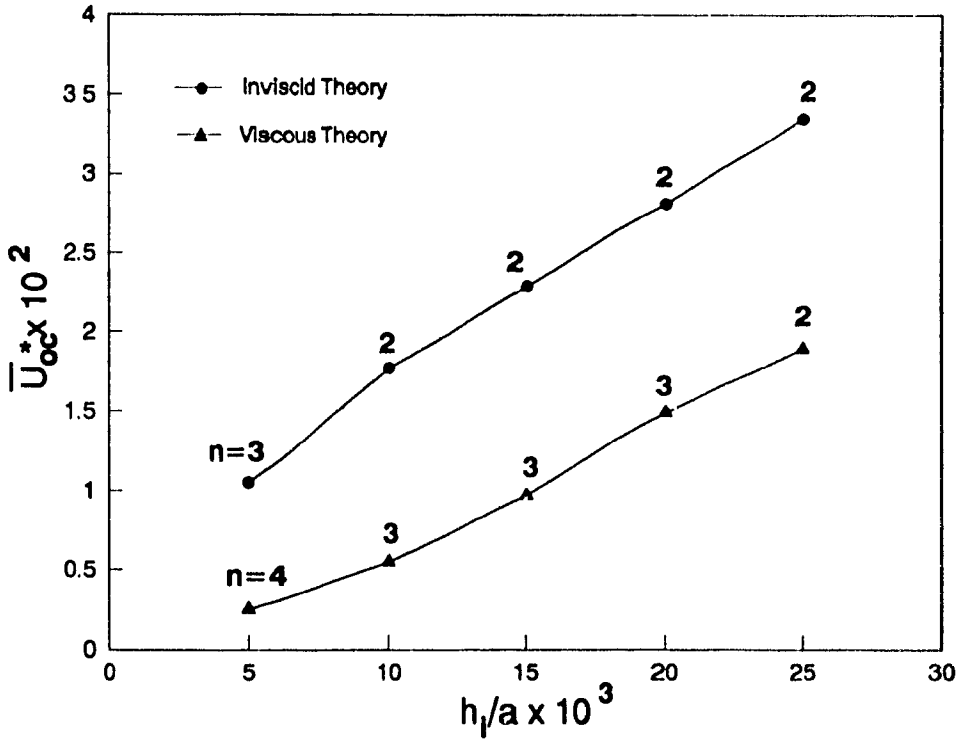

Figure 4.9: Comparison between stresses induced by internal viscous flow in the case of pinned-clamped or clamped-pinned system and those in the case of clamped-clamped system.

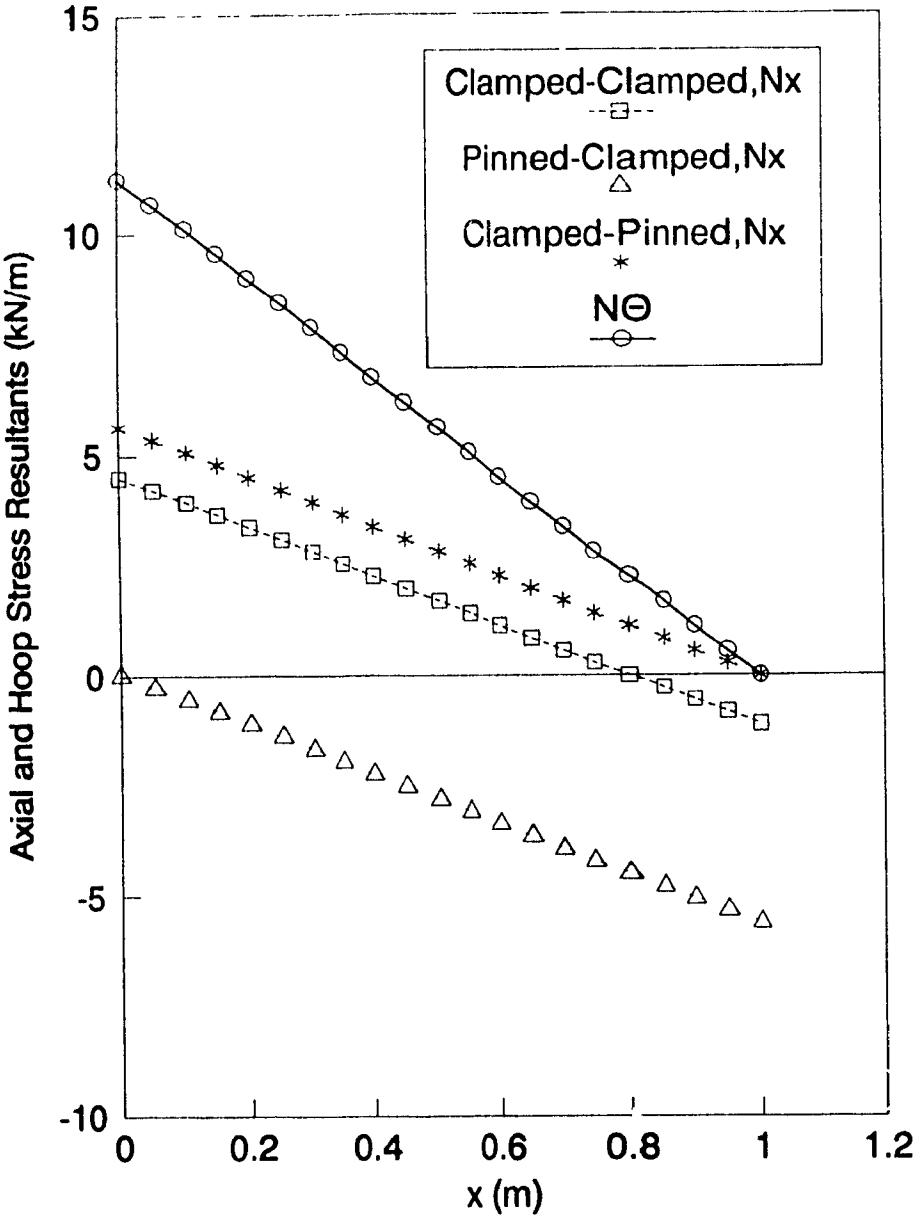

Figure 4.10: Comparison between stresses induced by annular viscous flow in the case of pinned-clamped or clamped-pinned system and those in the case of clamped clamped system.

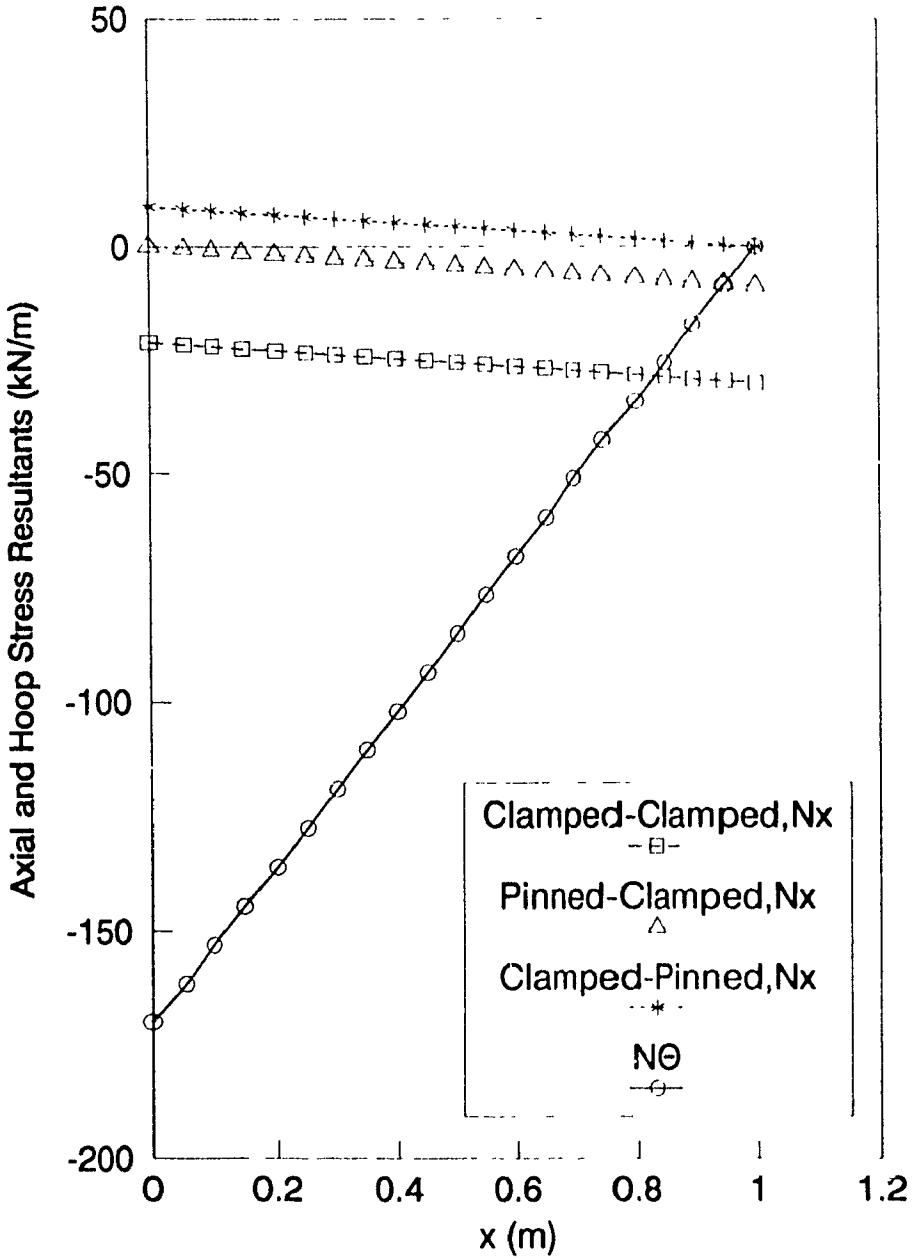

Chapter 5

Conclusion

5.1 Contributions of the Thesis

This thesis presented an analytical model for the study of the stability of pinned-clamped and clamped-pinned coaxial cylindrical shells subjected to internal and/or annular incompressible viscous fluid flow. The viscous nature of the fluid results in both steady and unsteady viscosity-related loads being exerted on the shells, the latter of which is neglected here and will be the subject of future investigation. Upstream pressurization of the flow (to overcome frictional pressure drop) and skin friction on the shell surfaces are taken into account, generating time-averaged normal and tangential loads on the shells. In this model, the shell motions were described by Flügge's shell equations, suitably modified to incorporate the time-averaged stress resultants arising from viscous effects. Such steady viscous effects were evaluated for clamped-pinned and pinned-clamped shells, using the same procedure previously proposed by Païdoussis, Misra and Chan (1985) for the system of clamped-clamped shells. The unsteady fluid-dynamic forces in these equations were formulated from potential flow theory: the perturbation pressures on the shells were determined from the perturba-

tion velocity potentials via the unsteady Bernoulli equation, these velocity potentials are governed by the Laplace equation, which was solved by the Fourier transform method.

For the clamped-pinned system, since the downstream end of the shell was simply supported, a so-called out-flow model was utilized in modelling the decay of flow perturbations beyond the pinned end.

The theory was first used to solve test problems involving pinned-clamped cylindrical shells: (i) the natural frequencies of a shell *in vacuo*, which were found to be in excellent agreement with the results obtained by Weingarten's (1964) theory; and (ii) the natural frequencies of a shell conveying inviscid flow, which was found to be in good agreement with the results obtained by beam theory.

The theory was then applied to investigate the dynamic behaviour of a pinned-clamped or clamped-pinned steel shell located coaxially within a rigid cylinder; the system had water flowing within the shell or in the annular region. The following were the main findings.

- In the case of internal flow, both systems lose stability by divergence, followed by the usual coupled-mode flutter, if the flow is inviscid; however, if the fluid is viscous, the system may lose stability by divergence first and then followed by coupled-mode flutter involving branches of the same mode. It was found that, for shell-type motions ($n \geq 2$), flow pressurization and skin friction stabilize the shell by a considerable amount, especially if the shell is long. The presence of the quiescent annular fluid lowers the natural frequencies by increasing the effective inertia of the system. A reduction in the annular gap destabilizes the system by increasing the virtual mass of the annular fluid and hence reducing

the effective stiffness of the system. It was also found that there is no difference between the pinned-clamped system and the clamped-pinned system when conveying inviscid fluid. This is because the comparison functions used (beam eigenfunctions) are not dependent on slope explicitly. However, in the case of inner viscous flow, the pressurization effect makes the pinned-clamped system effectively stiffer than the clamped-pinned system and hence, the former system loses stability at a greater flow velocity than the latter.

- In the case of annular flow, both systems lose stability by divergence, followed by normal type of coupled-mode flutter, if the flow is inviscid; however, if conveying viscous fluid, the system may lose stability by divergence first and then by either same-mode or the usual type of coupled-mode flutter (depending on the circumferential wave number, n). The principal effect of the steady viscous forces is to severely destabilize the system, due to the fact that pressurization of the annular flow results in inward-direction, crushing compressive loads acting on the shell. The value of U_{oc}^{*} is decreased as the length of the shell, L, is increased or its thickness, h_s, is reduced. If the flow is inviscid, the two systems have the same dynamic behaviour; however, viscous effects cause the pinned-clamped system to become more flexible than the clamped-pinned system. This is because the highest levels of hoop pre-stress occur at the upstream end, where the pinned-clamped system is *softest* and hence most susceptible to being softened by this pressurization effect.

- In the calculations, the slope effect of the pinned end of the clamped-pinned system was taken into account in the out-flow model. It was found that it has little influence upon the stability of the system. No difference in dynamic

behaviour was found between the two systems if the flow, either internal or annular, is inviscid; this is in contrast to the results obtained by Horáček and Zolotarev (1984); thus, perhaps due to the simplifications introduced by these researchers, their results must be wrong.

Comparison was made with the existing results for clamped-clamped (Païdoussis, Misra and Chan 1985) and clamped-free (Nguyen 1992) cases, which showed that the present theory is physically reasonable.

5.2 Suggestions for Future Work

Since the analytical model of this thesis neglected the unsteady viscous effects, a new analytical model with these effects taken into account should be developed. Also the results obtained by theory here should be tested experimentally.

Bibliography

[1] ANDERSON, G.L. 1972 A comparison of approximate methods for solving non-conservative problems of elastic stability. *Journal of Sound and Vibration*, **22**, 159-168.

[2] ARNOLD, R.N. and WARBURTON, G.B. 1949 Flexural vibrations of the walls of thin cylindrical shells having freely supported ends. *Proceedings of the Royal Society of London*, **197**, 238-256.

[3] ASHLEY, H. and HAVILAND, G. 1950 Bending vibrations of a pipeline containing flowing fluid. *Journal of Applied Mechanics*, **17**, 229-232.

[4] AU-YANG, M.K. 1976 Free vibration of fluid-coupled coaxial cylindrical shells of different lengths. *Journal of Applied Mechanics*, **98**, 480-484.

[5] BENJAMIN, T.B. 1961a Dynamics of a system of articulated pipes conveying fluid - I. Theory. *Proceedings of the Royal Society (London)*, **261**(A), 457-486.

[6] BENJAMIN, T.B. 1961b Dynamics of a system of articulated pipes conveying fluid - II. Experiments. *Proceedings of the Royal Society (London)*, **261**(A), 487-499.

[7] BRIGHTON, J.A. and JONES, J.B. 1964 Fully developed turbulent flow in annuli. *ASME Journal of Basic Engineering*, **86**, 835-844.

[8] BROWN, S.J. and LIEB, B.W. 1980 A comparison of experimental and theoretical vibration results for narrow gap, fluid-coupled, coaxial flexible cylinders. *American Society of Mechanical Engineers*, Paper No. 80-C2/PVP-104.

[9] CHEN, S.S. 1974 Dynamics of a rod-shell system conveying fluid. *Nuclear Engineering and Design*, **30**, 223-233.

[10] CHEN, S.S. 1975 Vibration of nuclear fuel bundles. *Nuclear Engineering and Design*, **35**, 399-422.

[11] CHEN, S.S. and JENDRZEJCYK, J.A. 1978 Experiments on fluidelastic vibration of cantilevered tube bundles. *ASME Journal of Mechanical Design*, **100**, 540-548.

[12] DOWELL, E.H. 1966 Flutter of infinitely long plates and shells. Part II: Cylindrical shells. *AIAA Journal*, **4**, 1510-1518.

[13] DOWELL, E.H. and WIDNALL, S.E. 1966 Generalized aerodynamic forces on an oscillating cylindrical shell. *Quarterly of Applied Mathematics*, **XXIV**, 1-17.

[14] EL CHEBAIR, A., MISRA, A.K. and PAÏDOUSSIS, M.P. 1990 Theoretical study of the effect of unsteady viscous forces on inner- and annular-flow-induced instabilities of cylindrical shells. *Journal of Sound and Vibration*, **138**, 457-478.

[15] EL CHEBAIR, A., PAÏDOUSSIS, M.P. and MISRA, A.K. 1989 Experimental study of annular flow-induced instabilities of cylindrical shells. *Journal of Fluids and Structures*, **3**, 349-364.

[16] FEODOS'EV, V.P. 1951 Vibrations and stability of a pipe when liquid flows through it. *Inzenernyi Sbornik*, **10**, 169-170.

[17] FLÜGGE, W. 1960 *Stresses in Shells.* Berlin: Springer-Verlag.

[18] GREGORY, R.W. and PAÏDOUSSIS, M.P. 1966a Unstable oscillation of tubular cantilevers conveying fluid - I. Theory. *Proceedings of the Royal Society (London)*, **293**(A), 512-527.

[19] GREGORY, R.W. and PAÏDOUSSIS, M.P. 1966b Unstable oscillation of tubular cantilevers conveying fluid - II. Experiments. *Proceedings of the Royal Society (London)*, **293**(A), 528-542.

[20] HANNOYER, M.J. and PAÏDOUSSIS, M.P. 1978 Instabilities of tubular beams simultaneously subjected to internal and external axial flows. *ASME Journal of Mechanical Design*, **100**, 328-336.

[21] HANNOYER, M.J. and PAÏDOUSSIS, M.P. 1979a Dynamics of slender tapered beams with internal or external axial flow. Part 1: Theory. *Journal of Applied Mechanics*, **46**, 45-51.

[22] HANNOYER, M.J. and PAÏDOUSSIS, M.P. 1979b Dynamics of slender tapered beams with internal or external axial flow. Part 2: Experiments. *Journal of Applied Mechanics*, **46**, 52-57.

[23] HOBSON, D.E. 1982 Fluid-elastic instabilities caused by flow in annulus. *Proceedings of the 3rd International Conference on Vibration of Nuclear Plant*, pp.440-463. Keswick, UK.

[24] HOLMES, P.J. 1978 Pipes supported at both ends cannot flutter. *Journal of Applied Mechanics*, **45**, 619-622.

[25] HORÁČEK, J. and ZOLOTAREV, I. 1984 Influence of fixing the edges of a cylindrical shell with conveying fluid on its dynamic characteristics. *Soviet Applied Mechanics*, **20**, pp.756-765.

[26] HOUSNER, G.W. 1952 Bending vibrations of a pipe line containing flowing fluid. *Journal of Applied Mechanics*, **19**, 205-208.

[27] JENDRZEJCZYK, J.A. and CHEN, S.S. 1985 Experiments on tubes conveying fluid. *Thin-Walled Structures*, **3**, 109-134.

[28] KRAJCINOVIC, D. 1974 Vibrations of two coaxial cylindrical shells containing fluid. *Nuclear Engineering and Design*, **30**, 242-248.

[29] LAUFER, J. 1953 The structure of turbulence in fully-developed pipe flow. NACA Technical Note 2954.

[30] LIU, H.S. and MOTE, C.D. 1974 Dynamic response of pipes transporting fluids. *ASME Journal of Engineering for Industry*, **96**, 591-596.

[31] MATEESCU, D. and PAÏDOUSSIS, M.P. 1985 The unsteady potential flow in an axially variable annulus and its effect in the dynamics of the oscillating rigid center-body. *ASME Journal of Fluids Engineering*, **107**, 421-427.

[32] MATEESCU, D. and PAÏDOUSSIS, M.P. 1987 Unsteady viscous effects on the annular-flow-induced instabilities of a rigid cylindrical body in a narrow duct. *Journal of Fluids and Structures*, **1**, 197-215.

[33] MATEESCU, D., PAÏDOUSSIS, M.P. and BÉLANGER, F. 1988 Unsteady pressure measurements on oscillating cylinder in narrow annular flow. *Journal of Fluids and Structures*, **2**, 615-628.

[34] MATEESCU, D., PAÏDOUSSIS, M.P. and BÉLANGER, F. 1989 A theoretical model compared with experiments for the unsteady pressure on a cylinder oscillating in turbulent annular flow. *Journal of Sound and Vibration*, **135**, 487-498.

[35] MATEESCU, D., PAÏDOUSSIS, M.P. and BÉLANGER, F. 1991 Computational solutions based on a finite difference formulation for unsteady internal flows. *Proceedings of the 29th Aerospace Sciences Meeting*, Paper No. AIAA 91-0724. Reno, Nevada.

[36] MULCAHY, T.M. 1983 Leakage flow-induced vibrations of reactor components. *Shock and Vibration Digest*, **15**, 11-18.

[37] NIORDSON, F.I. 1953 Vibrations of a cylindrical tube containing flowing fluid. *Kungliga Techniska Högskolans Handlingar (Stockholm)*, No. 73.

[38] NGUYEN, V.B. 1992 Theoretical and experimental study of the stability of clamped-free coaxial cylindrical shells subjected to internal and annular flows of viscous fluid. Ph.D. Thesis, Department of Mechanical Engineering, McGill University.

[39] NGUYEN, V.B., PAÏDOUSSIS, M.P. and MISRA, A.K. 1993 A new outflow model for cylindrical shells conveying fluid. *Journal of Fluids and Structures*, **7**, in press.

[40] PAÏDOUSSIS, M.P. 1966a Dynamics of flexible slender cylinders in axial flow. Part I: Theory. *Journal of Fluid Mechanics*, **26**, 717-736.

[41] PAÏDOUSSIS, M.P. 1966b Dynamics of flexible slender cylinders in axial flow. Part II: Experiments. *Journal of Fluid Mechanics*, **26**, 737-751.

[42] PAÏDOUSSIS, M.P. 1970 Dynamics of tubular cantilevers conveying fluid. *Journal of Mechanical Engineering Science*, **12**, 85-103.

[43] PAÏDOUSSIS, M.P. 1973 Dynamics of cylindrical structures subjected to axial flow. *Journal of Sound and Vibration*, **29**, 365-385.

[44] PAÏDOUSSIS, M.P. 1975 Flutter of conservative systems of pipes conveying incompressible fluid. *Journal of Mechanical Engineering Science*, **17**, 19-25.

[45] PAÏDOUSSIS, M.P. 1979 The dynamics of clusters of flexible cylinders in axial flow: theory and experiments. *Journal of Sound and Vibration*, **65**, 391-417.

[46] PAÏDOUSSIS, M.P. 1980 Flow-induced vibrations in nuclear reactors and heat exchangers. Practical experiences and state of knowledge. In *Practical Experiences with Flow-Induced Vibrations* (eds E. Naudascher and D. Rockwell), pp. 1-81. Berlin: Springer-Verlag.

[47] PAÏDOUSSIS, M.P. 1987 Flow-induced instabilities of cylindrical structures. *Applied Mechanics Reviews*, **40**, 163-175.

[48] PAÏDOUSSIS, M.P., CHAN, S.P. and MISRA, A.K. 1984 Dynamics and stability of coaxial cylindrical shells containing flowing fluid. *Journal of Sound and Vibration*, **97**, 201-235.

[49] PAÏDOUSSIS, M.P., CURLING, L.R. and GAGNON, J.O. 1982 Experiments on fluidelastic instability of cylinder clusters in axial flow. *ASME Journal of Fluids Engineering*, **104**, 342-349.

[50] PAÏDOUSSIS, M.P. and DEKSNIS, E.B. 1970 Articulated models of cantilevers conveying fluid: the study of a paradox. *Journal of Mechanical Engineering Science*, **12**, 288-300.

[51] PAÏDOUSSIS, M.P. and DENISE, J.-P. 1970 Instabilities of cylindrical shells containing flow. M.E.R.L. TN. 70-5, Department of Mechanical Engineering, McGill University.

[52] PAÏDOUSSIS, M.P. and DENISE, J.-P. 1971 Flutter of cylindrical shells conveying fluid. *Journal of Sound and Vibration*, **16**, 459-461.

[53] PAÏDOUSSIS, M.P. and DENISE, J.-P. 1972 Flutter of thin cylindrical shells conveying fluid. *Journal of Sound and Vibration*, **20**, 9-26.

[54] PAÏDOUSSIS, M.P. and ISSID, N.T. 1974 Dynamic stability of pipes conveying fluid. *Journal of Sound and Vibration*, **33**, 267-294.

[55] PAÏDOUSSIS, M.P., LUU, T.P. and LAITHIER, B.E. 1986 Dynamics of finite-length tubular beams conveying fluid. *Journal of Sound and Vibration*, **106**, 311-331.

[56] PAÏDOUSSIS, M.P., MATEESCU, D. and SIM, W.G. 1990 Dynamics and stability of a flexible cylinder in a narrow coaxial cylindrical duct, subjected to annular flow. *Journal of Applied Mechanics*, **57**, 232-240.

[57] PAÏDOUSSIS, M.P., MISRA, A.K. and CHAN, S.P. 1985 Dynamics and stability of coaxial cylindrical shells conveying viscous fluid. *Journal of Applied Mechanics*, **52**, 389-396.

[58] PAÏDOUSSIS, M.P., NGUYEN, V.B. and MISRA, A.K. 1991 A theoretical study of the stability of cantilevered coaxial cylindrical shells conveying fluid. *Journal of Fluids and Structures*, **5**, 127-164.

[59] PAÏDOUSSIS, M.P. and OSTOJA-STARZEWSKI, M. 1981 Dynamics of a flexible cylinder in subsonic axial flow. *AIAA Journal*, **19**, 1467-1475.

[60] PAÏDOUSSIS, M.P. and PETTIGREW, M.J. 1979 Dynamics of flexible cylinders in axisymmetrically confined axial flow. *Journal of Applied Mechanics*, **46**, 37-44.

[61] PAÏDOUSSIS, M.P. and SUSS, S. 1977 Stability of a cluster of flexible cylinders in bounded axial flow. *Journal of Applied Mechanics*, **44**, 401-408.

[62] PAÏDOUSSIS, M.P. and DES TROIS MAISONS, P.E. 1969 Free vibration of a heavy, damped cantilever in a plane inclined to the vertical. M.E.R.L. Report No. 69-6, Department of Mechanical Engineering, McGill University.

[63] PHAM, T.T. and MISRA, A.K. 1981 Dynamic stability of cylindrical shells subjected to axial flow and a linearly varying load. *Proceedings of the 8th Canadian Congress of Applied Mechanics*, Moncton, New Brunswick, pp. 143-144.

[64] SHARMA, C.B. 1978 Calculation of integrals involving characteristic beam functions. *Journal of Sound and Vibration*, **56**, 475-480.

[65] SHAYO, L.K. and ELLEN, C.H. 1974 The stability of finite length circular cross section pipes conveying inviscid fluid. *Journal of Sound and Vibration*, **37**, 535-545.

[66] SHAYO, L.K. and ELLEN, C.H. 1978 Theoretical studies of internal flow-induced instabilities of cantilevered pipes. *Journal of Sound and Vibration*, **54**, 463-474.

[67] WEAVER, D.S. and UNNY, T.E. 1973 On the dynamic stability of fluid conveying pipes. *Journal of Applied Mechanics*, **40**, 48-52.

[68] WEINGARTEN, V.I. 1964 Free vibration of thin cylindrical shells. *AIAA Journal*, **2**, 717-722.

[69] WEPPELINK, H. 1979 Free vibrations of finite circular cylindrical shells and tubes with and without a surrounding fluid. Ph.D. Thesis, Technische Hogeschool Twente, Enschede, The Netherlands.

[70] YEH, T.T. and CHEN, S.S. 1977 Dynamics of a cylindrical shell system coupled by viscous fluid. *Journal of the Acoustical Society of America*, **62**, 262-270.

[71] YU, Y.Y. 1955 Free vibrations of thin cylindrical shells having finite lengths with freely supported and clamped edges. *Journal of Applied Mechanics*, **22**, 547-552.

Appendix A

Definition of Eigenfunctions and Related Integrals

A.1 Comparison Functions

In order to satisfy all the boundary conditions (2.7)-(2.14) automatically, suitable comparison functions $\Phi_m(x)$ should be chosen for u, v and w [equations (2.29) and (2.30)]. In the present theory, the dimensionless comparison functions are beam functions $\Phi_j(\xi)$, which have the general form

$$\Phi_j(\xi) = (\cosh \lambda_j \xi - \cos \lambda_j \xi) - \sigma_j(\sinh \lambda_j \xi - \sin \lambda_j \xi) \tag{A.1}$$

and satisfy the equation

$$\Phi_j''''(\xi) = \lambda_j^4 \Phi_j(\xi), \tag{A.2}$$

where prime denotes differentiation with respect to the argument of the function, ξ; for a clamped-pinned beam, the constants σ_j are

$$\sigma_j = \frac{\cosh \lambda_j + \cos \lambda_j}{\sinh \lambda_j + \sin \lambda_j}, \tag{A.3}$$

and the eigenvalues λ_j are the roots of the transcendental equation

$$\tanh \lambda_j - \tan \lambda_j = 0. \tag{A.4}$$

The boundary conditions of a clamped-pinned beam are as follows:

at clamped end:

$$\begin{aligned} \Phi_j(0) &= 0, \\ \Phi_j'(0) &= 0, \\ \Phi_j''(0) &= 2\lambda_j^2, \\ \Phi_j'''(0) &= -2\sigma_j\lambda_j^3, \end{aligned} \tag{A.5}$$

at pinned end:

$$\begin{aligned} \Phi_j(1) &= 0, \\ \Phi_j'(1) &= \frac{2\lambda_j(-1)^j}{\sqrt{\sigma_j^2+1}+(-1)^j\sqrt{\sigma_j^2-1}}, \\ \Phi_j''(1) &= 0, \\ \Phi_j'''(1) &= \frac{2\lambda_j^3(-1)^{j+1}}{\sqrt{\sigma_j^2+1}+(-1)^{j+1}\sqrt{\sigma_j^2-1}} \end{aligned} \tag{A.6}$$

If the system is pinned-clamped, just let $\xi = 1-\eta$ and substitute it into (A.1), or

$${}^p\Phi_j(\eta) = \Phi_j(\xi) = \Phi_j(1-\eta), \tag{A.7}$$

where ${}^p\Phi_j(\eta)$ are beam eigenfunctions of a pinned-clamped beam with the constants σ_j and λ_j satisfying (A.3) and (A.4). There exist following relations:

$$\begin{aligned} {}^p\Phi_j(\eta) &= \Phi_j(\xi), \\ {}^p\Phi_j'(\eta) &= -\Phi_j'(\xi), \\ {}^p\Phi_j''(\eta) &= \Phi_j''(\xi), \\ {}^p\Phi_j'''(\eta) &= -\Phi_j'''(\xi), \end{aligned} \tag{A.8}$$

The corresponding boundary conditions of a pinned-clamped beam are as follows:

at pinned end:

$$\begin{aligned} {}^{p}\Phi_j(0) &= 0, \\ {}^{p}\Phi_j'(0) &= -\frac{2\lambda_j(-1)^j}{\sqrt{\sigma_j^2+1}+(-1)^j\sqrt{\sigma_j^2-1}}, \\ {}^{p}\Phi_j''(0) &= 0, \\ {}^{p}\Phi_j'''(0) &= -\frac{2\lambda_j^3(-1)^{j+1}}{\sqrt{\sigma_j^2+1}+(-1)^{j+1}\sqrt{\sigma_j^2-1}}, \end{aligned} \tag{A.9}$$

at clamped end:

$$\begin{aligned} {}^{p}\Phi_j(1) &= 0, \\ {}^{p}\Phi_j'(1) &= 0, \\ {}^{p}\Phi_j''(1) &= 2\lambda_j^2, \\ {}^{p}\Phi_j'''(1) &= 2\sigma_j\lambda_j^3, \end{aligned} \tag{A.10}$$

A.2 Integrals Involving Beam Eigenfunctions

A number of definite integrals involving beam eigenfunctions were encountered in Chapter 2 (Section 2.3.4), as a result of the Galerkin method being utilized to solve the equations of motion. Such integrals were denoted by the following constants in the case of the clamped-pinned system :

$$\begin{aligned} a_{km} &= \int_0^1 \Phi_k'(\xi)\Phi_m(\xi)d\xi, & \hat{a}_{km} &= \int_0^1 \xi\Phi_k(\xi)\Phi_m(\xi)d\xi, \\ b_{km} &= \int_0^1 \Phi_k'(\xi)\Phi_m'(\xi)d\xi, & \hat{b}_{km} &= \int_0^1 \xi\Phi_k'(\xi)\Phi_m'(\xi)d\xi, \\ c_{km} &= \int_0^1 \Phi_k(\xi)\Phi_m''(\xi)d\xi, & \hat{c}_{km} &= \int_0^1 \xi\Phi_k(\xi)\Phi_m''(\xi)d\xi, \\ d_{km} &= \int_0^1 \Phi_k'(\xi)\Phi_m'''(\xi)d\xi, & \hat{d}_{km} &= \int_0^1 \xi\Phi_k'(\xi)\Phi_m'''(\xi)d\xi, \end{aligned}$$

$$\delta_{km} = \int_0^1 \Phi_k(\xi)\Phi_m(\xi)d\xi = \begin{cases} 0 & \text{if } k \neq m, \\ 1 & \text{if } k = m, \end{cases}$$

where $\xi = x/L$ is a dimensionless length variable, defined in (2.53). If the system is pinned-clamped, the corresponding integrals should be denoted by the following constants:

$$\begin{aligned}
{}^p a_{km} &= \int_0^1 {}^p\Phi_k'(\eta)\,{}^p\Phi_m(\eta)d\eta, & {}^p\hat{a}_{km} &= \int_0^1 \eta\,{}^p\Phi_k(\eta)\,{}^p\Phi_m(\eta)d\eta, \\
{}^p b_{km} &= \int_0^1 {}^p\Phi_k'(\eta)\,{}^p\Phi_m'(\eta)d\eta, & {}^p\hat{b}_{km} &= \int_0^1 \eta\,{}^p\Phi_k'(\eta)\,{}^p\Phi_m'(\eta)d\eta, \\
{}^p c_{km} &= \int_0^1 {}^p\Phi_k(\eta)\,{}^p\Phi_m''(\eta)d\eta, & {}^p\hat{c}_{km} &= \int_0^1 \eta\,{}^p\Phi_k(\eta)\,{}^p\Phi_m''(\eta)d\eta, \\
{}^p d_{km} &= \int_0^1 {}^p\Phi_k'(\eta)\,{}^p\Phi_m'''(\eta)d\eta, & {}^p\hat{d}_{km} &= \int_0^1 \eta\,{}^p\Phi_k'(\eta)\,{}^p\Phi_m'''(\eta)d\eta,
\end{aligned}$$

where $\eta = x/L$ is a dimensionless length variable, and ${}^p\Phi_m(\eta)$ are beam eigenfunctions of a pinned-clamped beam defined in (A.7). To evaluate the above constants conveniently, following integrals are defined:

$$e_{km} = \int_0^1 \Phi_k(\xi)\Phi_m'''(\xi)d\xi, \qquad {}^p e_{km} = \int_0^1 {}^p\Phi_k(\eta)\,{}^p\Phi_m'''(\eta)d\eta.$$

The above integrals are evaluated using the same procedure as introduced by Gregory and Païdoussis (1966a). Firstly, we evaluate the following constants by integration by parts:

$$a_{km} = \frac{1}{\lambda_k^4 - \lambda_m^4}\left\{\lambda_k^4\Phi_k\Phi_m - \Phi_k'''\Phi_m' + \Phi_k''\Phi_m'' - \Phi_k'\Phi_m'''\right\}\Big|_0^1; \tag{A.11}$$

$$b_{km} = \frac{1}{\lambda_k^4 - \lambda_m^4}\left\{\lambda_k^4\Phi_k\Phi_m' - \Phi_k'''\Phi_m'' + \Phi_k''\Phi_m''' - \lambda_m^4\Phi_k'\Phi_m\right\}\Big|_0^1; \tag{A.12}$$

$$e_{km} = \frac{1}{\lambda_k^4 - \lambda_m^4}\left\{\Phi_k'''\Phi_m''' - \lambda_m^4\Phi_k''\Phi_m + \lambda_m^4\Phi_k'\Phi_m' - \lambda_m^4\Phi_k\Phi_m''\right\}\Big|_0^1; \tag{A.13}$$

But it is noted that when $k = m$ the above constants become undefined and should be reevaluated, which lead to:

$$a_{mm} = \frac{1}{2}\Phi_m^2\Big|_0^1, \tag{A.14}$$

$$b_{mm} = \frac{1}{4}\left\{3\Phi_m\Phi'_m + \xi\Phi'^2_m - 2\xi\Phi_m\Phi''_m - \frac{1}{\lambda_m^4}\Phi''_m\Phi'''_m + \frac{1}{\lambda_m^4}\xi\Phi'''^2_m\right\}\Big|_0^1, \quad \text{(A.15)}$$

$$e_{mm} = \frac{1}{2\lambda_m^4}\Phi'''^2_m\Big|_0^1. \quad \text{(A.16)}$$

Secondly, by integration by parts, and with the above constants we have:

$$\hat{a}_{km} = \frac{1}{\lambda_k^4 - \lambda_m^4}\{2(e_{km} - e_{mk}) + \xi[\Phi'''_k\Phi_m - \Phi''_k\Phi'_m + \Phi'_k\Phi_m - \Phi_k\Phi'''_m]_0^1\}, \quad \text{(A.17)}$$

$$\hat{b}_{km} = \frac{1}{\lambda_k^4 - \lambda_m^4}\left\{2(\lambda_m^4 e_{km} - \lambda_k^4 e_{mk}) + \left[\xi(\lambda_k^4\Phi_k\Phi'_m - \Phi'''_k\Phi''_m + \Phi''_k\Phi'''_m - \lambda_m^4\Phi'_k\Phi_m) + (\Phi'''_k\Phi'_m - \Phi'_k\Phi'''_m)\right]_0^1\right\}, \quad \text{(A.18)}$$

$$\hat{a}_{mm} = \frac{1}{8\lambda_m^4}\left\{2\xi[3\Phi_m\Phi'''_m - \Phi'_m\Phi''_m] + \xi^2[\lambda_m^4\Phi_m^2 + \Phi''^2_m - 2\Phi'_m\Phi'''_m] + 4\Phi'^2_m - 6\Phi_m\Phi''_m\right\}\Big|_0^1, \quad \text{(A.19, A.20)}$$

$$\hat{b}_{mm} = \frac{1}{8\lambda_m^4}\left\{2\xi[3\lambda_m^4\Phi_m\Phi'_m - \Phi''_m\Phi'''_m] + \xi^2[\lambda_m^4\Phi'^2_m + \Phi'''^2_m - 2\lambda_m^4\Phi''_m\Phi_m] + 4\Phi'''^2_m - 6\Phi'_m\Phi'''_m\right\}\Big|_0^1. \quad \text{(A.21, A.22)}$$

Finally, we can evaluate the remaining constants by using the above results and the boundary conditions (A.5)-(A.6):

$$c_{km} = -b_{km}, \quad \text{(A.23)}$$

$$d_{km} = -\lambda_m^4\delta_{km}, \quad \text{(A.24)}$$

$$\hat{c}_{km} = -\hat{b}_{km} - a_{mk}, \quad \text{(A.25)}$$

$$\hat{d}_{km} = -e_{km} - \lambda_m^4\hat{a}_{km}, \quad \text{(A.26)}$$

and then:

$$^p a_{km} = -a_{km}, \quad \text{(A.27)}$$

$$^p b_{km} = b_{km}, \quad \text{(A.28)}$$

$$^p c_{km} = -b_{km}, \quad \text{(A.29)}$$

$$ {}^{p}d_{km} = -\lambda_m^4 \delta_{km}, \tag{A.30} $$

$$ {}^{p}\hat{a}_{km} = \delta_{km} - \hat{a}_{km}, \tag{A.31} $$

$$ {}^{p}\hat{b}_{km} = b_{km} - \hat{b}_{km}, \tag{A.32} $$

$$ {}^{p}\hat{c}_{km} = -b_{km} - \hat{c}_{km}, \tag{A.33} $$

$$ {}^{p}\hat{d}_{km} = -\lambda_m^4 \delta_{km} - \hat{d}_{km}. \tag{A.34} $$

All of the above definite integrals expressed in terms of boundary conditions have been tested to be true by numerical integrations.

Appendix B

Expression for $H_{km}(\bar{\alpha})$ and ${}^{p}H_{km}(\bar{\alpha})$

$H_{km}(\bar{\alpha})$ was defined in Equation (2.63) as

$$H_{km}(\bar{\alpha}) = H_k(-\bar{\alpha})H_m(\bar{\alpha}), \tag{B.1}$$

where k and m are indices such that $1 \leq k,\ m \leq M$, and

$$H_j(\bar{\alpha}) = \int_0^1 \Phi_j(\xi)e^{i\bar{\alpha}\xi}d\xi. \tag{B.2}$$

In the above integral, $\Phi_j(\xi)$ are clamped-pinned beam eigenfunctions defined in (A.1).

By successive integration by parts, it is found that

$$H_j(\bar{\alpha}) = \frac{1}{\lambda_j^4 - \bar{\alpha}^4}\left[\Phi_j'''(\xi) - (i\bar{\alpha})\Phi_j''(\xi) + (i\bar{\alpha})^2\Phi_j'(\xi) - (i\bar{\alpha})^3\Phi_j(\xi)\right] e^{i\bar{\alpha}\xi}\Big|_0^1. \tag{B.3}$$

It is noted that $H_j(\bar{\alpha})$ becomes undefined when

$$\bar{\alpha} = \bar{\alpha}^* \equiv \pm\lambda_j,\ \pm i\lambda_j, \tag{B.4}$$

because the right hand side of (B.3) has the form 0/0; in such cases, applying L'Hospital's rule to equation (B.3) leads to

$$\begin{aligned} H_j(\bar{\alpha}^*) \;=\; & \frac{1}{4\bar{\alpha}^{*3}}\left\{\left[\bar{\alpha}^{*3}\Phi_j(\xi) + i\bar{\alpha}^{*2}\Phi_j'(\xi) - \bar{\alpha}^*\Phi_j''(\xi) - i\Phi_j'''(\xi)\right]\xi\right. \\ & \left. + \left[-3i\bar{\alpha}^{*2}\Phi_j(\xi) + 2\bar{\alpha}^*\Phi_j'(\xi) + i\Phi_j''(\xi)\right]\right\} e^{i\bar{\alpha}^*\xi}\Big|_0^1. \end{aligned} \tag{B.5}$$

The boundary conditions of a clamped-pinned beam are given by (A.5) and (A.6).

If the system is pinned-clamped, then using a pinned-clamped beam function ${}^{p}\phi_{j}(\eta)$ defined in (A.7) to replace $\Phi_j(\xi)$, we have:

$$\begin{aligned}
{}^{p}H_{km}(\bar{\alpha}) &= {}^{p}H_k(-\bar{\alpha})\,{}^{p}H_m(\bar{\alpha}) \\
&= \int_0^1 {}^{p}\Phi_k(\eta)e^{-\imath\bar{\alpha}\eta}d\eta \int_0^1 {}^{p}\Phi_m(\eta)e^{\imath\bar{\alpha}\eta}d\eta \\
&= \int_1^0 \Phi_k(\xi)e^{-\imath\bar{\alpha}(1-\xi)}d(1-\xi)\int_1^0 \Phi_m(\xi)e^{\imath\bar{\alpha}(1-\xi)}d(1-\xi) \\
&= \int_0^1 \Phi_k(\xi)e^{\imath\bar{\alpha}\xi}d\xi \int_0^1 \Phi_m(\xi)e^{-\imath\bar{\alpha}\xi}d\xi \\
&= H_k(\bar{\alpha})H_m(-\bar{\alpha}) = H_{mk}(\bar{\alpha})
\end{aligned}$$

or rewriting,

$$ {}^{p}H_{km}(\bar{\alpha}) = H_{mk}(\bar{\alpha}) \tag{B.6}$$

Appendix C

Out-Flow Model

In a recent study by Païdoussis *et al.* (1991), it was shown that, if the shells are cantilevered, the effect of flow perturbations beyond the downstream end of the shells must be taken into account. This also applies to clamped-pinned and pinned-pinned boundary conditions. Three different so-called out-flow models, previously introduced by Shayo & Ellen (1978) and Païdoussis *et al.* (1986), were examined by Païdoussis *et al.* (1991). Since the downstream flow perturbations vanish at $\xi = \ell$, ℓ should be sufficiently large for as gradual a decay as possible. However, numerical difficulties were experienced in previous studies. The non-convergence of the solution was therein identified as resulting from the non-existence of $\lim_{\ell\to\infty} N_{km}(\bar{\alpha})$, even though $N_{km}(\bar{\alpha})$ is finite for any value of ℓ. A similar example of non-convergence, because of the nature of the functional form involved, pertains to $\ell\cos\ell$; for any large ℓ, $\ell\cos\ell$ is finite, yet the limit, as $\ell\to\infty$, does not exist.

Therefore, a new outflow model with the requirement that the model *does not* lead to the numerical difficulties experienced in previous studies should be developed. This has been successfully accomplished by Nguyen *et al.* (1993) and is presented as follows.

The functional form of the new model is given by $R_m(\xi)$, defined over $1 \leq \xi \leq \ell$, where ℓ is the location at which flow perturbations vanish. $R_m(\xi)$ may be considered as an extension of the beam eigenfunctions (the admissible functions), $\Phi_m(\xi)$, beyond $\xi = 1$.

The characteristic function $R_m(\xi)$ of the new model satisfies the following boundary conditions:

$$R_m(\xi)|_{\xi=1} = \Phi_m(1), \quad R'_m(\xi)|_{\xi=1} = \Phi'_m(1),$$
$$R_m(\xi)|_{\xi=\ell,\ell\to\infty} = 0, \quad R'_m(\xi)|_{\xi=\ell,\ell\to\infty} = 0. \tag{C.1}$$

By intuition, $R_m(\xi)$ has been taken to be of the form

$$R_m(\xi) = (A\xi + B)e^{1-\xi}, \tag{C.2}$$

which automatically satisfies the last two boundary condition because of the term $e^{1-\xi}$. The constants A and B can easily be determined from the first two conditions; they are

$$A = \Phi_m(1) + \Phi'_m(1), \quad B = -\Phi'_m(1). \tag{C.3}$$

For the clamped-pinned system herein, $\Phi_m(1) = 0$, hence $R_m(\xi)$ can be written as:

$$R_m(\xi) = -\Phi'_m(1)(1-\xi)e^{1-\xi} \text{ for } 1 \leq \xi \leq \ell \tag{C.4}$$

In the process of obtaining the generalized fluid forces acting on the shells (Chapter 2), another function $N_{km}(\bar{\alpha})$ closely related to $R_m(\xi)$ was defined [equation (2.64)],

$$N_{km}(\bar{\alpha}) = H_k(-\bar{\alpha})N_m(\bar{\alpha}), \tag{C.5}$$

where

$$H_k(-\bar{\alpha}) = \int_0^1 \Phi_k(\xi)e^{-i\bar{\alpha}\xi}d\xi, \quad N_m(\bar{\alpha}) = \int_1^\ell R_m(\xi)e^{i\bar{\alpha}\xi}d\xi. \tag{C.6}$$

It should be recalled that $H_A(-\bar{\alpha})$ was completely determined in Appendix B; thus what remains to be done in this appendix is to evaluate $N_m(\bar{\alpha})$ corresponding to the new model.

In order to do so, the following functions are defined:

$$\hat{N}_0(\bar{\alpha}) = \int_1^\ell e^{(i\bar{\alpha}-1)\xi} d\xi = \frac{1}{i\bar{\alpha}-1}\left\{e^{(i\bar{\alpha}-1)\ell} - e^{i\bar{\alpha}-1}\right\}, \tag{C.7}$$

$$\hat{N}_1(\bar{\alpha}) = \int_1^\ell \xi e^{(i\bar{\alpha}-1)\xi} d\xi = -\frac{1}{(i\bar{\alpha}-1)^2}\left\{e^{(i\bar{\alpha}-1)\ell}(1 - i\bar{\alpha}\ell + \ell) - i\bar{\alpha}e^{i\bar{\alpha}-1}\right\}. \tag{C.8}$$

Finally, $N_m(\bar{\alpha})$ for the new model is determined from (C.2), together with (C.6), (C.7) and (C.8),

$$\begin{aligned} N_m(\bar{\alpha}) &= \int_1^\ell R_m(\xi) e^{i\bar{\alpha}\xi} d\xi \\ &= -\Phi'_m(1) e \int_1^\ell (1-\xi) e^{(i\bar{\alpha}-1)\xi} d\xi \\ &= \Phi'_m(1) e[\hat{N}_1(\bar{\alpha}) - \hat{N}_0(\bar{\alpha})]. \end{aligned} \tag{C.9}$$

Appendix D

Definition of [M], [C] and [K]

The following are the elements of [M], [C] and [K].

Matrix [M]

$$M_{km}^{1,1} = \varepsilon_i^2 b_{km};\ M_{km}^{2,2} = \delta_{km};\ M_{km}^{3,3} = \delta_{km} + q_{km}^{(1)};\ M_{km}^{3,6} = r_{km}^{(1)};$$

$$M_{km}^{4,4} = \varepsilon_o^2 b/\Omega_r^2;\ M_{km}^{5,5} = \delta_{km}/\Omega_r^2;\ M_{km}^{6,3} = s_{km}^{(1)};\ M_{km}^{6,6} = \delta_{km}/\Omega_r^2 + t_{km}^{(1)};$$

the remaining elements are zeros.

Matix [C]

$$C_{km}^{3,3} = 2q_{km}^{(2)};\ C_{km}^{3,6} = 2r_{km}^{(2)};\ C_{km}^{6,3} = 2s_{km}^{(2)};\ C_{km}^{6,6} = 2t_{km}^{(2)};$$

the remaining elements are zeros.

Matrix [K]: $[K] = [K_1] + [K_2]$

Each constituent part of [K] has a different physical basis. Matrix $[K_1]$ results from the strain energy associated with the standard Flügge's shell theory; matrix $[K_2]$ represents a change in the *effective* stiffness of the system due to steady viscous effects of the flowing fluid.

The elements of $[K_1]$ are:

$$
\begin{aligned}
K_{1km}^{1,1} &= -\frac{1}{2}n^2(1+k_i)(1-\nu_i)\varepsilon_i^2 b_{km} + \varepsilon_i^4 d_{km};\\
K_{1km}^{1,2} &= \frac{1}{2}n(1+\nu_i)\varepsilon_i^2 b_{km};\\
K_{1km}^{1,3} &= \left\{\nu_i - \frac{1}{2}n^2 k_i(1-\nu_i)\right\}\varepsilon_i^2 b_{km} - k_i\varepsilon_i^4 d_{km};\\
K_{1km}^{2,1} &= -\frac{1}{2}n(1+\nu_i)\varepsilon_i^2 c_{km};\\
K_{1km}^{2,2} &= -n^2\delta_{km} + \frac{1}{2}(1+3k_i)(1-\nu_i)\varepsilon_i^2 c_{km};\\
K_{1km}^{2,3} &= \frac{1}{2}nk_i(3-\nu_i)\varepsilon_i^2 c_{km} - n\delta_{km};\\
K_{1km}^{3,1} &= \left\{\frac{1}{2}n^2 k_i(1-\nu_i) - \nu_i\right\}\varepsilon_i^2 c_{km} + k_i\varepsilon_i^4\lambda_m^4\delta_{km};\ K_{1km}^{3,2} = K_{1km}^{2,3};\\
K_{1km}^{3,3} &= -[k_i(n^2-1)^2 + k_i\varepsilon_i^4\lambda_m^4 + 1]\delta_{km} + 2k_i n^2\varepsilon_i^2 c_{km} + q_{km}^{(3)};\ K_{1km}^{3,6} = r_{1km}^{(3)}\\
K_{1km}^{4,4} &= -\frac{1}{2}n^2(1+k_o)(1-\nu_o)\varepsilon_o^2 b_{km} + \varepsilon_o^4 d_{km};\\
K_{1km}^{4,5} &= \frac{1}{2}n(1+\nu_o)\varepsilon_o^2 b_{km};\\
K_{1km}^{4,6} &= \left\{\nu_o - \frac{1}{2}n^2 k_o(1-\nu_o)\right\}\varepsilon_o^2 b_{km} - k_o\varepsilon_o^4 d_{km};\\
K_{1km}^{5,4} &= -\frac{1}{2}n(1+\nu_o)\varepsilon_o^2 c_{km};\\
K_{1km}^{5,5} &= -n^2\delta_{km} + \frac{1}{2}(1+3k_o)(1-\nu_o)\varepsilon_o^2 c_{km};\\
K_{1km}^{5,6} &= \frac{1}{2}nk_o(3-\nu_o)\varepsilon_o^2 c_{km} - n\delta_{km};\\
K_{1km}^{6,4} &= \left\{\frac{1}{2}n^2 k_o(1-\nu_o) - \nu_o\right\}\varepsilon_o^2 c_{km} + k_o\varepsilon_o^4\lambda_m^4\delta_{km};\ K_{1km}^{6,5} = K_{1km}^{5,6};\\
K_{1km}^{6,6} &= -[k_o(n^2-1)^2 + k_o\varepsilon_o^4\lambda_m^4 + 1]\delta_{km} + 2k_o n^2\varepsilon_o^2 c_{km} + q_{km}^{(3)};\ K_{1km}^{6,3} = s_{1km}^{(3)}.
\end{aligned}
$$

the remaining elements are zeros.

The elements of matrix $[K_2]$ are:

$$
\begin{aligned}
K_{2km}^{1,1} &= \varepsilon_i^4\left[\hat{A}_{1i}\hat{d}_{km} + \hat{B}_{1i}d_{km}\right] - n^2\varepsilon_i^2\left[\hat{A}_{3i}\hat{b}_{km} + \hat{B}_{3i}b_{km}\right];\\
K_{2km}^{1,2} &= n\hat{B}_{2i}\varepsilon_i a_{km};\ K_{2km}^{1,3} = \hat{B}_{2i}\varepsilon_i a_{km} - \varepsilon_i^2\left[\hat{A}_{3i}\hat{b}_{km} + \hat{B}_{3i}b_{km}\right];\\
K_{2km}^{2,2} &= \varepsilon_i^2\left[\hat{A}_{1i}\hat{c}_{km} + \hat{B}_{1i}c_{km}\right] - n^2\left[\hat{A}_{3i}\hat{a}_{km} + \hat{B}_{3i}\delta_{km}\right];
\end{aligned}
$$

$$
\begin{aligned}
K_{2km}^{2,3} &= -n\left[\hat{A}_{3_i}\hat{a}_{km} + \hat{B}_{3_i}\delta_{km}\right];\ K_{2km}^{3,1} = \varepsilon_i^2\left[\hat{A}_{3_i}\hat{c}_{km} + \hat{B}_{3_i}c_{km}\right];\\
K_{2km}^{3,2} &= K_{2km}^{2,3};\ K_{2km}^{3,3} = \varepsilon_i^2\left[\hat{A}_{1_i}\hat{c}_{km} + \hat{B}_{1_i}c_{km}\right] - n^2\left[\hat{A}_{3_i}\hat{a}_{km} + \hat{B}_{3_i}\delta_{km}\right];\\
K_{2km}^{4,4} &= \varepsilon_o^4\left[\hat{A}_{1_o}\hat{d}_{km} + \hat{B}_{1_o}d_{km}\right] - n^2\varepsilon_o^2\left[\hat{A}_{3_o}\hat{b}_{km} + \hat{B}_{3_o}b_{km}\right];\\
K_{2km}^{4,5} &= n\hat{B}_{2_o}\varepsilon_o a_{km};\ K_{2km}^{4,6} = \hat{B}_{2_o}\varepsilon_o a_{km} - \varepsilon_o^2\left[\hat{A}_{3_o}\hat{b}_{km} + \hat{B}_{3_o}b_{km}\right];\\
K_{2km}^{5,5} &= \varepsilon_o^2\left[\hat{A}_{1_o}\hat{c}_{km} + \hat{B}_{1_o}c_{km}\right] - n^2\left[\hat{A}_{3_o}\hat{a}_{km} + \hat{B}_{3_o}\delta_{km}\right];\\
K_{2km}^{5,6} &= -n\left[\hat{A}_{3_o}\hat{a}_{km} + \hat{B}_{3_o}\delta_{km}\right];\ K_{2km}^{6,4} = \varepsilon_o^2\left[\hat{A}_{3_o}\hat{c}_{km} + \hat{B}_{3_o}c_{km}\right];\\
K_{2km}^{6,5} &= K_{2km}^{5,6};\ K_{2km}^{6,6} = \varepsilon_o^2\left[\hat{A}_{1_o}\hat{c}_{km} + \hat{B}_{1_o}c_{km}\right] - n^2\left[\hat{A}_{3_o}\hat{a}_{km} + \hat{B}_{3_o}\delta_{km}\right];
\end{aligned}
$$

the remaining elements are zeros.

In the above matrix elements, $\hat{A}$'s and $\hat{B}$'s are constants defined in (2.99), while for the clamped-pinned system constants $a_{km}, \ldots, d_{km}$ and $\hat{a}_{km}, \ldots, \hat{d}_{km}$ are defined in Appedix A. Constants $q_{km}^{(j)}$, $r_{km}^{(j)}$, $s_{km}^{(j)}$ and $t_{km}^{(j)}$ (with $j = 1, 2, 3.$) are defined in Chapter 2 in equation (2.65) and (2.67).

If the system is pinned-clamped, ${}^{p}\Phi_m(\xi)$ defined in Appendix A should replace $\Phi_m(\xi)$, and hence, in the above expressions, the constants $a_{km}, \ldots, d_{km}$ and $\hat{a}_{km}, \ldots, \hat{d}_{km}$ should be replaced by ${}^{p}a_{km}, \ldots, {}^{p}d_{km}$ and ${}^{p}\hat{a}_{km}, \ldots, {}^{p}\hat{d}_{km}$ respectively.

The elments of vector X are:

$$\{X\}^T = \{\bar{A}_m\ \bar{B}_m\ \bar{C}_m\ \bar{D}_m\ \bar{E}_m\ \bar{F}_m\}.$$

It should be noted that, since k and m are indices such that $1 \leq k, m \leq M$, each element of [M], [C], or [K] is in effect an $M \times M$ submatrix of scalars, and each element of X is a subvector of M (scalar) elements.

Appendix E

Computer Program Listing

Following is a listing of the computer program developed for Chapter 2. This program was written in FORTRAN 77 (Standard FORTRAN). It has the following characteristics:

- Most variables used in the program have the same physical meanings as those in the theory.
- All multi-dimensional arrays have the pseudo dimensions, which change automatically according to the data provided.
- All physical data are read in by the program; i.e. *all* changes in the data are made in the data file, *not* in the computer program.

```
C ... MAIN PROGRAM
C ... CLAMPED-PINNED AND PINNED-CLAMPED SHELLS USING THE INVISCID THEORY (WITH
C ... OR WITHOUT STEADY VISCOUS FORCES)
C ... INNER SHELL : FLEXIBLE, OUTER SHELL : RIGID
      IMPLICIT COMPLEX*16(A-H), REAL*8(O-Z)
      COMMON/CONST/PI,RGAMA,JSC,JIN,JOUT,IJOB,IOP1,IOP2
      COMMON/WORKSP/RWKSP(73748)
      COMMON  A(40000)
      CALL  IWKIN (73748)
      CALL  ERRSET (207,1,0,0,1,0)
      CALL  ERRSET (208,300,-1,1,1,0)
      CALL  ERRSET (209,1,0,0,1,0)
      NMAX= 40000
      READ (JIN,1000) MTIMES,INFO
      WRITE (JOUT,1000) MTIMES,INFO
      DO 250 ITIME=1,MTIMES
      CALL INPUT (NT)
      NR= NT*NT*3
      NS= 3*NT
      NX= 6*NT
      NO= 1
      N1= NO + 2*NR
      N2= N1 + NR
      N3= N2 + NS**2
      N4= N3 + NS**2
      N5= N4 + NS**2
      N6= N5 + NX**2
      N7= N6 + NX**2
      N8= N7 + NX
      N9= N8 + NX
      N10= N9 + NX**2
      NDIF= N10 - NMAX
      IF (NDIF)  20,20,300
   20 IF (INFO)  60,40,60
   40 CALL FORCES (A(NO),A(N1),NT,1)
      GO TO 250
   60 CALL FORCES (A(NO),A(N1),NT,2)
      READ (JIN,1000)  NTIMES
      DO 200  JTIME=1,NTIMES
      CALL CLEAR (A(N1),N10-N1)
      CALL FORCES (A(NO),A(N1),NT,3)
      CALL MCK (A(N1),A(N2),A(N3),A(N4),NT,NS)
      CALL DAMP (A(N1),A(N3),A(N4),NT,NS)
      IF (IOP1)  120,140,120
  120 CALL VISFOR (A(N4),NT,NS)
  140 CALL REDUCE (A(N2),A(N3),A(N4),A(N5),A(N6),NS,NX)
      CALL DGVCCG (NX,A(N5),NX,A(N6),NX,A(N7),A(N8),A(N9),NX)
      CALL OUTPUT (A(N5),A(N6),A(N7),A(N8),A(N9),NX)
  200 CONTINUE
  250 CONTINUE
      STOP
  300 WRITE (JOUT,2000) NDIF
      STOP
C 400 FORMAT (5X,2D25.16)
 1000 FORMAT (2I5)
 2000 FORMAT (53H * * *  PROGRAM STOPPED...  ALLOWED STORAGE EXCEEDED ,
     1        10HBY  NDIF =,I5)
      END
C
      COMPLEX FUNCTION  CIN*16 (A,N)
```

```
      IMPLICIT COMPLEX*16(A-H), REAL*8(O-Z)
      DOUBLE PRECISION  CDABS,DREAL,DIMAG
      COMMON/CONST/PI,RGAMA,JSC,JIN,JOUT,IJOB,IOP1,IOP2
      IF (CDABS(A).GE.20.D0)  GO TO 140
      AA= 0.5D0*A
      K= 0
      CIN= (0.D0,0.D0)
  100 CNEW= AA**(2*K)/RFAC(K)/RFAC(N + K)
      CIN= CIN + CNEW
      IF (CDABS(CNEW).LT.1.D-10)  GO TO 120
      K= K + 1
      GO TO 100
  120 CIN= CIN*AA**N
      RETURN
  140 CI= (0.D0,1.D0)
      CN1= (4.D0*N**2 - 1.D0)/(8.D0*A)
      CN2= CN1*(4.D0*N**2 - 9.D0)/(16.D0*A)
      CN3= CN2*(4.D0*N**2 - 25.D0)/(24.D0*A)
      CNA= CDEXP(A)/CDSQRT(2.D0*PI*A)
      CNB= CNA*CDEXP(-2.D0*A)
      IF (DIMAG(A))  160,200,180
  160 CIN= CNA*(1.D0-CN1+CN2-CN3)+(-1)**(N+1)*CI*CNB*(1.D0+CN1+CN2+CN3)
      RETURN
  180 CIN= CNA*(1.D0-CN1+CN2-CN3)+(-1)**N*CI*CNB*(1.D0+CN1+CN2+CN3)
      RETURN
  200 IF (DREAL(A))  220,240,240
  220 CIN= (-1)**N*CI*CNB*(1.D0 + CN1 + CN2 + CN3)
      RETURN
  240 CIN= CNA*(1.D0 - CN1 + CN2 - CN3)
      RETURN
      END

      COMPLEX FUNCTION  CKN*16 (A,N)
      IMPLICIT COMPLEX*16(A-H), REAL*8(O-Z)
      DOUBLE PRECISION  CDABS,DREAL,DIMAG
      COMMON/CONST/PI,RGAMA,JSC,JIN,JOUT,IJOB,IOP1,IOP2
      IF (CDABS(A).GE.15.D0)  GO TO 200
      AA= 0.5D0*A
      B= (0.D0,0.D0)
      IF (N.EQ.0)  GO TO 150
      K= 0
  100 BNEW= (-1)**K*RFAC(N-K-1)/(RFAC(K)*AA**(N-2*K))
      B= B + BNEW
      IF (N-1-K)  140,140,120
  120 K= K + 1
      GO TO 100
  140 B= 0.5D0*B
  150 K= 0
      CKN= (0.D0,0.D0)
  160 CNEW= (AA**(2*K)/RFAC(K)/RFAC(N + K))*(0.5D0*(RFI(K) + RFI(N + K))
     1                                          - (CDLOG(AA) + RGAMA))
      CKN= CKN +CNEW
      IF (CDABS(CNEW).LT.1.D-10)  GO TO 180
      K= K + 1
      GO TO 160
  180 CKN= CKN*(-AA)**N + B
      RETURN
  200 CN1= (4.D0*N**2 - 1.D0)/(8.D0*A)
      CN2= CN1*(4.D0*N**2 - 9.D0)/(16.D0*A)
      CN3= CN2*(4.D0*N**2 - 25.D0)/(24.D0*A)
      CNA= CDEXP(-A)*CDSQRT(0.5D0*PI/A)
```

```
      CKN= CNA*(1.DO + CN1 + CN2 +CN3)
      IF (DREAL(A))  220,240,240
  220 IF (DIMAG(A))  240,260,240
  240 RETURN
  260 B= -A
      CNA= CDEXP(-B)*CDSQRT(0.5D0*PI/B)
      CKN= CKN + (-1)**N*CNA*(1.D0 - CN1 + CN2 - CN3)
      RETURN
      END
C
      SUBROUTINE  CLEAR (CF,N)
      IMPLICIT COMPLEX*16(A-H)
      DIMENSION  CF(1)
      DO 20  I=1,N
   20 CF(I)= (0.D0,0.D0)
      RETURN
      END
C
      SUBROUTINE  DAMP (CQ,CXC,CXK,NT,NS)
      IMPLICIT COMPLEX*16(A-H), REAL*8(O-Z)
      COMMON/ISHELL/DHI,DVI,QI,REI,SKI,PSI
      COMMON/CONST/PI,RGAMA,JSC,JIN,JOUT,IJOB,IOP1,IOP2
      DIMENSION  CQ(NT,NT,1),CXC(NS,1),CXK(NS,1)
      IF (IOP2)  20,60,20
C ... MODIFY MATRICES C AND K TO ACCOUNT FOR HYS. AND VIS. DAMPING
   20 DO 40  I=1,NS
      DO 40  J=1,NS
      CXC(I,J)= CXC(I,J) + DVI*CXK(I,J)
   40 CXK(I,J)= DHI*CXK(I,J)
C ... ADD TO THE STIFFNESS MATRIX K THE GENERALIZED FORCES CQ(K,M,3)
   60 DO 80  M=1,NT
      J= M + 2*NT
      DO 80  K=1,NT
      I= K + 2*NT
   80 CXK(I,J)= CXK(I,J) + CQ(K,M,3)
      RETURN
      END
C
      BLOCK  DATA
C ... DATA FOR CLAMPED-FREE BEAMS
      IMPLICIT REAL*8(O-Z)
      COMMON/CONST/PI,RGAMA,JSC,JIN,JOUT,IJOB,IOP1,IOP2
      COMMON/COAX/RLA(10),RHO(10),OMR,RINT,NINT,N,IOP3
      COMMON/SVFOR/SAL(11),SBT(11),RDI,RDO,RGI,RGO,VISI,VISA,SL
      DATA  PI/3.141592653589793D0/, RGAMA/0.5772156649015328D0/,
     1      JSC/4/, JIN/5/, JOUT/6/, IJOB/2/
      DATA  RLA/ 3.926602312047912D0, 7.068582745628738D0,
     1           10.21017612281303D0, 13.35176877775410D0,
     2           16.49336143134641D0, 19.63495408493620D0,
     3           22.77654673852600D0, 25.91813939211580D0,
     4           29.05973204570559D0, 32.20132469929538D0 /,
     5      RHO/ 1.000777311907269D0, 1.000001449897657D0,
     6           1.000000002707595D0, 1.000000000005056D0,
     7           1.000000000000010D0, 1.000000000000000D0,
     8           1.000000000000000D0, 1.000000000000000D0,
     9           1.000000000000000D0, 1.000000000000000D0 /
      DATA SAL/0.06411D0,0.1D0,0.2D0,0.3D0,0.4D0,0.5D0,0.6D0,
     1           0.7D0,0.8D0,0.9D0,1.0D0/, SBT/ 0.56388D0,
     2         0.63925D0,0.72964D0,0.78990D0,0.83964D0,0.88330D0,
     3         0.92316D0,0.95143D0,0.97183D0,0.98919D0,1.0D0/
      END
```

```
C
      SUBROUTINE  FORCES (FR,CQ,NT,ID)
C ... CALCULATE UNSTEADY INVISCID FORCES
      IMPLICIT COMPLEX*16(A-H), REAL*8(O-Z)
      DOUBLE PRECISION  DABS,DREAL
      COMMON/IFLUID/RHOI,UI,UIR
      COMMON/AFLUID/RHOA,UA,UAR
      COMMON/ISHELL/DHI,DVI,QI,REI,SKI,PSI
      COMMON/OSHELL/DHO,DVO,QO,REO,SKO,PSO
      COMMON/CONST/PI,RGAMA,JSC,JIN,JOUT,IJOB,IOP1,IOP2
      COMMON/COAX/RLA(10),RHO(10),OMR,RINT,NINT,N,IOP3
      COMMON/SVFOR/SAL(11),SBT(11),RDI,RDO,RGI,RGO,VISI,VISA,SL
      DIMENSION  FR(NT,NT,1),CQ(NT,NT,1),XG(2),WGT(2),WG(2)
      DATA  XG/-0.577350269189626D0,0.577350269189626D0/, WGT/1.D0,1.D0/
      GO TO (20,360,420), ID
   20 DO 100  J=1,2
  100 WG(J)= 0.5D0*RINT*WGT(J)
      RLIM= 0.5D0*RINT*NINT
      FN= N
      MT= 6*NT*NT
      CALL  CLEAR (FR,MT)
      DO 300  I=1,NINT
      RLOW= RINT*(I - 1) - RLIM
      RHI= RLOW + RINT
      DO 300  J=1,2
      WT= WG(J)
      RA= 0.5D0*(RLOW + RHI + RINT*XG(J))
      AEI= RA*REI
      RALFA= RA*REO
      AEO= RALFA
      B1= CIN(AEI,N)
      B2= CIN(AEI,N+1)
      CON1= B1/(B1*FN/AEI + B2)
      C1= CKN(AEI,N)
      C2= CKN(AEI,N+1)
      IF (DABS(RALFA).GT.87.D0)  GO TO 120
      B3= CIN(AEO,N)
      B4= CIN(AEO,N+1)
      C3= CKN(AEO,N)
      C4= CKN(AEO,N+1)
      CON= (B3*FN/AEO+B4)*(C1*FN/AEI-C2)-(B1*FN/AEI+B2)*(C3*FN/AEO-C4)
      CON2= ( (B3*FN/AEO + B4)*C1 - B1*(C3*FN/AEO - C4) )/DREAL(CON)
      GO TO 140
  120 CON= (C1*FN/AEI - C2)
      CON2= C1/DREAL(CON)
  140 DO 200  IT=1,3
      RB= RA**(IT - 2)
      DO 200  M=1,NT
      DO 200  K=1,NT
      HN= GH(RA,K,M,2)
      FR(K,M,IT)= FR(K,M,IT) + WT*RB*HN*DREAL(CON1)
  200 FR(K,M,3+IT)= FR(K,M,3+IT) + WT*RB*HN*DREAL(CON2)
  300 CONTINUE
      DO 320  IT=1,6
      DO 320  M=1,NT
      DO 320  K=1,NT
  320 WRITE (JOUT,2000)  FR(K,M,IT)
      RETURN
C ... READ IN VALUES OF INTEGRALS IN EXPRESSIONS OF FLUID FORCES
  360 DO 380  IT=1,6
      DO 380  M=1,NT
```

```
      DO 380  K=1,NT
  380 READ (JSC,2000)  FR(K,M,IT)
      RETURN
C ... READ DATA FOR THE INTERNAL AND ANNULAR FLUIDS
  420 READ (JIN,1000)  VISI,RHOI,UIR
      READ (JIN,1000)  VISA,RHOA,UAR
      DO 600  IT=1,3
      IF (IT - 2)  440,460,480
  440 R1=  RHOI*UI**2/(2.D0*PI*QI*REI**2)
      R2= -RHOA*UA**2/(2.D0*PI*QI*(REO*OMR)**2)
      GO TO 500
  460 R1= -RHOI*UI**2*UIR/(PI*QI*REI)
      R2=  RHOA*UA**2*UAR/(PI*QI*REO*OMR)
      GO TO 500
  480 R1=  RHOI*UI**2*UIR**2/(2.D0*PI*QI)
      R2= -RHOA*UA**2*UAR**2/(2.D0*PI*QI)
  500 DO 600  M=1,NT
      DO 600  K=1,NT
  600 CQ(K,M,IT)= R1*FR(K,M,IT) + R2*FR(K,M,3+IT)
      RETURN
 1000 FORMAT (3D15.6)
 2000 FORMAT (5X,2D25.16)
      END
C
      SUBROUTINE  INPUT (NTERMS)
      IMPLICIT COMPLEX*16(A-H), REAL*8(O-Z)
      COMMON/ISHELL/DHI,DVI,QI,REI,SKI,PSI
      COMMON/OSHELL/DHO,DVO,QO,REO,SKO,PSO
      COMMON/IFLUID/RHOI,UI,UIR
      COMMON/AFLUID/RHOA,UA,UAR
      COMMON/COAX/RLA(10),RHO(10),OMR,RINT,NINT,MODE,IOP3
      COMMON/CLFR/RL,MODEL
      COMMON/CONST/PI,RGAMA,JSC,JIN,JOUT,IJOB,IOP1,IOP2
      COMMON/SVFOR/SAL(11),SBT(11),RDI,RDO,RGI,RGO,VISI,VISA,SL
C ... READ DATA FOR THE INNER AND OUTER SHELLS
      READ (JIN,1000)  YNI,PSI,SDENI,THIKI,RDI,RGI,SHI,SVI
      READ (JIN,1000)  YNO,PSO,SDENO,THIKO,RDO,RGO,SHO,SVO
      WRITE (JOUT,1000)  YNI,PSI,SDENI,THIKI,RDI,RGI,SHI,SVI
      WRITE (JOUT,1000)  YNO,PSO,SDENO,THIKO,RDO,RGO,SHO,SVO
C ... READ VARIOUS PARAMETERS FOR THE COMPUTATION
      READ(JIN,1100) SL,RL,RINT,NINT,MODEL,MODE,NTERMS,IOP1,IOP2,IOP3
      WRITE(JOUT,1100)SL,RL,RINT,NINT,MODEL,MODE,NTERMS,IOP1,IOP2,IOP3
C ... GENERATE SPECIFIC DATA FOR LATER USE
      SKI= (THIKI/RDI)**2/12.D0
      SKO= (THIKO/RDO)**2/12.D0
      REI= RDI/SL
      REO= RDO/SL
      QI= YNI*THIKI*SL/(RDI**2*(1.D0 - PSI**2))
      QO= YNO*THIKO*SL/(RDO**2*(1.D0 - PSO**2))
      UI= DSQRT(YNI/(SDENI*(1.D0 - PSI**2)))
      UA= DSQRT(YNO/(SDENO*(1.D0 - PSO**2)))
      OMR= RDI*UA/(RDO*UI)
      CI= (0.D0,1.D0)
      DHI= 1.D0 + SHI*CI
      DHO= 1.D0 + SHO*CI
      DVI= SVI*UI*CI/RDI
      DVO= SVO*UA*CI/RDO
      RETURN
 1000 FORMAT (3D20.12/3D20.12/3D20.12)
 1100 FORMAT (3D15.8,4I5,3I2)
      END
```

```
C
      SUBROUTINE  MCK (CQ,CXM,CXC,CXK,NT,NS)
      IMPLICIT COMPLEX*16(A-H), REAL*8(O-Z)
      COMMON/COAX/RLA(10),RHO(10),OMR,RINT,NINT,N,IOP3
      COMMON/ISHELL/DHI,DVI,QI,REI,SKI,PSI
      COMMON/OSHELL/DHO,DVO,QO,REO,SKO,PSO
      DIMENSION  CQ(NT,NT,1),CXM(NS,1),CXC(NS,1),CXK(NS,1)
      DIMENSION  AM(3,3),AC(3,3),AK(3,3)
      DO 200  M=1,NT
      DO 200  K=1,NT
      CALL CLEAR (AM,9)
      CALL CLEAR (AC,9)
      CALL CLEAR (AK,9)
      U1= RE1(K,M)
      V2= RE4(K,M,2)
      V3= -V2
      V4= RE2(K,M,4)
      W1= N
      W2= W1**2
C ... CALCULATE ELEMENTS OF THE MASS MATRIX  M
      AM(1,1)= REI**2*V2
      AM(2,2)= U1
      AM(3,3)= U1 + CQ(K,M,1)
C ... CALCULATE ELEMENTS OF THE DAMPING MATRIX  C
      AC(3,3)= CQ(K,M,2)
C ... CALCULATE ELEMENTS OF THE STIFFNESS MATRIX  K
      AK(1,1)= -0.5D0*W2*(1.D0 + SKI)*(1.D0 - PSI)*REI**2*V2 + REI**4*V4
      AK(2,1)= -0.5D0*W1*(1.D0 + PSI)*REI**2*V3
      AK(3,1)= ( 0.5D0*W2*SKI*(1.D0 - PSI) - PSI )*REI**2*V3
     1         + SKI*(REI*RLA(M))**4*U1
      AK(1,2)= 0.5D0*W1*(1.D0 + PSI)*REI**2*V2
      AK(2,2)= -W2*U1 + 0.5D0*(1.D0 + 3.D0*SKI)*(1.D0 - PSI)*REI**2*V3
      AK(3,2)= W1*( -U1 + 0.5D0*SKI*(3.D0 - PSI)*REI**2*V3 )
      AK(1,3)= (PSI-0.5D0*W2*SKI*(1.D0-PSI))*REI**2*V2 - SKI*REI**4*V4
      AK(2,3)= W1*( 0.5D0*SKI*(3.D0 - PSI)*REI**2*V3 - U1 )
      AK(3,3)= -(SKI*((W2 - 1.D0)**2 + (REI*RLA(M))**4) + 1.D0)*U1
     1         + 2.D0*SKI*(W1*REI)**2*V3
      DO 100  J=1,3
      JJ= M + NT*(J - 1)
      DO 100  I=1,3
      II= K + NT*(I - 1)
      CXM(II,JJ)= AM(I,J)
      CXC(II,JJ)= AC(I,J)
  100 CXK(II,JJ)= AK(I,J)
  200 CONTINUE
      RETURN
      END
C
      SUBROUTINE  OUTPUT (AP,AQ,EIGA,EIGB,EIGVEC,NX)
      IMPLICIT COMPLEX*16(A-H), REAL*8(O-Z)
      COMMON/CONST/PI,RGAMA,JSC,JIN,JOUT,IJOB,IOP1,IOP2
      COMMON/IFLUID/RHOI,UI,UIR
      COMMON/AFLUID/RHOA,UA,UAR
      COMMON/SVFOR/SAL(11), SBT(11),RDI,RDO,RGI,RGO,VISI,VISA,SL
      DIMENSION  AP(1),AQ(1),EIGA(1),EIGB(1),EIGVEC(1)
      WRITE (JOUT,2000)  UIR,UAR
C ... CALCULATE THE PERFORMANCE INDEX
      PFINX= DGPICG(NX,NX,AP,NX,AQ,NX,EIGA,EIGB,EIGVEC,NX)
      WRITE (JOUT,2020)  PFINX
C ... CALCULATE THE EIGENVALUES
C ... CON= UI/RDI
```

```
      DO 100  I=1,NX
  100 EIGA(I)=-EIGA(I)/EIGB(I)
      CALL SORT (EIGA,NX)
      DO 200  I=1,NX
  200 WRITE (JOUT,2040)  I,EIGA(I)
      RETURN
 2000 FORMAT (54H * * *  VALUES OF NON-DIMENSIONALIZED FLUID VELOCITIES,
     1       //20X,5HUIR =,D15.6,10X,5HUAR =,D15.6//
     2         35H * * *  RESULTS FOR THE FREQUENCIES/)
 2020 FORMAT (/28H > > >  PERFORMANCE INDEX = ,F8.3/)
 2040 FORMAT (4H I =,I5,5X,8HOM  =  (,2D24.16,2H ))
      END
C
      SUBROUTINE  REDUCE (CXM,CXC,CXK,AP,AQ,NS,NX)
      IMPLICIT COMPLEX*16(A-H)
      DIMENSION  CXM(NS,1),CXC(NS,1),CXK(NS,1),AP(NX,1),AQ(NX,1)
      MX= NX*NX
      CALL CLEAR (AP,MX)
      CALL CLEAR (AQ,MX)
      DO 100  I=1,NS
      AP(I,NS+I)= (1.D0,0.D0)
  100 AQ(I,I)= (-1.D0,0.D0)
      DO 200  J=1,NS
      DO 200  I=1,NS
      AP(NS+I,J)= CXK(I,J)
      AP(NS+I,NS+J)= CXC(I,J)
  200 AQ(NS+I,NS+J)= CXM(I,J)
      RETURN
      END
C
      DOUBLE PRECISION FUNCTION  RFAC (N)
      IMPLICIT REAL*8(O-Z)
      RFAC= 1.D0
      IF (N.LE.1)  RETURN
      X= 2.D0
      DO 20  I=2,N
      RFAC= RFAC*X
   20 X= X + 1.D0
      RETURN
      END
C
      DOUBLE PRECISION FUNCTION  RFI (N)
      IMPLICIT REAL*8(O-Z)
      RFI= 0.D0
      IF (N.EQ.0)  RETURN
      X= 1.D0
      DO 20  I=1,N
      RFI= RFI + 1.D0/X
   20 X= X + 1.D0
      RETURN
      END
C
      SUBROUTINE  SORT (DT,NX)
      IMPLICIT COMPLEX*16(A-H), REAL*8(O-Z)
      DOUBLE PRECISION  DREAL
      DIMENSION  DT(1)
      NMIN= NX - 1
  100 IFLAG= 0
      DO 200  I=1,NMIN
      C1= DT(I)
      C2= DT(I+1)
```

```
      IF (DREAL(C1).GE.DREAL(C2))  GO TO 200
      DT(I)= C2
      DT(I+1)= C1
      IFLAG= 1
  200 CONTINUE
      IF (IFLAG.EQ.1)  GO TO 100
      RETURN
      END
C
      SUBROUTINE  VISFOR (CXK,NT,NS)
C ... CALCULATE STEADY VISCOUS FORCES FOR CLAMPED-PINNED AND PINNED-CLAMPED
C ... SHELLS
      IMPLICIT COMPLEX*16(A-H), REAL*8(O-Z)
      DOUBLE PRECISION  DLOG10,DSQRT
      COMMON/IFLUID/RHOI,UI,UIR
      COMMON/AFLUID/RHOA,UA,UAR
      COMMON/ISHELL/DHI,DVI,QI,REI,SKI,PSI
      COMMON/COAX/RLA(10),RHO(10),OMR,RINT,NINT,N,IOP3
      COMMON/SVFOR/SAL(11),SBT(11),RDI,RDO,RGI,RGO,VISI,VISA,SL
      DIMENSION  CXK(NS,1),CV(3,3)
      R13= 0.33333333333333330
C     RM= DSQRT(0.5D0*(RDO**2 - RDI**2)/DLOG(RDO/RDI))
C ... DETERMINE THE LOCATION OF THE MAXIMUM VELOCITY USING A MULTILINEAR
C ... REPRESENTATION OF THE CURVE BY BRIGHTON \& JONES (1963)
      RAB= RDI/RDO
      DO 5  I=1,11
      IF (RAB-SAL(I)) 10,5,5
    5 CONTINUE
   10 SBETA= SBT(I-1)+(RAB-SAL(I-1))*(SBT(I)-SBT(I-1))/(SAL(I)-SAL(I-1))
      RM= RDO*(RAB + 0.5D0*SBETA*(1.D0 - RAB))
      IF (UIR)  40,40,20
   20 RNI= 2.D0*(UIR*UI)*RDI/VISI
      WFAI= 0.0055D0*(1.D0 + (2.D+04*RGI + 1.D+06/RNI)**R13)
      WFI= -0.5D0/DLOG10(RGI/3.7D0 + 2.51D0/(RNI*DSQRT(WFAI)))
      UTI= UI*UIR*WFI/DSQRT(8.D0)
      GO TO 60
   40 UTI= 0.D0
   60 IF (UAR)  100,100,80
   80 RNA= 2.D0*(UAR*UA)*(RDO - RDI)/VISA
      WFAOI= 0.0055D0*(1.D0 + (2.D+04*RGI + 1.D+06/RNA)**R13)
      WFAOO= 0.0055D0*(1.D0 + (2.D+04*RGO + 1.D+06/RNA)**R13)
      WFOI= -0.5D0/DLOG10(RGI/3.7D0 + 2.51D0/(RNA*DSQRT(WFAOI)))
      WFOO= -0.5D0/DLOG10(RGO/3.7D0 + 2.51D0/(RNA*DSQRT(WFAOO)))
      UTOI= UA*UAR*WFOI*DSQRT((RM**2 - RDI**2)/(8.D0*RDI*(RDO - RDI)))
      UTOO= UA*UAR*WFOO*DSQRT((RDO**2 - RM**2)/(8.D0*RDO*(RDO - RDI)))
      GO TO 120
  100 UTOI= 0.D0
      UTOO= 0.D0
  120 WBI= RHOI*UTI**2 + RHOA*UTOI**2
      WCI= 2.D0*(RHOI*UTI**2/RDI - RDO*RHOA*UTOO**2/(RDO**2 - RM**2))
      WDI= -SL*WCI
      RCONI= 1.D0/(QI*REI**2)
      A1I= -RCONI*WBI
      B1I= -A1I
      B2I=  RCONI*WBI*REI
      A3I= -RCONI*WCI*RDI
      B3I= -RCONI*WDI*REI
      EN= N
      DO 300  K=1,NT
      DO 300  M=1,NT
      CALL CLEAR (CV,9)
```

```
      CV(1,1)= REI**4*( A1I*RE3(K,M,4) + IOP3*B1I*RE2(K,M,4) )
     1       - (EN*REI)**2*( A3I*RE3(K,M,2) + B3I*RE2(K,M,2) )
      CV(3,1)= REI**2*( A3I*RE3(K,M,3) + B3I*RE2(K,M,3) )
      CV(1,2)= B2I*EN*REI*RE2(K,M,1)
      CV(2,2)= REI**2*( A1I*RE3(K,M,3) + IOP3*B1I*RE2(K,M,3) )
     1       - EN**2*( A3I*RE3(K,M,1) + B3I*RE1(K,M))
      CV(3,2)= -EN*( A3I*RE3(K,M,1) + B3I*RE1(K,M) )
      CV(1,3)= REI*(B2I*RE2(K,M,1)-REI*(A3I*RE3(K,M,2)+B3I*RE2(K,M,2)))
      CV(2,3)= CV(3,2)
      CV(3,3)= CV(2,2)
      DO 200  J=1,3
      JJ= M + NT*(J - 1)
      DO 200  I=1,3
      II= K + NT*(I - 1)
  200 CXK(II,JJ)= CXK(II,JJ) + CV(I,J)
  300 CONTINUE
      RETURN
      END

C
      COMPLEX FUNCTION  GH*16 (RA,K,M,ID)
C ... FUNCTIONS  GKM AND HKM FOR CLAMPED-PINNED OR PINNED-CLAMPED BEAMS
      IMPLICIT COMPLEX*16(A-H), REAL*8(O-Z)
      COMMON/COAX/RLA(10),RHO(10),OHMR,RINT,NINT,N,IOP3
      CI= (0.D0,1.D0)
      GH= HH(RA,K,-1)*(HH(RA,M,1)+IOP3*CN(RA,M) )
C ... ID=1 FOR GKM, ID=2 FOR HKM
      GO TO (100,200), ID
  100 GH= CI*RA*GH
  200 RETURN
      END
C
      COMPLEX FUNCTION  HH*16 (RA,M,I)
C ... FUNCTIONS  HK AND HM FOR CLAMPED-PINNED AND PINNED-CLAMPED BEAMS
      IMPLICIT COMPLEX*16(A-H), REAL*8(O-Z)
      COMMON/COAX/RLA(10),RHO(10),OHMR,RINT,NINT,N,IOP3
C ... I=-1 FOR HK, I=+1 FOR HM
      CI= (0.D0,1.D0)
      CA= CI*RA*I
      CB=CA*(-1)**(IOP3+1)
      RM= RLA(M)
      RDIF= DABS(RA) - RM
      IF (DABS(RDIF).LT.1.D-16)  GO TO 50
      H1=CB**3*RFB(M,2,1)-CB**2*RFB(M,2,2)+CB*RFB(M,2,3)-RFB(M,2,4)
      H2=CB**3*RFB(M,1,1)-CB**2*RFB(M,1,2)+CB*RFB(M,1,3)-RFB(M,1,4)
      HH=(CDEXP(CB)*H1-H2)/(RA**4-RM**4)
      HH=CDEXP(CA*(1-IOP3))*HH
      RETURN
   50 H1=CB**3*RFB(M,2,1)-CB**2*RFB(M,2,2)+CB*RFB(M,2,3)-RFB(M,2,4)
     +   +3.D0*CB**2*RFB(M,2,1)-2.D0*CB*RFB(M,2,2)+RFB(M,2,3)
      H2=3.D0*CB**2*RFB(M,1,1)-2.D0*CB*RFB(M,1,2)+RFB(M,1,3)
      HH=(CDEXP(CB)*H1-H2)/CB**4/4.D0
      HH=CDEXP(CA*(1-IOP3))*HH
      RETURN
      END
C
      COMPLEX FUNCTION CN*16 (RA,M)
      IMPLICIT COMPLEX*16(A-H),REAL*8(O-Z)
      COMMON/COAX/RLA(10),RHO(10),OHMR,RINT,NINT,N,IOP3
      COMMON/CONST/PI,RGAMA,JSC,JIN,JOUT,IJOB,IOP1,IOP2
      COMMON/CLPI/RL,MODEL
```

```
      CN=(0.D0,0.D0)
      IF (MODEL) 20,20,40
   20 RETURN
   40 RB=RFB(M,2,2)
      RD=RL-1.D0
      CI=(1.D0,0.D0)
      CJ=(0.D0,1.D0)
      CA=CJ*RA
      CD=CA-CI
      CE=CD*RD
      CF=CDEXP(CA)
      CG=CDEXP(CE)
C ... THE NEW OUTFLOW-MODEL
      CN=-RB*CF*(CG*(CD*RD+1.D0)-1.D0)/CD**2
      RETURN
      END
C

      DOUBLE PRECISION FUNCTION RFB (M,ID1,ID2)
C...  BOUNDARY CONDITIONS OF CLAMPED-PINNED BEAMS
      IMPLICIT REAL*8(O-Z)
      COMMON/COAX/RLA(10),RHO(10),OHMR,RINT,NINT,N,IOP3
      GO TO (100,200),ID1
C...  ID1=1 MEANS THE LEFT END  X=0
100   GO TO (10,20,30,40),ID2
10    RFB = 0.0D+00
      RETURN
20    RFB = 0.0D+00
      RETURN
30    RFB = 2.0D+00*RLA(M)**2
      RETURN
40    RFB =-2.0D+00*RLA(M)**3*RHO(M)
      RETURN
C...  ID1=2 MEANS THE RIGHT END X=L
200   GO TO (50,60,70,80),ID2
50    RFB = 0.0D+00
      RETURN
60    RFB = 2.D0*RLA(M)*(-1)**M/(DSQRT(RHO(M)**2+1.D0)
     +       +(-1)**M*DSQRT(RHO(M)**2-1.D0))
      RETURN
70    RFB = 0.0D+00
      RETURN
80    RFB = 2.D0*RLA(M)**3*(-1)**(M+1)/(DSQRT(RHO(M)**2+1.D0)
     +       +(-1)**(M+1)*DSQRT(RHO(M)**2-1.D0))
      RETURN
      END


      DOUBLE PRECISION FUNCTION  RE1 (K,M)
C ... INTEGRALS INVOLVING CHARAC. FUNCTIONS OF CL-PI AND PI-CL BEAMS
      IMPLICIT REAL*8(O-Z)
      COMMON/COAX/RLA(10),RHO(10),OHMR,RINT,NINT,N,IOP3
  100 IF (K.EQ.M)  GO TO 120
      RE1= 0.D0
      RETURN
  120 RE1= 1.D0
      RETURN
      END
C
      DOUBLE PRECISION FUNCTION  RE4 (K,M,ID)
C ... INTEGRALS INVOLVING CHARAC. FUNCTIONS OF CLAMPED-PINNED BEAMS
```

```
C ... AND PINNED-CLAMPED BEAMS
      IMPLICIT REAL*8(O-Z)
      COMMON/COAX/RLA(10),RHO(10),OHMR,RINT,NINT,N,IOP3
      RK= RLA(K)
      RM= RLA(M)
      IF (K.EQ.M)  GO TO 100
      GO TO (20,40,60), ID
   20 T1=RK**4*RFB(K,2,1)*RFB(M,2,1)-RFB(K,2,4)*RFB(M,2,2)
     +         +RFB(K,2,3)*RFB(M,2,3)-RFB(K,2,2)*RFB(M,2,4)
      T2=RK**4*RFB(K,1,1)*RFB(M,1,1)-RFB(K,1,4)*RFB(M,1,2)
     +         +RFB(K,1,3)*RFB(M,1,3)-RFB(K,1,2)*RFB(M,1,4)
      RE4=(T1-T2)/(RK**4-RM**4)
      RETURN
   40 T1=RK**4*RFB(K,2,1)*RFB(M,2,2)-RFB(K,2,4)*RFB(M,2,3)
     +  +RFB(K,2,3)*RFB(M,2,4)-RFB(K,2,2)*RFB(M,2,1)*RM**4
      T2=RK**4*RFB(K,1,1)*RFB(M,1,2)-RFB(K,1,4)*RFB(M,1,3)
     +  +RFB(K,1,3)*RFB(M,1,4)-RFB(K,1,2)*RFB(M,1,1)*RM**4
      RE4=(T1-T2)/(RK**4-RM**4)
      RETURN
   60 T1=RFB(K,2,4)*RFB(M,2,4)+(-RFB(K,2,3)*RFB(M,2,1)
     +  +RFB(K,2,2)*RFB(M,2,2)-RFB(K,2,1)*RFB(M,2,3))*RM**4
      T2=RFB(K,1,4)*RFB(M,1,4)+(-RFB(K,1,3)*RFB(M,1,1)
     +  +RFB(K,1,2)*RFB(M,1,2)-RFB(K,1,1)*RFB(M,1,3))*RM**4
      RE4=(T1-T2)/(RK**4-RM**4)
      RETURN
  100 GO TO (120,140,160),ID
  120 RE4=0.D0
      RETURN
  140 T1=RFB(M,2,2)*RFB(M,2,2)-RFB(M,2,3)*RFB(M,2,4)/RM**4
     +  +RFB(M,2,4)*RFB(M,2,4)/RM**4
      T2=-RFB(M,1,3)*RFB(M,1,4)/RM**4
      RE4=(T1-T2)/4.D0
      RETURN
  160 RE4=0.5D0*(RFB(M,2,4)*RFB(M,2,4)
     +          -RFB(M,1,4)*RFB(M,1,4))/RM**4
      RETURN
      END
C
      DOUBLE PRECISION FUNCTION  RE5 (K,M,ID)
C ... INTEGRALS INVOLVING CHARAC. FUNCTIONS OF CLAMPED-PINNED BEAMS
C ... AND PINNED-CLAMPED BEAMS
      IMPLICIT REAL*8(O-Z)
      COMMON/COAX/RLA(10),RHO(10),OHMR,RINT,NINT,N,IOP3
      RK= RLA(K)
      RM= RLA(M)
      IF (K.EQ.M) GO TO 60
      GO TO (20,40), ID
   20 RE5=( RFB(K,2,4)*RFB(M,2,1)-RFB(K,2,3)*RFB(M,2,2)
     +     +RFB(F,2,2)*RFB(M,2,3)-RFB(K,2,1)*RFB(M,2,4)
     +     -2.D0*RE4(M,K,3)+2.D0*RE4(K,M,3))/(RK**4-RM**4)
      RETURN
   40 RE5=(RK**4*RFB(K,2,1)*RFB(M,2,2)-RFB(K,2,4)*RFB(M,2,3)
     +          +RFB(K,2,3)*RFB(M,2,4)-RFB(K,2,2)*RFB(M,2,1)*RM**4
     +          +RFB(K,2,4)*RFB(M,2,2)-RFB(K,2,2)*RFB(M,2,4)
     +   -2.D0*RK**4*RE4(M,K,1)+2.D0*RM**4*RE4(K,M,1))/(RK**4-RM**4)
      RETURN
   60 GO TO(80,100),ID
   80 T1=2.D0*(3.D0*RFB(M,2,1)*RFB(M,2,4)-RFB(M,2,2)*RFB(M,2,3))
     ++(RM**4*RFB(M,2,1)**2+RFB(M,2,3)**2-2.D0*RFB(M,2,2)*RFB(M,2,4))
     +    +4.D0*RFB(M,2,2)**2-6.D0*RFB(M,2,1)*RFB(M,2,3)
      T2=  4.D0*RFB(M,1,2)**2-6.D0*RFB(M,1,1)*RFB(M,1,3)
```

```
      RE5=(T1-T2)/8.D0/RM**4
      RETURN
  100 T1=2.D0*(3.D0*RFB(M,2,1)*RFB(M,2,2)*RM**4-RFB(M,2,3)*RFB(M,2,4))
     ++RM**4*(RFB(M,2,2)**2-2.D0*RFB(M,2,3)*RFB(M,2,1))+RFB(M,2,4)**2
     +    +4.D0*RFB(M,2,3)**2-6.D0*RFB(M,2,2)*RFB(M,2,4)
      T2=  4.D0*RFB(M,1,3)**2-6.D0*RFB(M,1,2)*RFB(M,1,4)
      RE5=(T1-T2)/8.D0/RM**4
      RETURN
      END
C
      DOUBLE PRECISION FUNCTION  RE2 (K,M,ID)
C ... INTEGRALS INVOLVING CHARAC. FUNCTIONS OF CLAMPED-PINNED BEAMS
C ... AND PINNED-CLAMPED BEAMS
      IMPLICIT REAL*8(O-Z)
      COMMON/COAX/RLA(10),RHO(10),OHMR,RINT,NINT,N,IOP3
      RK= RLA(K)
      RM= RLA(M)
      GO TO (20,40,60,80),ID
   20 RE2=(-1)**(IOP3+1)*RE4(K,M,1)
      RETURN
   40 RE2=RE4(K,M,2)
      RETURN
   60 RE2=-RE4(K,M,2)
      RETURN
   80 RE2=-RM**4*RE1(K,M)
      RETURN
      END
C
      DOUBLE PRECISION FUNCTION  RE3 (K,M,ID)
C ... INTEGRALS INVOLVING CHARAC. FUNCTIONS OF CLAMPED-PINNED BEAMS
C ... AND PINNED-CLAMPED BEAMS
      IMPLICIT REAL*8(O-Z)
      COMMON/COAX/RLA(10),RHO(10),OHMR,RINT,NINT,N,IOP3
      RK= RLA(K)
      RM= RLA(M)
      GO TO (20,40,60,80),ID
   20 RE3=(-1)**(IOP3+1)*RE5(K,M,1)+(1-IOP3)*RE1(K,M)
      RETURN
   40 RE3=(-1)**(IOP3+1)*RE5(K,M,2)+(1-IOP3)*RE2(K,M,2)
      RETURN
   60 RE3=(-1)**(IOP3+1)*(-RE4(M,K,1)-RE5(K,M,2))+(1-IOP3)*RE2(K,M,3)
      RETURN
   80 RE3=(-1)**(IOP3+1)*(-RE4(K,M,3)-RM**4*RE5(K,M,1))
     +           +(1-IOP3)*RE2(K,M,4)
      RETURN
      END


    1    1
          2.0000D+11              0.30D+00        7.8000000D+03
          0.5000D-03   0.09090909091D+00             0.00D+00
          0.0000D+00             0.000D+00
          2.0000D+11              0.30D+00        7.8000000D+03
          0.5000D-03   0.10000000000D+00             0.00D+00
          0.0000D+00             0.000D+00
     1.0000D+00        3.00D+00       2.000D+00  200    3    3    6 0 0 1
    1
   1.121000D-06   1.000000D+03     0.02000D+00    1
   1.121000D-06   1.000000D+03     0.00000D+00

    1    1
```

```
 0.2000000000000D+12  0.3000000000000D+00  0.7800000000000D+04
 0.5000000000000D-03  0.9090909091000D-01  0.0000000000000D+00
 0.0000000000000D+00  0.0000000000000D+00
 0.2000000000000D+12  0.3000000000000D+00  0.7800000000000D+04
 0.5000000000000D-03  0.1000000000000D+00  0.0000000000000D+00
 0.0000000000000D+00  0.0000000000000D+00
0.10000000D+01 0.30000000D+01 0.20000000D+01  200    3    3    6 0 0 1
* * *  VALUES OF NON-DIMENSIONALIZED FLUID VELOCITIES

                    UIR =   0.200000D-01          UAR =   0.000000D+00

* * *  RESULTS FOR THE FREQUENCIES


> > >  PERFORMANCE INDEX =  550.750

I =    1     OM  =  (  0.3486091897466983D+01   0.1039543870264284D-13 )
I =    2     OM  =  (  0.3347329169784129D+01  -0.7647929192126422D-13 )
I =    3     OM  =  (  0.3228825238110891D+01   0.8385120647854616D-13 )
I =    4     OM  =  (  0.3133065037988444D+01  -0.2862784199760782D-14 )
I =    5     OM  =  (  0.3062476956661809D+01  -0.2608736068596212D-14 )
I =    6     OM  =  (  0.3019154164656023D+01  -0.1006989456891162D-14 )
I =    7     OM  =  (  0.2240326917869975D+01   0.2338137875847423D-14 )
I =    8     OM  =  (  0.2028610077240330D+01  -0.1792545860097676D-14 )
I =    9     OM  =  (  0.1946327646016872D+01   0.1355707837505615D-14 )
I =   10     OM  =  (  0.1879598819915037D+01   0.3154402237765462D-14 )
I =   11     OM  =  (  0.1828208326939845D+01  -0.6715131398261934D-15 )
I =   12     OM  =  (  0.1793089007203285D+01  -0.1657128807190817D-15 )
I =   13     OM  =  (  0.4485857047500065D-01   0.7022883434978871D-15 )
I =   14     OM  =  (  0.3094610549019855D-01  -0.4114248720879916D-15 )
I =   15     OM  =  (  0.2054619149802507D-01  -0.2510996102895470D-14 )
I =   16     OM  =  (  0.1177916767588317D-01   0.1560478595473382D-14 )
I =   17     OM  =  (  0.5080333746931395D-02  -0.1110705123751779D-14 )
I =   18     OM  =  (  0.9663690915345615D-03   0.2506741895573173D-14 )
I =   19     OM  =  ( -0.9663690915361852D-03   0.2504991747857112D-14 )
I =   20     OM  =  ( -0.5080333746806315D-02  -0.1104722823258334D-14 )
I =   21     OM  =  ( -0.1177916767699853D-01   0.1558440983910724D-14 )
I =   22     OM  =  ( -0.2054619149350455D-01  -0.2459499534541495D-14 )
I =   23     OM  =  ( -0.3094610550539888D-01  -0.4584217604226748D-15 )
I =   24     OM  =  ( -0.4485857045468787D-01   0.7303670266083322D-15 )
I =   25     OM  =  ( -0.1793089007203285D+01  -0.1266337031486691D-15 )
I =   26     OM  =  ( -0.1828208326939847D+01  -0.4587570802467386D-15 )
I =   27     OM  =  ( -0.1879598819915022D+01   0.3023587763280680D-14 )
I =   28     OM  =  ( -0.1946327646016879D+01   0.2338400356301398D-14 )
I =   29     OM  =  ( -0.2028610077240312D+01  -0.3148459903657773D-14 )
I =   30     OM  =  ( -0.2240326917869974D+01   0.2357380351744562D-14 )
I =   31     OM  =  ( -0.3019154164656041D+01  -0.2680124780395467D-15 )
I =   32     OM  =  ( -0.3062476956661864D+01  -0.2236056351176150D-14 )
I =   33     OM  =  ( -0.3133065037988432D+01  -0.4337701635713217D-14 )
I =   34     OM  =  ( -0.3228825238110839D+01   0.8454349435231693D-13 )
I =   35     OM  =  ( -0.3347329169784118D+01  -0.7765204592868956D-13 )
I =   36     OM  =  ( -0.3486091897466920D+01   0.1113458223487697D-13 )
```